THÈSE EN COTUTELLE PRÉSENTÉE
POUR OBTENIR LE GRADE DE

DOCTEUR DE

L'UNIVERSITÉ DE BORDEAUX

ET DE L'UNIVERSITÉ DU PAYS BASQUE (UPV/EHU)

ÉCOLE DOCTORALE DES SCIENCES CHIMIQUES
SPÉCIALITÉ: CHIMIE-PHYSIQUE

Par Alejandro PEÑA TORRES

CONTRIBUTION TO THE THEORETICAL DESCRIPTION OF N_2 DYNAMICS ON W(100)

Sous la direction de: Cédric CRESPOS
Co-directeur: Iñaki JUARISTI

Soutenue le 10/12/2018

Membres de jury:

M. BONNET, Laurent	Directeur de Recherche au CNRS	Université de Bordeaux	Président
M. DONG, Wei	Directeur de Recherche	Ecole Normale Supérieure de Lyon	Rapporteur
Mme. MARCOS, Maria Luisa	Professeure	Universidad Autónoma de Madrid	Rapporteur
Mme. DÍAZ, Cristina	"Ramón y Cajal" Research Fellow	Universidad Autónoma de Madrid	Examinateur
M. DÍEZ MUIÑO, Ricardo	Directeur de Recherche	Donostia International Physics Center	Examinateur
M. BUSNENGO, Fabio	Professeur	Universidad Nacional de Rosario	Examinateur
M. CRESPOS, Cédric	Maître de Conférence	Université de Bordeaux	Directeur de thèse
M. JUARISTI, Iñaki	Professeur	Universidad del País Vasco (UPV/EHU)	Co-directeur de thèse

Titre: Contribution à l'étude théorique de la dynamique réactionnelle du système N_2/W(100)

Résumé: Les processus élémentaires à l'interface gaz-solide suscitent un grand intérêt dans de nombreux domaines scientifiques. Ainsi, les réactions molécule-surface jouent un rôle clé dans l'étude des processus de catalyse hétérogènes, dans l'analyse des interactions plasma-paroi (fusion thermonucléaire, rentrées atmosphériques), dans la chimie des milieux atmosphériques, et l'astrochimie, mais également dans les procédés de fonctionnalisation de surface, etc... Le but de ce travail de thèse est d'analyser la dynamique de plusieurs mécanismes présents lorsque des molécules de N2 entrent en collision avec une surface W (100). Le système N_2 / W constitue l'un des systèmes de référence les plus emblématiques dans le domaine des sciences de surface. Des simulations de dynamique moléculaire quasi-classique ont été réalisés en utilisant une surface d'énergie potentielle construite à partir de calculs de structure électronique prenant en compte des interactions non locales, telles que les forces de van der Waals, au travers de la théorie de la fonctionnelle de la densité. Parmi les processus réactifs étudiés, nous nous sommes concentrés sur la caractérisation de l'adsorption dissociative et non dissociative, de la diffusion non réactive et de la recombinaison Eley-Rideal. Les simulations prennent en compte les différents canaux de dissipation de l'énergie de la molécule liés à l'excitation des phonons de surface et les excitations électroniques de type électron-trou.

Mots clés: Dynamique, interface gaz-solide, surface d'énergie potentiell

---

Title: Contribution to the theoretical description of N_2 dynamics on W(100)

Abstract: Elementary processes at the gas-solid interface are of great interest in many scientific domains. Thus molecule-surface reactions play a key role in the study of: heterogeneous catalysis processes, plasma-wall interactions in the context of thermonuclear fusion or atmospheric re-entries technologies, chemistry of atmospheric media, astrochemistry, surface functionalization etc... The main goal of this thesis work is to analyse the dynamics of several processes that occur when N2 molecules collide with a W(100) surface. The N2/W system constitutes one of the most emblematic benchmark system in the surface science field.

Quasi-classical molecular dynamics are performed making use of a potential energy surface based on density functional theory calculations that include non-local interactions such as van der Waals forces. Among the reactive processes studied, we focus on the characterization of the dissociative and non-dissociative adsorption, non-reactive scattering and Eley-Rideal recombination. The non-adiabaticity of the dynamics was accounted for by introducing energy dissipation channels to surface phonons and electron-hole pair excitations in the simulations.

Keywords: Dynamics, gas-solid interface, potential energy surface

Unité de recherche

Institut des Sciences Moléculaires – Université de Bordeaux CNRS UMR 5255
B*â*timent A12, 351 cours de la libération
33405 TALENCE cedex
FRANCE

université de BORDEAUX

eman ta zabal zazu
Universidad del País Vasco
Euskal Herriko Unibertsitatea

DOCTORAL THESIS

Contribution to the theoretical description of N_2 dynamics on W(100)

Author:
Alejandro Peña Torres

Supervisors:
Cedric Crespos, PhD.
Iñaki Juaristi, PhD.

A thesis submitted in fulfillment of the requirements for the degree of Doctor of Philosophy

in the programs

Chemical Physics - Université de Bordeaux
Physics of Nanostructures and Advanced Materials - Universidad del País Vasco

December, 2018

"Do, or do not... There is no try."

Yoda

Acknowledgements

It was less than three years ago when I started to work in this thesis. Back then I didn't really know what to expect. Crossing the ocean to start a new life away from the loved ones is not an easy transition and it was indeed a bit scary. Luckily, I ended up working with two amazing supervisors such as Cédric Crespos and Iñaki Juaristi. I want to start by deeply thanking them for guiding me in this journey. I cannot thank them enough for being always available and supporting me in any way I needed. I truly admire their passion for science and the patience to teach (and correct my drafts and huge mistakes, of course). None of this work could have been done without their advices.

I want to express my sincere gratitude to Fabio Busnengo for letting me spend a couple of months in Rosario and teaching me the basis of a great part of this work. It has been a great opportunity to share many spaces with Fabio throughout my thesis and to learn from all of his experience, whether it was from the scientific point of view in the office or from the personal point of view drinking some beers. I want to also thank Pascal and Maite, who were also willing to help me with anything I needed. It didn't matter if I was in Bordeaux or Donostia, I knew that there was always someone to help me out.

The good thing about doing the thesis in two cities is that you get to know a lot of people. The bad thing is that you will probably forget to thank them all, but I will try. First of all, I want to thank the people that I have met in the ISM in Bordeaux: Raphaël, Fred, Phillipe, Alain, Laurent, Lionel, Thierry, Miguel, Dianailys, Rémi, Nosir, Claire, Angelos, Kasia, Manoj, César, Alberto, Laurie... Having a good atmosphere in the group was essential for me to feel so comfortable. I really enjoyed the scientific and the not-so-scientific debates throughout my thesis. Next, I want to thank the people from the CFM and DIPC in Donostia, starting with Carlos, for hosting me when I couldn't find a place to stay and for being a really good friend, gracias asere! Also thanks to Irene, Mario, Raúl, Oihana, Paula, Daniel, Carla, Jorge, Cristina, Thomas, Alejandro, and the rest (I tried). I had an amazing time with all of you, the football, the beers, the games, the nonsensical

chit-chat, I enjoyed it all.

I want to thank of course the University of Bordeaux for funding this project under the "Initiative d'excellence de l'Université de Bordeaux" (IdEX). Moreover, a great part of my work was possible thanks to the administrative and computer services from the UB and the CFM/DIPC. Also thanks to all the developers of open source and free software packages, I have used them quite a lot during this time.

Quiero agradecer enormemente a María, quien desde el momento en el que la conocí ha estado apoyándome a pesar de lo difícil que puedo llegar a ser. El proceso de escritura no habría sido el mismo sin ella y sin Tara.

Finalmente, quiero agradecer a toda mi familia. Todos y cada uno me han apoyado desde la distancia, sin saber ni siquiera qué es lo que estaba haciendo exactamente. Todo lo que soy como persona se debe a ellos, Diego, David, Pocho, Juan, Paula, Lore, Daniel, Julie, Pipe, Ángela, César, Glorita, Aura, Roci, Angie, Clau, Alberto, Edgar... No puedo nombrarlos a todos, pero siempre los tengo presente. Pero sobre todo, quiero agradecer a mis padres, sin ellos no habría podido llegar a donde estoy. Espero poder retribuirles algún día todos los sacrificios que han hecho por mi. Y esto va dedicado a ellos.

¡Gracias a todos!
Merci à tous!
Eskerrik asko denoi!
Thank you all!

Contents

List of Figures

To JL

Publications

Publications related to this thesis

1. **A. Peña-Torres**, H. F. Busnengo, J. I. Juaristi, P. Larregaray and C. Crespos, *Dynamics of N_2 sticking on W(100): The decisive role of van der Waals interactions*, Physical Chemistry Chemical Physics, 20, 19326 (2018), DOI: 10.1039/C8CP03515F

2. **A. Peña-Torres**, H. F. Busnengo, J. I. Juaristi, P. Larregaray and C. Crespos, *Energy Dissipation Effects on the Adsorption Dynamics of N_2 on W(100)*, Submitted

3. C. Ibargüen-Becerra, P. Larregaray, **A. Peña-Torres** and C. Crespos, *Inelastic Scattering of N_2 off W(001): Reconciling Experiment and Theory at Low Collision Energies*, Submitted.

4. **A. Peña-Torres**, J. I. Juaristi, P. Larregaray and C. Crespos, *Revisiting the dynamics of N_2 Eley-Rideal recombination on W(100) : effect of van der Waals interactions*, In preparation

Chapter 1

Introduction

The role of heterogeneous catalysis in our society is truly remarkable. Nowadays, a wide variety of technological developments relies on industrial processes based on reactions at surfaces. For example, catalytic reactions are crucial for the economy in developed countries [1]. This includes the reactions involved in petrol refinement into less polluting substances [2, 3], production of fibers and different types of materials or industrial production of ammonia, among many others. It is precisely because of the importance of this type of reactions, that the study of heterogeneous elementary processes has always been widely addressed. Usually, the prototype elementary gas-surface reactions involves a diatomic molecule interacting with a crystal surface. This represents the simplest example for a molecule reacting on a surface. Among these simple diatomic molecule-surface reactions, one that stands out is the dissociation of N_2 molecules on metallic surfaces. It constitutes the rate-limiting step in the ammonia synthesis process [4]. The elucidation of this mechanism granted Gerhard Ertl the Nobel Prize in chemistry in 2007. The N_2 molecule is also involved in many processes of interest in atmospheric research given its presence in the interstellar media [5, 6]. The reaction of diatomic molecules such as N_2 and O_2 can contribute up to a third of the heat flux in the outer walls of an spatial vehicle during atmospheric reentries [7]. Furthermore, these reactions play a key role in the description of plasma-wall interactions in the efforts to build a fusion reactor (ITER) [8]. All in all, an accurate theoretical description of heterogeneous reactive processes is essential, and it constitutes an active field of research.

The apparent simplicity of a diatomic molecule reacting on a surface can be deceiving. In reality, the presence of impurities, defects, temperature fluctuations and many other parameters can influence the possible outcomes of the reaction. All of these variables make the theoretical work to be more difficult since several

approximations need to be made to study these reactions while catching the essential physics of the problem. Another problematic item when it comes to the study of these reactions, is the superposition of processes that occur at the same time on the surface. Fortunately, experimentalists have developed tools to differentiate between some of these processes, making it easier to compare with theoretical simulations. Some of the possible processes that can occur in the interaction of a diatomic molecule and a surface are schematically shown in Fig. 1.1, and they correspond to:

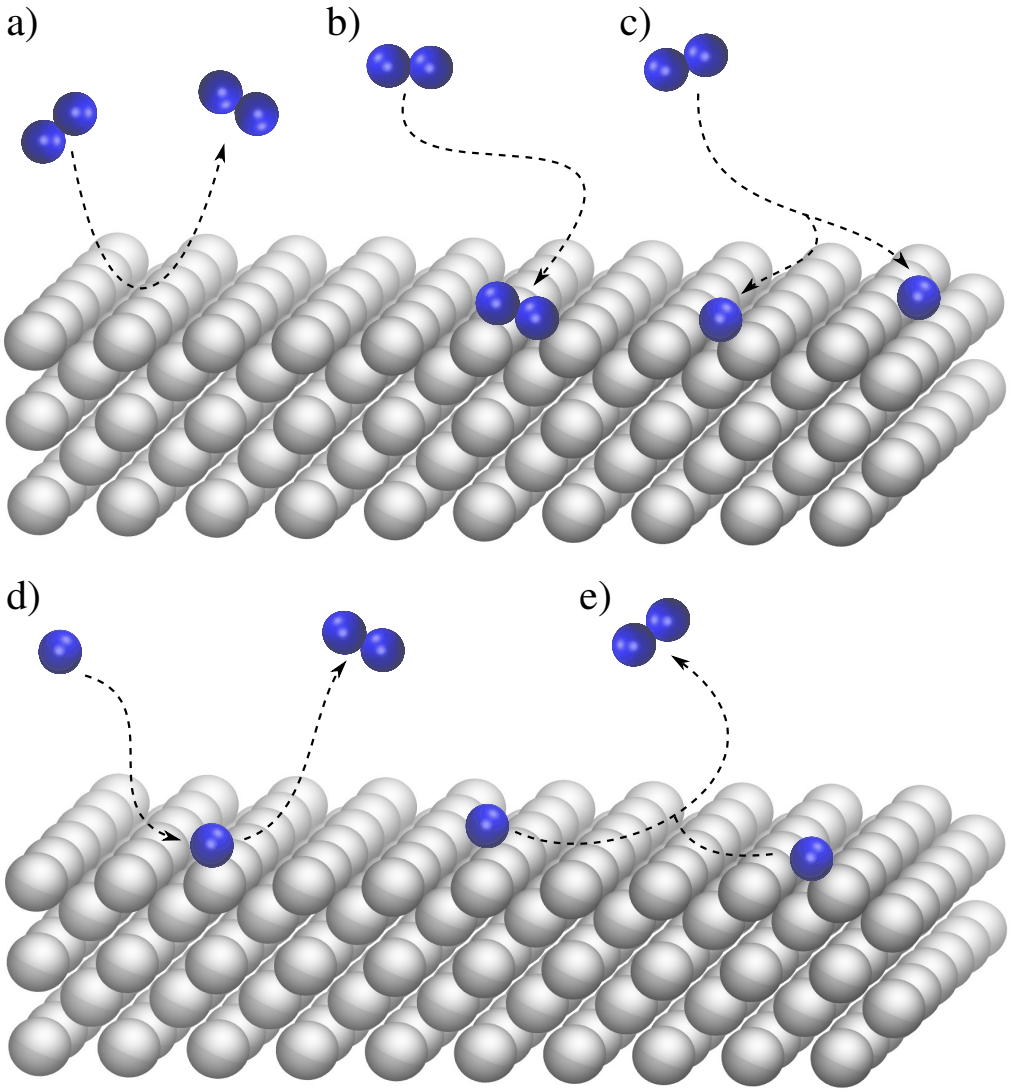

FIGURE 1.1: Some elementary molecule-surface processes. (a) Reflection; (b) Non-dissociative adsorption; (c) Dissociative adsorption; (d) Eley-Rideal recombination; (e) Langmuir-Hinshelwood recombination.

- Reflection: Takes place when the molecule impinging on the surface is reflected back to the gas phase. It is referred to as elastic reflection if the energy of the molecule is the conserved after being reflected. Otherwise, if there is an energy difference (positive or negative) it is said to be an inelastic process.
- Adsorption
  - Non-dissociative adsorption: Also known as molecular adsorption, it occurs when the projectile (impinging molecule) sticks to the surface upon collision. This is usually observed when the molecule reaches a molecular configuration which is favorable in energy without breaking the internuclear bond.
  - Dissociative adsorption: It happens when the internuclear bond breaks and the two atoms bond separately on the surface.
- Eley-Rideal (ER) recombination: When an atom is pre-adsorbed on the surface, one atom coming from the gas phase can hit the adsorbed one to form a molecule that subsequently goes back to the gas phase. If the impinging atom diffuses on the surface before colliding with the adsorbed one, the process is called *Hot atom* (HA) recombination.
- Langmuir-Hinshelwood (LH) recombination: Takes place when the two atoms that form the molecule going back to the gas phase were both previously adsorbed on the surface.
- Absorption: It takes place when the molecule (or an atom) collides the metal and penetrates into the subsurface finding a stable configuration inside the bulk. This is normally seen when the impinging atoms are small in size, like hydrogen.

As stated before, there has always been great experimental efforts to distinguish and characterize the different type of mechanisms in gas-surface reactions. One of the most fundamental experiments in this area is the molecular beams (MB) technique [9]. These beams are generated by a supersonic expansion of a gas flowing through a nozzle to a chamber at ultra high vacuum (UHV). The main advantages of MB experiments, is the great control of the user over the beams [10]. For instance, the translational energy of the molecules can be controlled by changing the temperature or by mixing different gases (seeding gases). In addition, laser irradiation can be used to obtain the desired initial vibrational and rotational states. Since the molecular degrees of freedom (DOF) are well defined, the dependency of a reaction on the internal DOF can also be studied [11]. Controlling all of these

parameters, MB techniques allow to measure sticking probabilities (combination of non-dissociative and dissociative probabilities) in very specific ways. Furthermore, these experiments are often coupled to other techniques that can measure properties of the scattered (reflected) or adsorbed molecules. To obtain information about the scattered molecules, resonance enhanced multiphoton ionization (REMPI) spectroscopy [12] is often used. Whereas for the adsorbed species, time-resolved surface spectroscopy techniques come in handy. Other techniques such as the femtosecond transition-state spectroscopy (FTS) [13] and laser induce fluorescence (LIF) [14] can be use to detect transition states during the reaction.

Working hand by hand with the experiments, theoretical advances on the description of the dynamics involved in the elementary processes have been extraordinary in the past two decades. Great developments in theoretical simulations from first principles (*ab initio*) along with the enormous improvement in computational capabilities have been crucial to this aim. A great amount of gas-surface problems have been tackled successfully using *ab initio* calculations [15, 16]. Nowadays, computational resources have developed in such a way that efficient algorithms have emerged to solve numerically the complex equations that govern the gas-surface interaction at quantum level. However, this does not imply that all of the simulations can reproduce the experimental data, there are several other cases in which there is still plenty refinement to be done. Theoretical studies are usually cheaper to carry out than experimental ones. For this reason, one of the goals in this area of research would be to be able to screen theoretically numerous possible catalysts to then work experimentally with the one that performs the best. However, given that the current theory is still unable to reproduce all experimental data, there is still the need to constantly test new experiments without having the theoretical backup. The aim of the present thesis is to contribute in the ongoing theoretical research in gas-surface dynamics.

Ideally, the theoretical study of a molecule-surface reaction would have to deal with the whole system in a quantum manner. This involves solving the time-dependent Schödinger equation (TDSE) for all the electrons and nuclei defining the system. This can be done for a very limited number of atoms. As the size of the system increases, the number of particles (and hence the DOF) increases as well, making the full quantum description computationally expensive for cases beyond the diatomic molecules interacting with a surface. In view of this, different approaches have been proposed to deal with the description of large molecule-surface problems. Within the so-called Born-Oppenheimer approximation, nuclei

and electronic problems are treated separately. The electronic part of the problem is usually tackled performing calculations based on density functional theory (DFT), which has proven to be an adequate tool to study large systems.

As mentioned above, a great and useful amount of informations can be extracted from MB experiments, particularly when they are performed in a very controlled way (i.e. for a given incidence angle, certain impact energy, clean surface). The results of these experiments can shed some light about the shape and features of the potential energy surface of the system. Any computational approach trying to reproduce experimental data involves the analytical or numerical representation of a continuous potential energy surface (PES) making use of several approximations to overcome the issue related to the large number of DOF. With a PES for a given system, molecular dynamics simulations allow to model molecular beam experiments by integrating the dynamics equations. If the full multidimensional PES is obtained, classical simulations of relatively long time scales (several ps) can be performed while keeping the full dimensionality of the system. However, the building of a continuous multidimensional PES is not a straightforward process. An accurate fitting or interpolating procedure of previously obtained potential energies becomes difficult to make as the DOF of the system increase. The way of overcoming these constraints will be discussed and developed in the following pages. Considering all of the above, this thesis is dedicated to the theoretical contribution and understanding of the N_2 dynamics over a W(100) surface.

It has been stated that the N_2 molecule reacting on different metallic surfaces constitutes one of the most representative examples in elementary reaction dynamics. In particular, the reactive scattering of N_2 on W surfaces has been an attractive subject to researchers due to large crystallographic anisotropies observed in early experimental measurements [17, 18]. Since then, reactivity on tungsten surfaces (i.e. W(100) and W(110)) have been widely addressed both experimentally by means of MB techniques [19–22] and theoretically using multidimensional potential energy surfaces based on DFT calculations [23–27]. Even though the theoretical methodologies used so far have been able to reach an agreement with MB experiments in, for example, scattering properties such as angular distributions, [28, 29] energy distributions [29, 30] and diffraction peak positions [31, 32] of scattered particles, a full understanding of other processes like dissociation probabilities is still lacking. One interesting result concerning the dissociation of N_2 on W surfaces is the large dependence on the surface geometry. [23] It has been observed that the dissociation for low-energy N_2 beams at high values of surface

temperature is around two orders of magnitude smaller on the W(110) face than in the W(100) face. In fact, the W(100) face exhibits a considerable probability of sticking under these conditions [22]. This has been associated with the fact that in the W(100) face, the N_2 molecules can find a path leading to dissociation without any energy barrier. [25] This is usually referred to as a non-activated system. On the other hand, the W(110) surface behaves as a so-called activated system given the low sticking probability ($\approx 10^{-3}$) displayed when low-energy N_2 beams are used. Although having such a low sticking probability makes the theoretical evaluation more challenging (in terms of the numbers of simulations needed to have statistical meaning), a relatively good agreement between theory and experiments for the dissociation probability on the W(110) has been achieved in the full range of energies. In contrast, the description of the N_2 reactivity on the W(100) surface, particularly for low-energy N_2 molecules has not been fully understood. This is a very undesirable situation since, as stated above, it is of great importance to have a full comprehension of the most basic heterogeneous processes.

To tackle this problem, the present work brings a significant contribution to the theoretical description of the N_2/W(100) dynamics by trying to solve some the long-standing problems concerning the disagreement between theory and experiments. For this, a new potential energy surface based on DFT calculations was built. One of the main points in this work, is the inclusion of van der Waals (vdW) interactions in the DFT calculations. Based on recent studies, we have seen that the use of non-local functionals that account for long range vdW interactions can have a strong effect in the dynamics of several molecule-surface systems [33, 34]. Afterwards, several approximations are made in order to deal with the large number of DOF. On one hand, the mathematical treatment is done under the Born-Oppenheimer (BO) approximation. In addition, the so-called frozen surface approximation is used to keep the surface atoms fixed at their equilibrium positions, reducing the dimensionality and hence computational cost. The energies obtained from DFT calculations are interpolated using the corrugation reducing procedure method (CRP) [35] to get a multidimensional PES (See Chapter 2). Then, quasi-classical trajectories (QCT) are performed on the obtained PES to model reactive dynamics processes such as adsorption, scattering and ER recombination. In this work, we also study the inclusion of energy dissipation effects in the dynamics studies. We will allow for surface motion during the interaction of the molecule with the surface, also accounting for the surface temperature, to incorporate the energy exchange between the molecule and the lattice in the dynamics (phonon excitations). Additionally, nonadiabaticity will be introduced via a friction model

to account for electron-hole pair excitations. In addition, a brief part of the thesis is devoted to the *ab initio* molecular dynamics (aiMD) performed for the studied system. It is known that aiMD is a very expensive computational method, given that the forces acting on the nuclei must be calculated at each step of the numerical integration (*on the fly*), making possible the calculation of a reduced amount of trajectories. However, it can provide useful information about the system that can complement the results obtained using a precalculated PES.

This thesis is structured as follows:

- In Chapter 2 a detailed overview of the theoretical methods used throughout this work is presented. It starts with the basics of the molecule-surface interactions, deals with the electronic structure problem introducing and briefly reviewing the density functional theory (DFT), paying special attention to the van der Waals functionals. Next, the potential energy surfaces, its practical issues and main features are addressed, as well as the corrugation reducing procedure, which is the interpolation method used in this work. Finally, molecular dynamics are discussed. A transition between quantum and classical dynamics is presented, together with the approximations to include energy dissipation effects in the classical dynamics calculations. Finally, *ab initio* molecular dynamics are briefly reported.

- Chapter 3 deals with the description of the procedure to build the potential energy surface for the N_2/W(100) system based on DFT calculations and the corresponding test to check the quality of the PES. Furthermore, a characterization of the static features of the PES (e.g. adsorption sites, energy barriers) is addressed. In addition, a topological comparison with previous PESs obtained using a different functional is discussed, emphasizing the role of the van der Waals forces in the long range interactions between N_2 and the W surface.

- In chapter 4 we present an overview of the historic experiments and theoretical contributions to the sticking dynamics of N_2 on W(100). The details of the quasi-classical dynamics calculations for the dissociative adsorption of N_2 on the W(100) surface within the adiabatic frozen surface approximation are presented. The simulations are performed on the precalculated frozen potential energy surface. A complete analysis of the non-activated character of the PES for low-energy N_2 molecules is carried out.

- In chapter 5 we introduce the energy dissipation effects included in this work. On one hand, electron-hole pair excitations are included in the dynamics calculations through the use of the local density friction approximation. On the other hand, surface motion and surface temperature effects are taken into account by means of the generalized langevin oscillator model. Results for the sticking probability are discussed in relation to those obtained within the adiabatic frozen surface approximation and to the measured values in molecular beam experiments. In addition, we present results from *ab initio* molecular dynamics where we let the surface W atoms move. First, the surface thermalization procedure is explained, followed by the description of the method to choose the initial conditions of the simulation for the positions and velocities of the N_2 molecule and the W surface atoms. The results are compared to those obtained with the precalculated PES in terms of the characterization of the adsorption wells and energy barriers.

- Chapter 6 deals with two different processes. On the one hand, we present results for the non-reactive scattering of N_2, including both energy dissipation channels and comparing the results to the available experimental data. On the other hand, the Eley-Rideal recombination, in which an atomic N projectile recombines with another N atom already preadsorbed on the surface is studied. A comparison is made between the present results for different observables with those obtained in previous theoretical works. The role played by van der Waals interactions and the energy dissipation effects due to phonons excitations are addressed as well.

- Finally, chapter 7 summarizes the most relevant results of the work presented here and the outlook for future research based on our findings is discussed.

Chapter 2

Theoretical Background

The aim of this chapter is to provide an introduction to the theoretical framework used throughout the manuscript. In Sec. 2.1 a description of the treatment of the molecule-surface interaction is given. Next, in Sec. 2.2 a brief description of the density functional theory (DFT) including a discussion on the van der Waals (vdW) functionals is presented. Sec 2.3 reviews the general methods for modelling the system and the construction of a potential energy surface. Finally, Sec. 2.4 deals with the different approaches used to perform molecular dynamics.

2.1 Molecule-surface interactions

The determination of the molecule-surface interactions is based on first principle calculations. Let us start considering a system formed by n electrons and N nuclei. Spin will not be taken into account for simplification. We can define the set of electronic and nuclear coordinates as $\mathbf{r} \equiv \mathbf{r}_i$ $(i = 1, \ldots, n)$ and $\mathbf{R} \equiv \mathbf{R}_I$ $(I = 1, \ldots, N)$, respectively. The time-independent Schrödinger equation to be solved for this many-body problem is:

$$H\Psi(\mathbf{r}_i, \mathbf{R}_I) = E\Psi(\mathbf{r}_i, \mathbf{R}_I), \tag{2.1}$$

where H is the many-body Hamiltonian acting on the wave-function Ψ and E is the total energy of the system. The non-relativistic Hamiltonian can be written as a sum of of five terms

$$H = T_e + T_N + V_{ee} + V_{NN} + V_{eN}, \tag{2.2}$$

where T_e and T_N correspond to the kinetic energy of the electrons and nuclei respectively, V_{ee} represents the Coulomb interaction between electrons, V_{NN} is the interaction between nuclei and V_{eN} is the attractive electrostatic interaction of the

electrons and the nuclei. In atomic units ($m_e = \hbar = e = 1$) each of these terms can be written as

$$T_e = -\frac{1}{2}\sum_{i=1}^{n}\nabla_i^2, \tag{2.3}$$

$$T_N = -\frac{1}{2}\sum_{I=1}^{N}\frac{1}{m_I}\nabla_I^2, \tag{2.4}$$

$$V_{ee} = \sum_{i=1}^{n}\sum_{j>i}^{n}\frac{1}{|\mathbf{r}_i - \mathbf{r}_j|}, \tag{2.5}$$

$$V_{NN} = \sum_{I=1}^{N}\sum_{J>i}^{N}\frac{Z_I Z_J}{|\mathbf{R}_I - \mathbf{R}_J|}, \tag{2.6}$$

$$V_{eN} = -\sum_{i=1}^{n}\sum_{I=i}^{N}\frac{Z_I}{|\mathbf{r}_i - \mathbf{R}_I|}, \tag{2.7}$$

where m_I and $Z_{I,J}$ represent the mass and charge of the nuclei, respectively. Up to this point, we have a many-body problem that includes both electronic and nuclear degrees of freedom. However, as it is known, this can only be solved for systems of very few atoms. For this reason, the computational simulations of molecule-surface systems are based on several approximations.

Generally, the Born-Oppenheimer (BO) approximation [36] is one of the first approximations to be considered. The main idea consists in the separation of the electronic and nuclear degrees of freedom. The BO approximation has been widely accepted given that an electron is ≈ 2000 times lighter than the hydrogen atom. This means that from the electronic frame of reference the nuclei appear to be static as the electrons move. From this, we can write the time-independent Schrödinger equation for the moving electrons around the fixed nuclei at the position $\mathbf{R}_I$ as:

$$H_{el}\Psi_{el}(\mathbf{r}_i, \mathbf{R}_I) = E_{el}(\mathbf{R}_I)\Psi_{el}(\mathbf{r}_i, \mathbf{R}_I), \tag{2.8}$$

where the so-called electronic Hamiltonian H_{el} has the form

$$H_{el} = T_e + V_{ee} + V_{NN} + V_{eN}. \tag{2.9}$$

In Eq. 2.8, E_{el} represents the electronic energy levels of the system. Note that

the internuclear term V_{NN} inside H_{el} does not depend on $\mathbf{r}_i$ but only parametrically on the nuclei coordinates, so it is treated as a constant. Moreover, the nuclear kinetic energy term T_N is not involved in Eq. 2.8 given that it does not act on the variables of the electronic wavefunction Ψ_{el}. Within the BO approximation, and after solving H_{el}, the next step is to re-inject the solution of the electronic equation in the total Schrödinger equation 2.1 defining what is called the nuclear Schrödinger equation. We can write the time-independent Schrödinger equation for the nuclei as

$$H_N \Psi_N(\mathbf{R}_I) = (T_N + E_{el}(\mathbf{R}_I))\Psi_N(\mathbf{R}_I). \tag{2.10}$$

Thus, the $E_{el}(\mathbf{R}_I)$ term is acting as a potential term for the nuclei problem. $E_{el}(\mathbf{R}_I)$ is defined as the ground state PES on which the dynamics of the nuclei can be studied. The BO approximation can be well justified for several cases. For example, the electronic states for a molecule in gas phase are usually well separated. For low kinetic energies, electronic transitions are not expected and the BO approximation can successfully describe the ground state properties. However, if the molecule is no longer in vacuum but interacting with a metallic surface, a quasi-continuous spectra of excited electronic states is observed. In this case, the BO approximation is said to break down and its validity can no longer be proven. Nonetheless, it can be used as a starting point to introduce later non-adiabatic corrections. In practice, the use of the BO approximation in molecule-surface problems consists in obtaining the electronic ground state PES by using Eq. 2.8 and performing nuclear dynamics on that PES (the latter will be addressed in Section 2.4). However, even after reducing the degrees of freedom of the system, more approximations are to be made due to the computational cost associated. We will start by describing the methodology used to obtain the PES E_{el}.

A wide variety of first principle methods have been developed to solve the electronic Schrödinger equation. Many of them, such as Møller-Plesset perturbation theory (MP), coupled cluster (CC) or configuration interactions (CI) are referred as post Hartree-Fock (post-HF) methods since they try to recover the electronic correlation energy that the HF theory is unable to achieve. These methods can be used and refined to compute highly accurate energies. However, the computational cost of these methods scales exponentially with the number of particles treated. Post-HF methods require at least a N^5 scaling, where N is the number of basis functions. This has been the bottleneck of the so-called wavefunction based methods given that even for small systems (<20 atoms) the computational cost

can be elevated. In view of this, HF based methods are not the first choice when it comes to studying molecule-surface reactions where the surface of the solid is formally described by an infinite number of atoms (periodic system). To study larger systems or periodic systems as it is the case for gas-surface problems, a compromise between chemical accuracy and computational efficiency has to be made, and in this case, DFT is the go-to theory.

2.2 Density Functional Theory

The density functional theory can help to overcome the most complicated part of an electronic structure calculation: the electron-electron interaction. Normally, an N-electron system is described by a wavefunction that depends on $3N$ spatial coordinates. As the size of the system increases, the number of electronic degrees of freedom increases and the solution becomes unfeasible using wavefunction based methods. In view of this, and based on a unique property that characterizes a quantum system, such as the electronic density ρ, Hohenberg and Kohn (HK) established the fundations of the density functional theory [37].

The first HK theorem states that the potential that determines the electronic Hamiltonian H_{el} is a unique functional of the electronic density ρ. This simplifies the high dimensional issue, given that the density, and as a consequence the functional, depends solely on 3 spatial coordinates regardless the size of the system. The theorem also states that there is a one-to-one correspondence between the external potential and ρ. Since all physical information is given by H_{el}, all the information is embedded in the ground state density. So, the electronic energy can be written as a functional of the electron density $\rho(\mathbf{r})$

$$E[\rho(\mathbf{r})] = T_e[\rho(\mathbf{r})] + V_{ee}[\rho(\mathbf{r})] + V_{eN}[\rho(\mathbf{r})] = V_{eN}[\rho(\mathbf{r})] + F_{HK}[\rho(\mathbf{r})], \tag{2.11}$$

where $F_{HK}[\rho(\mathbf{r})]$ is the HK functional that contais T_e and V_{ee}, these last two terms are universal and do not depend on the external potential and are generic for a given Coulomb interaction.

In the second HK theorem, the authors state that the total energy of the system is minimal for the ground state electronic density. Any other density will yield a higher energy than the one obtained with the ground state density. Thus, the variational principle can be used to determine the exact ground state density and

energy. At this point, an expression for F_{HK} would suffice to obtain the exact energy of a given system, unfortunately, this functional remains unknown and approximations are needed. First, the electron-electron interaction term can be expanded as

$$F_{HK}[\rho(\mathbf{r})] = T_e[\rho(\mathbf{r})] + V_{ee}[\rho(\mathbf{r})] = T_e[\rho(\mathbf{r})] + E_H[\rho(\mathbf{r})] + G_{XC}[\rho(\mathbf{r})], \tag{2.12}$$

where E_H is the classical electrostatic repulsion energy of the electron density as calculated at the HF level given by

$$E_H[\rho(\mathbf{r})] = \frac{1}{2}\int \frac{\rho(\mathbf{r})\rho(\mathbf{r'})}{|\mathbf{r}-\mathbf{r'}|} d\mathbf{r}d\mathbf{r'}, \tag{2.13}$$

and G_{XC} is a term that contains the quantum mechanical many-body effects, commonly referred to as exchange-correlation functional. To tackle the problem of not having an exact analytical form of the functional, Kohn and Sham [38] developed an efficient scheme to obtain the ground state density based on the HK theorems.

The main idea was to introduce a non-interacting reference system that has an associated wave function constructed with single particle orbitals ϕ_i (named Kohn-Sham (KS) orbitals) that yield the electron density of the original system,

$$\rho(\mathbf{r}) = \sum_{i=1}^{n} \phi_i^*(\mathbf{r})\phi_i(\mathbf{r}). \tag{2.14}$$

With the introduction of this reference system, the total kinetic energy can be separated in a non-interacting contribution T_s and an unknown component T_c that deals with many-body effects corrections. The former can be evaluated as

$$T_s = -\frac{1}{2}\sum_{i=1}^{N} \int \phi_i^*(\mathbf{r})\nabla^2\phi_i(\mathbf{r})d\mathbf{r}, \tag{2.15}$$

while T_c is a functional of the density that coupled to G_{xc} forms what is known as the exchange-correlation (XC) functional:

$$E_{xc}[\rho] = G_{xc}[\rho] + T_x[\rho]. \tag{2.16}$$

This means that everything that is not known is embedded in E_{xc}, which makes it the key term in the whole theory. All in all, we can rewrite Eq. 2.11 as

$$E[\rho] = T_s[\rho] + V_{Ne}[\rho] + E_H[\rho] + E_{xc}[\rho]. \tag{2.17}$$

From all of the above, now we can write the Schrödinger equation separated into individual ones (so-called KS equations) [38]

$$\left(-\frac{1}{2}\nabla^2 + v_{eff}\right)\phi_i(\mathbf{r}) = \epsilon_i\phi_i(\mathbf{r}), \tag{2.18}$$

where v_{eff} is an effective potential that can be expanded as $v_{eff} = v_{eN} + v_H + v_{xc}$. The three terms on the right side are functional derivatives with respect to the density of the corresponding energy functionals:

$$v_{eN} = -\sum_{I=1}^{N}\frac{Z_I}{|\mathbf{r} - \mathbf{R}_I|}, \tag{2.19}$$

$$v_H = \int \frac{\rho(\mathbf{r}')}{|\mathbf{r} - \mathbf{r}'|}d\mathbf{r}', \tag{2.20}$$

$$v_{xc} = \frac{\delta E_{xc}[\rho(\mathbf{r})]}{\delta\rho(\mathbf{r})}. \tag{2.21}$$

Given that these derivatives that enter the KS equations (2.18) depend on the density, and consequently, on ϕ_i, the KS equations have to be solved in a self-consistent way. Normally, an initial guess for the density is needed to obtain the derivatives, and from there, the KS equations are solved until convergence is achieved.

2.2.1 Exchange-Correlation functionals

The first and simplest approximations for the XC functional is called the *local dentisty approximation* (LDA) and it was proposed again by Kohn and Sham [38]. The approximation makes the assumption that the contribution of each point in the space to the XC energy corresponds to that of an homogeneous electron gas of the same density, and is written as

$$E_{xc}^{LDA}[\rho(\mathbf{r})] = \int \rho(\mathbf{r})\varepsilon_{xc}[\rho(\mathbf{r})]d\mathbf{r}, \tag{2.22}$$

where ε_{xc} is usually expressed as the sum of two contributions, $\varepsilon_{xc} = \varepsilon_x + \varepsilon_c$, and it refers to the XC energy per electron in the homogeneous electron gas. The exchange part is exact and has the form

$$\varepsilon_x(\rho) = -\frac{3}{4}\left(\frac{3\rho}{\pi}\right)^{\frac{1}{3}}, \tag{2.23}$$

on the other hand, the correlation has no analytical form and therefore it has to be calculated. This is usually done using quantum Monte-Carlo methods [39] and the results are used subsequently to form a functional of ρ. This process is not straightforward and requires parametrization methods [40, 41].

Although the LDA stood for a long time as the most widely used approximation for the XC functional, it comes with disadvantages, such as the underestimation of bond lengths and overestimation of binding energies [42]. Because of this, more advanced XC functionals that include the gradient of the electronic density have been developed. These are referred to as the *generalized gradient approximation* (GGA) XC functionals, and can be expressed as:

$$E_{xc}^{GGA}[\rho(\mathbf{r})] = \int \rho(\mathbf{r})\varepsilon_{xc}[\rho(\mathbf{r}), \nabla\rho(\mathbf{r})]d\mathbf{r}. \tag{2.24}$$

In GGA-XC functionals, the exchange-correlation energy for a given electron density and its gradient can be chosen rather freely, giving more flexibility at the time of constructing GGAs. There are several ways to obtain new GGAs, for example, one can use exact quantum mechanical constraints to derive the parameters in approximate functionals. This is the case of the PBE functional [43], widely used in the solid state physics research due to its accuracy for many systems. Another way to develop a GGA, is to simply fit the parameters to particular systems. A representative example of this is perhaps the BLYP functional [44, 45], most commonly used in computational chemistry. In general, for gas-surface reactions, among the most used functionals are the PBE [43], the RPBE [46] (which is a revised version of the PBE), the PW91 [47] and recently, the so-called van der Waals (vdW) functionals. One of these vdW functionals (namely vdW-DF2) is the one used in this work to perform the DFT calculations.

On the van der Waals functionals

In spite of the success in numerous applications of GGA and other types of functionals (e.g. Meta-GGA, Hybrid functionals), the inclusion of non-local effects such as vdW forces are necessary to properly describe the interaction at sparse electron densities. The exact XC functional contains all of these non-local effects, however, as it is unknown, several approximations have been and are currently

being made to include them in the DFT.

Although vdW interactions have been known for more than a century, the work and development within the DFT started to grow exponentially in the past two decades. At first, the inclusion of vdW forces was included as asymptotic interactions between fragments [48]. Afterwards, the vdW-DF functional was published and tested for layered structures and particular geometries [49, 50], yielding good results for the description of the dispersion in several systems. Nevertheless, it underestimates the H-bond strength [51, 52] and the equilibrium separations are overestimated [53–57].

The basic idea behind these vdW functionals, comes from dividing the correlation energy functional in two terms,

$$E_c[n] = E_c^0[n] + E_c^{nl}[n], \tag{2.25}$$

where $E_c^{nl}[n]$ incorporates the vdW interaction by including some long range non-local terms, which are expressed in terms of an interaction formula that contains a parametrized kernel. This kernel works with parameters that are obtained in terms of the local density an its gradient. Although the $E_c^0[n]$ term is also non-local, it approaches the LDA in the limit of a slowly varying density, whereas $E_c^{nl}[n]$ approaches zero. For the case of the vdW-DF correlation functional, the numerical development uses Eq 2.25 coupled with the RPBE exchange functional. However, RPBE tends to overestimate the equilibrium separations, and it showed spurious binding due to the exchange alone. Because of this, different exchange functionals were tested, and as a result, the vdW-DF2 functional emerged from coupling it to the PW86 exchange functional [58]. This appeared to be more chemically accurate, agreeing with wavefunction based methods, in addition to the vanishing of the spurious binding present in other functionals.

In view of this, several studies have made use of functionals that account for vdW corrections in the past few years [33, 34], improving in some cases the dynamical observables in gas-surface systems. For this reason we have decided to use it for the work presented in this thesis. For a more detailed read of the vdW functionals, we recommend the reviews of Ref. [59, 60] and the references therein. All in all, the development of new functionals is an active research field, and the fact that a functional works well for a given system does not guarantee that it will

work for a different one. However, regarding the gas-surface systems, the vdW-type functionals appear quite promising, as we will discuss in the next chapters.

2.3 Modelling the system

In the previous section, we have briefly provided the theoretical tools to solve the Schrödinger equation, here we will address the practical issues. We have seen that the approach to perform a DFT calculation reduces to solve the KS equations (2.18). Hence, the first step is to choose the basis set to represent the KS orbitals ϕ_i. Among the different types of basis functions that we can use (e.g. Slater-type orbitals, Gaussian-type orbitals, Numerical Atomic orbitals), plane waves are notably well suited for solid state systems due to their intrinsic periodicity [61]. For this reason, the DFT calculations in this work were carried out with this type of basis functions.

Given that the potential in a solid is periodic and has the same periodicity as the lattice, we can make use of the Bloch theorem [62] to write the eigenstates (i.e. the KS orbitals) as

$$\phi_{i,\mathbf{k}}(\mathbf{r}) = u_{i,\mathbf{k}}(\mathbf{r})e^{i\mathbf{k}\cdot\mathbf{r}}, \tag{2.26}$$

where $\mathbf{k}$ is a wavevector within the first Brillouin zone and $u_{i,\mathbf{k}}$ is a function with the periodicity of the lattice. We can then expand $u_{i,\mathbf{k}}$ in the plane wave basis set and rewrite the KS orbitals as

$$\phi_{i,\mathbf{k}}(\mathbf{r}) = \frac{1}{\sqrt{\Omega}}\sum_{\mathbf{G}} C_{i,\mathbf{k}}(\mathbf{G})e^{i(\mathbf{k}+\mathbf{G})\cdot\mathbf{r}}, \tag{2.27}$$

with $\frac{1}{\sqrt{\Omega}}$ being a normalization factor and $\mathbf{G}$ corresponding to the reciprocal lattice vectors. If we introduce Eq. 2.27 into the KS equations (2.18), we obtain the matrix eigenvalue equation:

$$\sum_{\mathbf{G}'}\left(\frac{1}{2}(\mathbf{k}+\mathbf{G})^2 + v_{eff}(\mathbf{G}-\mathbf{G}')\right)c_{i,\mathbf{k}+\mathbf{G}'} = \epsilon_i(\mathbf{k})c_{i,\mathbf{k}+\mathbf{G}}, \tag{2.28}$$

where v_{eff} is the Fourier transform of the effective potential. Given a plane waves basis set, Eq 2.28 can be solved using Fast Fourier Transformations (FFT). However, in practice, the number of plane waves representing the wave function has to be finite. Usually, only the plane waves with an associated kinetic energy below the so-called cut-off energy are considered,

$$\frac{1}{2}(\mathbf{k}+\mathbf{G}^2) \leq E_{cutoff}. \tag{2.29}$$

In practice, to obtain a reasonable value for the cut-off energy, several calculations should be performed increasing the value for E_{cutoff} and stop when the property of interest converges.

One of the main drawbacks of plane waves basis sets arises close to the nuclei, where the single-particle states shows significant oscillations due to the strong attractive potential. This means that a too large number of plane waves would be necessary to properly describe this region. An effective approach to deal with this issue, is to neglect the explicit consideration of the core electrons, given that they do not play a key role in the interaction with other atoms. This is commonly known as the *pseudopotential* approximation. In this approach, only the valence electrons remain explicitly considered, and a pseudopotential replaces the strong Coulomb potential of a nucleus with a softer potential of a pseudo-atom, which contains the nucleus, the core electrons, and the interaction between them. Furthermore, the associated pseudo-wavefunction is built in a way that is as smooth inside a cut-off radius r_c and reproduces the true wavefunction outside r_c. At first, pseudopotentials were called *norm-conserving* since the norm of each pseudo-wavefunction outside r_c had to be exactly the same that the corresponding electron wavefunction [63]. This was a simple approach that it is still used, however the E_{cutoff} needed was still too large. Trying to minimize the value for E_{cutoff} required, *ultrasoft* (US) pseudopotentials [64, 65] and *projector-augmented waves* [66, 67] (PAW) were later introduced. PAW pseudopotentials are known to be more accurate than US pseudopotentials due to the fact that they keep the full wavefunction (with all electrons) in the core region. Throughout this work, PAW pseudopotentials were used to perform the DFT calculations.

Another computational bottleneck of these calculations is the continuous sampling of the Brillouin zone since now we have to compute a finite number of eigenstates at an infinite number of **k**–points in a single unit cell. Nonetheless, at a large volume the **k**-points become a dense continuum and here we can consider electronic wavefunctions to be the same at **k**-points that are close together. Hence, the wavefunctions in single **k**-point can represent can represent the wavefunction in a region of the **k**-space,

$$\frac{1}{V_{BZ}}\int_{BZ} d\mathbf{k} \approx \frac{1}{(2\pi)^3}\sum_{\mathbf{k}} w_{\mathbf{k}}. \tag{2.30}$$

Here, only **k**-points from the irreducible Brillouin zone weighted by a symmetry factor w need to be computed. In this thesis, a useful scheme developed by Monkhorst and Pack [68] to generate the **k**-point grid was used.

When it comes to modelling a gas-surface system using periodic boundary conditions, one must take into account that the initial three-dimensional periodicity is not real. The surface is not periodic in the axis normal to the surface (z), where it goes from the metallic bulk structure to the vacuum. To tackle this, the *supercell* approach is often used. A simple scheme of this approach is shown in Fig. 2.1. In the model, the surface is represented as a set of finite atomic planes (slab) alternated with a layer of vacuum in the z direction. To properly describe a system of this kind, one must ensure that the cell is large enough so that spurious interaction with the periodic image molecules are avoided. Likewise, the vacuum region between slabs must be large enough so there is no interaction at all between the slabs. Finally, the thickness of the slab should be such that the atoms in the middle have the properties of bulk atoms. All in all, one must find the compromise between the system size and the computational cost that guarantees a good representation of the system.

2.3.1 Construction of an adiabatic potential energy surface

The total energy of a given nuclear configuration is determined by using the methodology detailed in the previous section. Then, in order to simulate dynamics of nuclei, energy has to be known for any configuration of the system. It is necessary to determine a continuous representation of the multi-dimensional PES. For this, several high symmetry sites of the surface are selected to calculate the electronic energies (DFT data). This set of DFT data is consequently interpolated with respect to all the degrees of freedom to obtain the full PES. In this case, one must ensure that the intermediate values obtained are accurate for the description of the PES.

Nowadays there are several schemes that allow an interpolation of the DFT data. Among these one can find models that include physically justified parameters, such as the embedded atom method [69] and the LEPS potential [70–72]. Although these models work with some physical insight of the system, the desired accuracy is not always trivial to obtain. On the other hand, there are models that are purely mathematical and require only the DFT energies to interpolate. These schemes, such as the neural network approximation [73], the modified Shepard interpolation [74], and the corrugation reducing procedure [35] have provided good

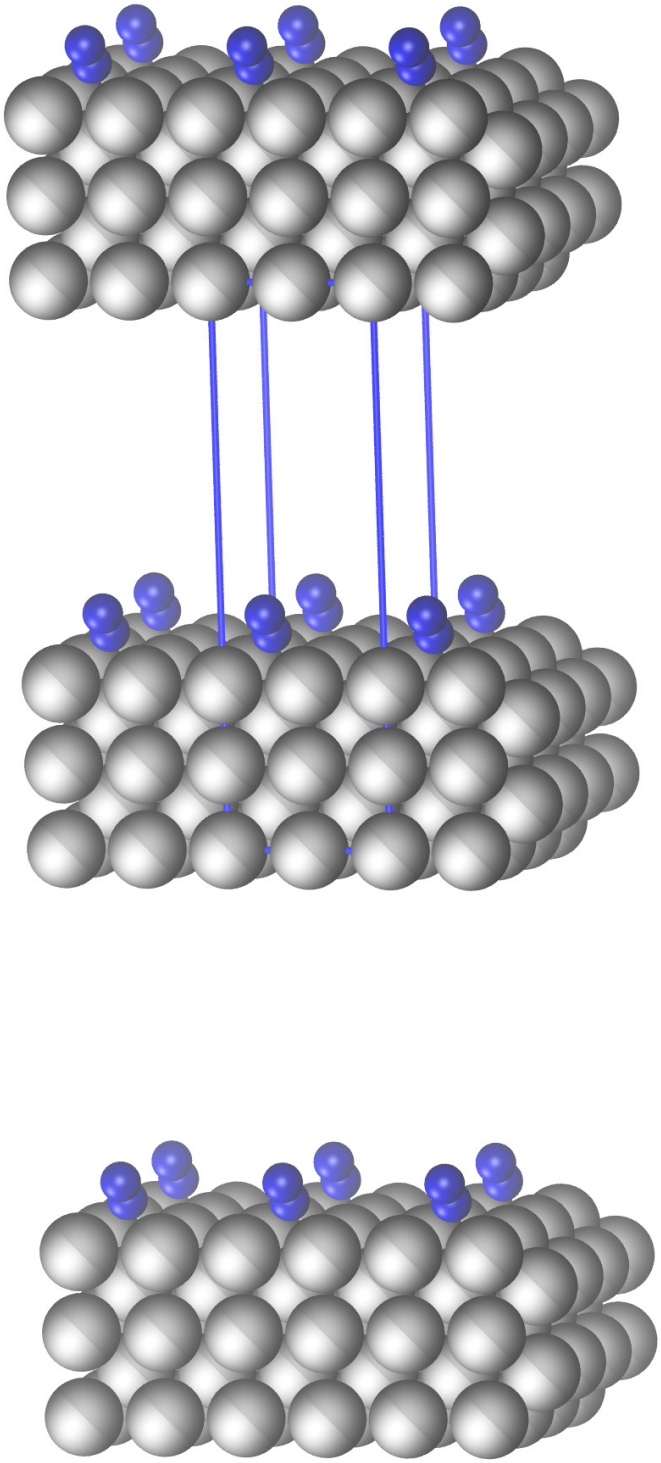

FIGURE 2.1: Representation of a typical 2×2 supercell (blue box) of a primitive surface unit cell and a diatomic molecule. The surface is modelled by a five-layer slab separated from its periodic image by a vacuum along the z axis.

accuracy given their flexibility. However, the number of DFT data points needed to accurately describe the PES increases with the number of degrees of freedom considered. Hence, it is commonly accepted to freeze the surface degrees of freedom and only consider the molecular ones, relying on the fact that these are the most relevant in the interaction. This approach, called the *frozen surface approximation* is used in this thesis. Varying only the diatomic molecular degrees of freedom and keeping the surface atoms fixed we end up with a six-dimensional (6D) PES.

The coordinate system used to perform all DFT calculations is illustrated in Fig. 2.2. The six molecular degrees of freedom correspond to the position in X, Y and Z of the center of mass, the internuclear distance r and to the molecular orientation relative to the surface determined by the polar (θ) and azimuthal (ϕ) angles. As mentioned above, the first step in the construction of a multi-dimensional PES is to compute a dense grid of DFT data points and then use of one the interpolation schemes to obtain the a continuous surface. In this thesis, the *corrugation reducing procedure* was used for this end.

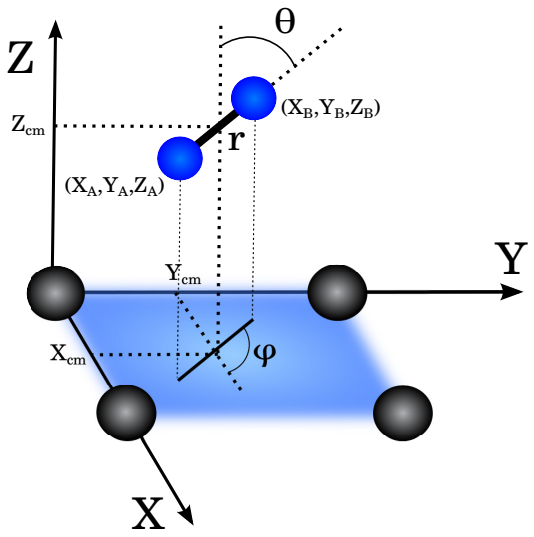

FIGURE 2.2: Schematic representation of the coordinate system used in the calculations. Surface atoms are shown in grey and molecular atoms in blue. The origin of the coordinate system is place on top of a surface atom.

Corrugation Reducing Procedure

The corrugation reducing procedure (CRP) method was developed by Busnengo *et.al.* in 2000 to build specifically potential energy surfaces of diatomic molecules

reacting with a surface [35]. Since then, it has been widely used leading to accurate results for different gas-surface systems [23, 24, 75–80]. The major problem when dealing with the parametrization of a molecular potential near the surface is its large variation when looking at different configurations of the molecule. This is usually referred to as corrugation. The main idea behind the CRP is that this corrugation can be reduced. The key of the method relies on the fact that most of the corrugation in a molecule-surface PES comes from the individual atomic interactions with the surface. Hence, if we subtract the atom-surface potentials V_A^{3D} and V_B^{3D} from the 6D molecule-surface potential V_{6D}, we obtain a smoother function I^{6D}. Then, it is possible to interpolate separately the highly corrugated terms V^{3D} and the so called "interpolation function" that presents smoother variations.

$$\begin{aligned} I^{6D}(X,Y,Z,r,\theta,\phi) =& V^{6D}(X,Y,Z,r,\theta,\phi) - \\ & V^{3D}(X_A,Y_A,Z_A) - V^{3D}(X_B,Y_B,Z_B). \end{aligned} \tag{2.31}$$

Usually, standard numerical interpolation methods are used to interpolate I_{6D}. The following steps are commonly followed:

- 2D cubic splines are used to interpolate the (r,Z) dependence of the I^{6D} function.
- Interpolation over the polar and azimuthal angles (θ,ϕ) is carried out making use of basis functions (trigonometric functions) that fulfill the symmetry requirements of the system.
- Finally, interpolation over (X,Y) is performed using 2D periodic cubic splines.

Once I^{6D} has been interpolated, the atomic-surface potential values V_A^{3D} and V_B^{3D} are added again to obtain the desired 6D-potential V^{6D}.

From this, it becomes clear that in addition to the initial set of molecular energies over the surface, a grid of atom-surface DFT energies is needed to obtain the corresponding V^{3D}. For the cases of homonuclear diatomic molecules, a single grid of atomic-surface potential is enough. In addition, the number of points in the atomic grid is smaller than in the molecular case since only three degrees of freedom are considered. The strong variation in the atomic potential makes V^{3D} also highly corrugated. To deal with this corrugation, we can make an additional decomposition as in Eq. 2.31

$$I^{3D}(\mathbf{R}) = V^{3D}(\mathbf{R}) - \sum_{i=1}^{n} V^{1D}(|\mathbf{R} - \mathbf{R_i}|), \tag{2.32}$$

where one-dimensional pair potentials V^{1D} describe the interaction between one atom of the molecule and one surface atom located at positions $\mathbf{R}$ $\equiv$(X,Y,Z) and $\mathbf{R_i}$ $\equiv$(X_i,Y_i,Z_i) respectively. Usually, the V^{1D} potential is chosen as the one obtained over a surface atom (top configuration). In order to interpolate I^{3D}, 3D splines over X,Y and Z can be easily computed. When the construction of the PES is finished, it is important to test its accuracy. This is usually done by comparing some interpolated values with DFT energies that were not included in the initial set of data points. If it were necessary, more DFT points can be added to the grid to improve the accuracy of the PES, hence the flexibility of the procedure.

Summing up, the CRP for a 6D-PES involves the following steps:

1. Obtain V^{1D}, V^{3D} and V^{6D} from DFT calculations
2. Construct I^{3D} = V^{3D} - $\sum V^{1D}$ and interpolate it
3. Recover V^{3D} = I^{3D} + $\sum V^{1D}$
4. Construct I^{6D} = V^{6D} - V_A^{3D} - V_B^{3D} and interpolate it
5. Recover the final V^{6D} = I^{6D} + V_A^{3D} - V_B^{3D}
6. Test the accuracy of the PES

The reader can find detailed information about the interpolation procedure in Appendix B.

Exploration of the PES

Once the interpolation procedure is done and the accuracy of the obtained PES has been tested, several characteristics of the static PES can provide useful information about the reaction dynamics (e.g. Minimum energy reaction paths, energy barriers, depth of potential wells). Usually the most important of the static PES features is the adsorption well of the molecule, which has an associated binding energy. For many systems, this quantity is experimentally reported, giving DFT-based PES the chance to compare directly with experiments before performing dynamics on the PES.

However, exploring a PES is not always a straightforward task, particularly if there are several local minima apart from the global one. If this is the case, one has to choose starting configurations that could lead to possible local minima and evaluate them. Here it comes in handy having a fully interpolated PES since it allows for quickly visualization of large portions of it. In Chapter 3 we will show in detail how the characterization of the PES was carried out.

2.4 Molecular Dynamics

In spite of the valuable information that we can obtain from the static analysis of the PES, molecular dynamics simulations are essential to gain understanding of the reactive mechanisms. Here we will describe the theoretical models used in this thesis to perform adiabatic and non-adiabatic simulations within the classical framework.

2.4.1 Classical dynamics on a PES

Dynamics calculations of gas-surface reactions involve taking into account the motion of all the atoms. Within the Born-Oppenheimer approximation described in Sec 2.1, the nuclear motion can be uncoupled from the motion of the electrons. In principle, nuclear motion should be treated quantum mechanically, however, with a high number of degrees of freedom, dynamics based on quantum mechanics become computationally costly. So it becomes necessary to transition from quantum to classical equations of motion. Treating nuclei as classical particles can be justified as follows: First, considering that the curvature of the potential where the nuclei move is large enough, their mass is sufficiently large so that the associated wavepacket is localized. Moreover, exchange effects can be neglected from the wavefunction given that they appear only at very low temperatures. Based on these arguments, several studies have shown a reasonable agreement between dynamics observables (e.g. adsorption probabilities, reflection) obtained with quantum and classical dynamics [15, 81, 82].

To make the transition between the quantum expressions to the classical ones, a good starting point is to take the Ehrenfest theorem [83]. According to this theorem, one can write the time evolution of the expectation values of position $\langle R_i \rangle$ and momentum $\langle P_i \rangle$ of the atoms of the diatomic molecule as

$$i\frac{d\langle \mathbf{R}_i \rangle}{dt} = \langle |H, \mathbf{R}_i| \rangle = i\frac{\langle \mathbf{P}_i \rangle}{M_i}, \tag{2.33}$$

$$i\frac{d\langle \mathbf{P}_i \rangle}{dt} = \langle |H, \mathbf{P}_i| \rangle = -i\langle \nabla_i V^{6D}(\mathbf{R}_i, \mathbf{R}_j) \rangle \text{ with } i \neq j. \tag{2.34}$$

These expressions lead to the Newtonian equation of motion of the form

$$\frac{d^2\langle \mathbf{R}_i \rangle}{dt^2} = -\frac{1}{M_i}\langle \nabla_i V^{6D}(\mathbf{R}_i, \mathbf{R}_j) \rangle \text{ with } i \neq j. \tag{2.35}$$

Since nuclei are treated classically, their wavefunction can be approximated as a product of Dirac's δ-functions with centers placed at the classical position. Hence, within this approximation, Eq. 2.35 can be written as

$$\frac{d^2\langle \mathbf{R}_i \rangle}{dt^2} = -\frac{1}{M_i}\nabla_i V^{6D}(\mathbf{R}_i, \mathbf{R}_j) \text{ with } i \neq j. \tag{2.36}$$

The Hamilton equations of motion equivalent to Eq. 2.36

$$\frac{d\mathbf{R}_i}{dt} = \frac{\partial H}{\partial \mathbf{P}_i}\,, \frac{d\mathbf{P}_i}{dt} = -\frac{\partial H}{\partial \mathbf{R}_i} \tag{2.37}$$

are solved in this thesis to perform the classical dynamics calculations. For this task, we have used a predictor-corrector algorithm of type Bulirsh-Stoer [84]. This provides an accurate expression for the velocities and the energy is conserved as it should be in adiabatic calculations. One thing to note is that classical equations ignore the vibrational zero-point energy (ZPE) conservation of the molecule. Nonetheless, depending on the reaction, this conservation can be crucial to study the reaction mechanism. To deal with this, calculations are usually done in the so-called quasi-classical way, where the internuclear distance and radial momenta are initially sampled in such a way that the vibrational energy corresponds to the ZPE. In this work, we perform quasi-classical calculations, even if the difference with purely classical results is not significant, as it will be shown later.

2.4.2 Energy dissipation effects in classical dynamics

Up to this point, we have introduced the concept of dynamics calculations within the frozen surface approximation, which is used to reduce the dimensionality of the system, simplifying the equations and thus, reducing the computational cost. Even though this approach has proven to successfully describe the reactivity in many gas-surface systems, to have dynamics results with more physical meaning one has to introduce energy dissipation channels in the dynamics calculations. To this aim, we have included in our calculations the two main energy dissipation channels, which are the energy exchange between the surface phonons and the molecular and the electronic excitations. On the other hand, the energy exchange

between the electrons of the surface and the molecule. To model these dissipation channels we make use of the generalized Langevin oscillator (GLO) model and the local density friction approximation (LDFA), respectively.

Generalized Langevin Oscillator Model

The GLO [85–88] is a simple model that allows to keep the good accuracy of the 6D-PES while making possible to model surface motion and surface temperature effects. In the model, the surface is described by a 3D harmonic oscillator with the mass of a surface atom m_s, a position vector $\mathbf{R}_s$ and an associated 3×3 frequency matrix $\hat{\omega}_s$. To account for thermal fluctuations, a so-called 3D ghost oscillator with a position vector $\mathbf{R}_g$, mass m_g and a 3×3 associated frequency $\hat{\omega}_g$ is coupled to the first oscillator through the coupling matrix $\hat{\lambda}_{gs}$. The equations of motion for the molecule and the 3D oscillators become

$$M_i \frac{d^2\mathbf{R}_i}{dt^2} = -\nabla_i V^{6D}(\mathbf{R}_i - \mathbf{R}_s, \mathbf{R}_j - \mathbf{R}_s), \tag{2.38}$$

$$m_s \frac{d^2\mathbf{R}_s}{dt^2} = -\nabla_s V^{6D}(\mathbf{R}_i - \mathbf{R}_s, \mathbf{R}_j - \mathbf{R}_s) - \hat{\omega}_s^2 \mathbf{R}_s + \hat{\lambda}_{gs}\mathbf{R}_g, \tag{2.39}$$

$$m_s \frac{d^2\mathbf{R}_g}{dt^2} = -\hat{\omega}_g^2 \mathbf{R}_g + \hat{\lambda}_{gs}\mathbf{R}_s - \hat{\gamma}_g \frac{d\mathbf{R}_g}{dt} + \mathbf{F}_r(t). \tag{2.40}$$

The 3D ghost oscillator is subjected to a friction force with damping matrix $\hat{\gamma}_g$ and to a random fluctuation force $\mathbf{F}_r(t)$. The latter models the heating of the surface atoms due to motion of the bulk atoms, and is in essence a Gaussian white noise with variance

$$Var(\mathbf{F}_r(t)) = \frac{2k_B T_s \gamma_g}{m_s \Delta t}, \tag{2.41}$$

being Δt the integration step, k_B the Boltzmann constant and T_s the surface temperature. The fluctuation-dissipation theorems links both the friction and the random fluctuation forces to guarantee that the surface atoms are indeed coupled to a thermal bath with temperature T_s. The frequency matrices corresponding to the surface and ghost oscillators are taken equal and diagonal, making $(\hat{\omega}_s)_{ii} = (\hat{\omega}_g)_{ii} = 2\omega_i^2$ and $(\hat{\lambda}_{gs})_{ii} = \omega_i^2$. And the values are obtained from the surface phonon frequencies $\omega_i (i = x, y, z)$ at the edges of the Brillouin zone of the metal surface, following Refs [87, 88]. Finally, the damping matrix in Eq. 2.40 is assumed isotropic as proposed in Ref. [89] and obtained using the Debye frequency ω_D

$$\hat{\gamma}_g = \frac{\pi}{6}\omega_D \mathbf{I}, \tag{2.42}$$

where $\mathbf{I}$ corresponds to the identity matrix.

Local Density Friction Approximation

There is numerous experimental evidences of electronic excitations being present in gas-surface reactions [90, 91]. This has lead to the development of a variety of methods to introduce this non-adiabatic effect in dynamics calculations [92–95]. Among these methods, the LDFA [96] has proven to be suitable to perform multidimensional molecular dynamics while keeping the accuracy and at the same time, not increasing the computational cost. The basic idea of this approximation comes from taking $e-h$ pair excitations created by a moving atom over a metallic surface as excitations created by the atom moving in a free electron gas (FEG) with the density of that of the surface at the atomic position. This is quite useful, since it helps to reduce the problem to that of an atom moving in an homogeneous FEG.

To apply the model in practice, one first has to calculate the electronic density $n(\mathbf{R}_i)$ for the surface alone at each position along the trajectory for each atom in the projectile. This electronic density can be obtained easily with a DFT calculation that has to be done under the same conditions as the calculations performed to obtain the PES. Then, the energy losses of the molecule caused by $e-h$ pair excitations are obtained in terms of a friction coefficient that is, as stated before, approximated at each point by the corresponding friction coefficient in a homogeneous FEG with density equal to that of the bare surface at that point.

The dissipative force that is included in the dynamics equations can be written as a friction coefficient proportional to the velocity of the projectile:

$$\mathbf{F}_{diss} = -\eta \mathbf{v} = n_0 \mathbf{v} k_F \sigma_{tr}(k_F), \tag{2.43}$$

where n_0 is the electronic density with an associated Fermi momentum k_F and $\sigma_{tr}(k_F)$ is the transport cross section at the Fermi level. We can understand the dissipative force in Eq 2.43 as the result of the momentum transfer per unit time to a uniform current of independent electrons $(n_0 v)$ scattered by a fixed impurity potential. The friction coefficient reads

$$\eta = n_0 k_F \sigma tr(k_F). \tag{2.44}$$

This friction coefficient has been used to calculate accurately the stopping power of atoms and ions in metal solids and surfaces [97–100]. Furthermore, the calculation of the transport cross section is done in terms of the scattering phase shifts $\delta(k_F)$ at the Fermi level, which are calculated from DFT scattering potential of an atom within the free electron gas model,

$$\sigma_{tr}(k_F) = \frac{4\pi}{k_F^2}\sum_{l=0}^{\infty}(l+1)sin^2(\delta_l(k_F) - \delta_{l+1}(k_F)). \tag{2.45}$$

Lastly, the dissipative force has to be included in the classical equations of motion for each recombining atom as

$$M_i\frac{d^2\mathbf{R}_i}{dt^2} = -\nabla_i V^{6D}(\mathbf{R}_i, \mathbf{R}_j) - \eta(\mathbf{R}_i)\frac{d\mathbf{R}_i}{dt}, \tag{2.46}$$

where in addition to the adiabatic force coming from the 6D-PES $V^{6D}(\mathbf{R}_i, \mathbf{R}_j)$ there is now the term for the dissipative force experienced by each atom of the projectile. All in all, the LDFA has been extensively used to study the role of $e-h$ pair excitations atomic and molecular dynamics on metallic surfaces [30, 96, 101–103].

In practice, we need to solve Newton equations when accounting for energy dissipation effects. Hamilton equations 2.37 cannot be solved given that the energy is not conserved. For this, numerical integrators such as the Verlet [104] or the Beeman algorithm [105] can be helpful. We use the latter to solve the resulting Newton equations of motion within the GLO model (Eq. 2.38,2.39 and 2.40) and within the LDFA (Eq. 2.46).

2.4.3 *Ab Initio* Molecular Dynamics

As we have mentioned in this section, quasi-classical dynamics performed on a precalculated 6D-PES often give good results when comparing to experimental data, and the main advantage over quantum calculations lies on the fact that they can be done considerably fast and easier to interpret in terms of dynamics analysis. This allows to have statistical meaningful results by calculating a great number of trajectories (in the order of thousands). On the other hand, the frozen surface approximation associated to the GLO model, is only able to quantify the energy exchange between the molecule and the surface phonons but not the dynamical coupling between surface atoms and molecular degrees of freedom. Although not allowing the surface atoms to move individually is a more than reasonable approximation given the compromise that we must make between accuracy and

computational cost, it still lacks the full description of all degrees of freedom in the system. For this, *Ab Initio* molecular dynamics (AIMD) is usually performed. The idea is to perform DFT calculations at each step of the dynamics (*on the fly*) to calculate the forces on the atoms. In AIMD calculations, both the atoms forming the molecule and the surface atoms are allowed to move according to the forces acting on them allowing the energy exchange between the molecule and the lattice. Because of this, each trajectory calculation is computationally expensive, and as a consequence the good statistical meaning that classical dynamics provide is lost. However, a lot of useful information can be extracted from these calculations.

Depending on the system, the explicit individual motion of the surface atoms might not have a big effect on the description of the reactivity of the system, but for the sake of comparison and in order to see how the reactive dynamics of the system treated in this work are affected, we have performed AIMD calculations. In Chapter 5 the corresponding procedure and results of these calculations are shown.

Chapter 3

Potential Energy Surface for N_2 on W(100)

This chapter will be devoted to the explanation of the procedure to build the potential energy surface for the N_2/W(100) system and to analyze the main features of it, such as the adsorption sites and potential energy barriers. The impact of accounting for non-local effects in the chosen XC functional will be addressed comparing the long and short range barriers with previous theoretical results.

In Sec. 3.1 we present the methodology used to calculate the DFT energies in the molecule-surface interaction followed by the interpolation procedure to obtain the continuous PES. Then, in Sec. 3.2 we analyze the features of the PES using 1D and 2D-cuts to obtain information about the potential minima and the energy barriers present in the PES. Finally, we summarize in Sec. 3.3.

3.1 Constructing the adiabatic potential energy surface

The interaction between the N_2 molecules and the W(100) surface is described by a 6D-PES that, following the frozen surface approximation, only depends on the degrees of freedom corresponding to the N_2 molecule. Here we illustrate the procedure to build the PES using the corrugation reducing procedure [35]. All the DFT calculations were performed using the vdW-DF2 functional [58] as implemented in the Vienna *ab initio* simulation package (VASP) [106–109]. The electron-core interaction was treated in the plane augmented wave (PAW) approximation [67].

To work within the supercell approach, we first need to calculate the W lattice parameter a for the vdW-DF2 functional. To that aim, we minimized the energy of the bulk while varying the value of a. The cut-off energy used was 500 eV for the plane-wave basis set and a $8\times8\times8$ Monkhorst-Pack grid of special $\mathbf{k}$-points was

used. Under these conditions, we obtained a lattice constant a=3.24 Å as shown in Fig. 3.1. The obtained value overestimates the experimental low-temperature value of 3.16 Å [110]. This overestimation has been noticed when using corrections in the XC functional to account for van der Waals interactions.

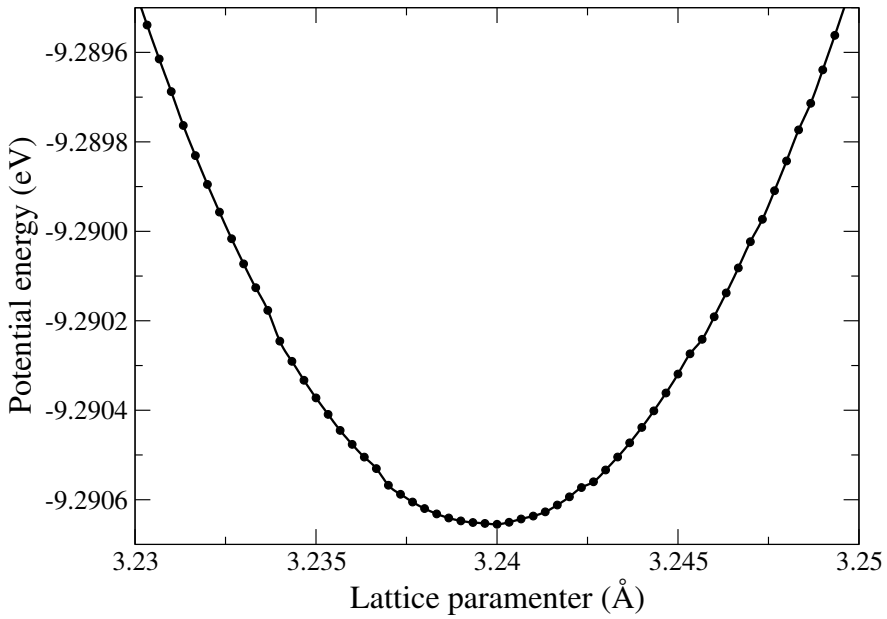

FIGURE 3.1: Potential energy as a function of the lattice parameter for the W(100) bulk.

The supercell is modelled by a five-layer thick slab (using a 2×2 surface unit cell) and 15.5 Å of vacuum. The large vacuum is necessary to properly represent a projectile approaching from the gas phase without it interacting with the periodic bulk images. After relaxing the top two layers, an interlayer distance of 0.437a between the top two and of 0.517a between the second and middle layer was obtained. This represents a contraction of 0.2 Å, 0.06 Å higher than the one observed with low-energy electron diffraction (LEED) experiments [111].

A total of 14 824 DFT energies were calculated for different atomic and molecular configurations of N and N_2 over the W(100) surface. To sample the Brillouin zone of the supercell, an 8×8×1 Monkhorst-Pack grid of special **k**-points was used. The zero of the potential is taken as the energy of the N_2 molecule at its equilibrium distance (r_{eq}=1.11 Å) in the middle of two slabs (i.e. 7.5Å above the topmost layer). We assume that in this region, the molecule does not interact with the surface or its periodic images. To justify this, we calculate the energy of the molecule alone and compare it to the obtained energy halfway between the bulk

and its periodic image. The energy difference in this case is below 5 meV. Explanatory figures showing how several of the parameters used in the calculations were obtained is shown in Appendix A.

As explained in Chapter 2, the coordinate system used in the calculations involves six degrees of freedom: X, Y and Z of the center of mass, molecular orientation represented by the polar (θ) and azimuthal (ϕ) angles, and the internuclear distance r. To build the PES, 35 different configurations (defined by X,Y,θ,ϕ) of the N_2 molecule over the surface were chosen. For each configuration, a 2D-cut of the PES in r and Z was calculated while keeping fixed the position of the center of mass of the molecule over the surface (X,Y) and its orientation (θ,ϕ). For each 2D-cut, r varied from 0.71 Å to 3 Å in a 14-point grid, and the range in Z started from 0.5 Å up to 7.5 Å in a 29-point grid with a 0.25 Å step size. These 2D-cuts have been calculated in the high symmetry points within the irreducible surface unit cell. In Fig. 3.2 a detailed scheme of the sites were calculations were performed is shown.

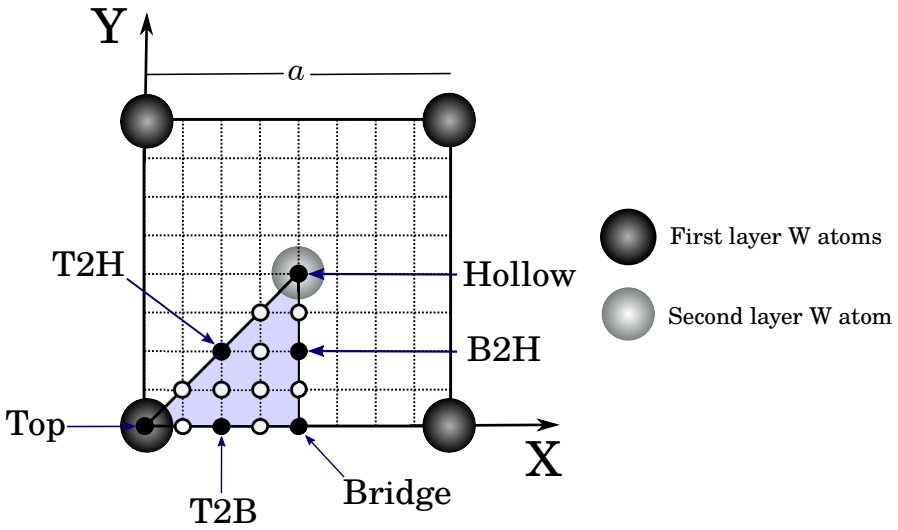

FIGURE 3.2: Top-view of the W(100) unit cell. Black and white circles mark the positions for which DFT calculations of the 3D N/W(100) were carried out. N_2 molecular DFT energies were calculated with the center of mass over the sites marked with black circles.

The 35 different configurations are divided as follows:

- Five configurations with the center of mass over the top site ($X = 0$, $Y = 0$): $\theta = 0°$; $\theta = 90°$ with $\phi = 0°$ and $\phi = 45°$; $\theta = 45°$ with $\phi = 0°$ and $\phi = 45°$.

- Five configurations over the bridge site ($X = a/2$, $Y = 0$): $\theta = 0°$; $\theta = 90°$ with $\phi = 0°$ and $\phi = 45°$; $\theta = 45°$ with $\phi = 0°$ and $\phi = 90°$.
- Five configurations over the hollow site ($X = a/2$, $Y = a/2$): $\theta = 0°$; $\theta = 90°$ with $\phi = 0°$ and $\phi = 45°$; $\theta = 45°$ with $\phi = 0°$ and $\phi = 45°$.
- Seven configurations over the top-to-hollow (t2h) site ($X = a/4$, $Y = a/4$): $\theta = 0°$; $\theta = 90°$ with $\phi = 45°$ and $\phi = 135°$; $\theta = 45°$ with $\phi = 45°$, $\phi = 90°$, $\phi = 135°$ and $\phi = 225°$.
- Six configurations over the top-to-bridge (t2b) site ($X = a/4$, $Y = 0$): $\theta = 0°$; $\theta = 90°$ with $\phi = 0°$ and $\phi = 90°$; $\theta = 45°$ with $\phi = 0°$, $\phi = 90°$ and $\phi = 80°$.
- Seven configurations over the bridge-to-hollow (b2h) site: ($X = a/2$, $Y = a/4$): $\theta = 0°$; $\theta = 90°$ with $\phi = 0°$, $\phi = 45°$ and $\phi = 90°$; $\theta = 45°$ with $\phi = 0°$, $\phi = 90°$ and $\phi = 270°$.

The corresponding atomic potentials (V_A^{3D}, V_B^{3D}) are needed to perform the 6D interpolation. These atomic potentials are substracted from the full V^{6D} to obtain the less corrugated function I^{6D} which is subsequently interpolated. After I^{6D} has been successfully interpolated, V_A^{3D} and V_B^{3D} are added again giving as a result the full 6D-PES. To calculate the 3D N/W(100) PES, a set of spin-polarized DFT calculations was performed over the 15 sites marked with black and white circles in Fig. 3.2. For each site, a 47-point grid in Z ranging from -2 Å to 6Å was used. The interpolation of I^{6D} is carried out first in r and Z using using 2D cubic splines. Afterwards, Fourier series expansions are used to interpolate over θ and ϕ. Finally, 2D periodic cubic splines help to interpolate over X and Y. A more detailed explanation of the CRP is given in Appendix B.

To test the accuracy of the final interpolated 6D-PES, several configurations not included in the interpolation procedure used to build the PES were chosen. An example of the test is shown in Fig 3.3, where the DFT energies are compared to those obtained with the interpolated PES. After a thorough analysis of the PES, it shows that in average, the interpolation errors are below 50 meV. On the other hand, the largest errors occurs in some configurations close to the surface where the potential variations are large. However, these regions are not important for the dynamics, unlike adsorption sites and minimum energy barriers, where the error is kept below 10 meV.

In highly corrugated surfaces, the most challenging degrees of freedom to interpolate accurately are those corresponding to the molecular orientation (θ, ϕ).

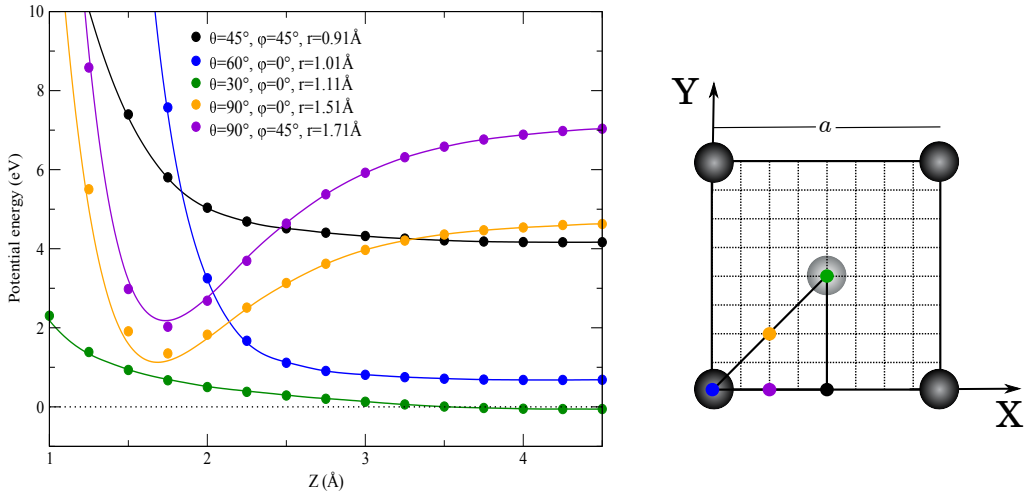

FIGURE 3.3: Potential energy as a function of the N_2 center of mass altitude over the surface Z for different molecular configurations. The DFT energies are represented as solid circles and the continuous lines represent the interpolation. The molecular orientation and internuclear distance for each configuration is shown in the legend, and the position over the unit cell is shown on the right hand side.

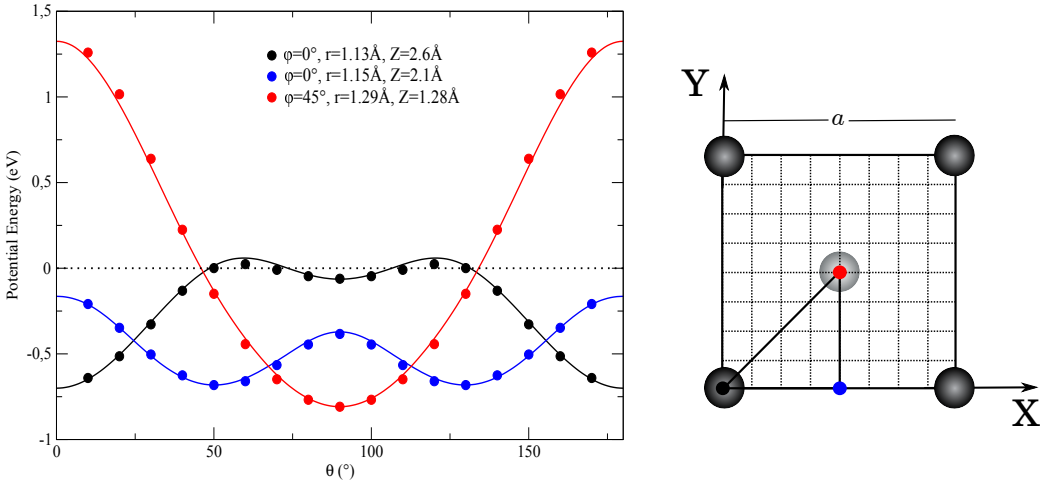

FIGURE 3.4: Potential energy as a function of the N_2 polar angle θ. The DFT energies are represented as solid circles and the continuous lines represent the interpolation. The azimuthal angle ϕ, internuclear distance r and altitude Z are shown for each configuration, and the position over the unit cell is shown on the right hand side.

In Fig 3.4 we show an interpolation in θ for different configurations, and as it is observed, the DFT points used to build the PES are enough to obtain a high accuracy, specially in the regions of the PES with a negative potential, which are of great importance for the study of the reactivity.

3.2 Characterization of the 6D-PES

To begin the analysis of the PES, we generate a series of 1D-cuts of the potential energy for several molecular configurations. This is useful to have a first idea of which configurations face a barrier when approaching the surface. In Fig. 3.5, the potential energy as a function of Z is represented for several (X, Y, θ, ϕ) configurations, r being equal to the equilibrium value of N_2 in the gas phase. After testing several configurations within the irreducible unit cell we noticed that at distances from the surface around 3 Å $< Z <$ 3.5 Å the PES presents an energy barrier for most of the configurations. The only cases were this is not true is for configurations approaching along the W-W bond with a molecular orientation close to vertical for the top site (X=0; Y=0; $\theta = 0°$) and more tilted if the approach is done towards the bridge site (X=0.5; Y=0; $\theta = 50°$; $\phi = 0°$).

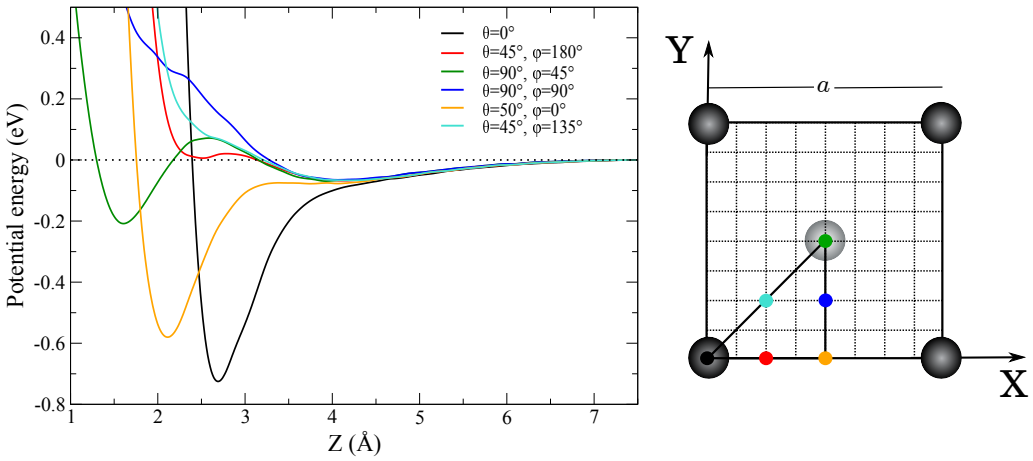

FIGURE 3.5: Potential energy as a function of the N_2 center of mass altitude over the surface Z for several molecular configurations. The internuclear distance corresponds to the equilibrium distance r_{eq} for all cases. The molecular orientation and internuclear distance for each configuration is shown in the legend, and the position over the unit cell is shown on the right side.

This observation differs from what was reported in Ref. [25]. In the latter case, using the PW91-PES, the only available entrance channel without barriers was observed for configurations around the top sites (i.e. above the W atoms) with a molecular orientation close to vertical. This means that the inclusion of vdW interactions in the description of the XC functional increases the attraction in the zone around Z=3 Å, which is of crucial importance to the dynamics as stated before. To visualize the energy barriers in the entrance channel in a better way, in

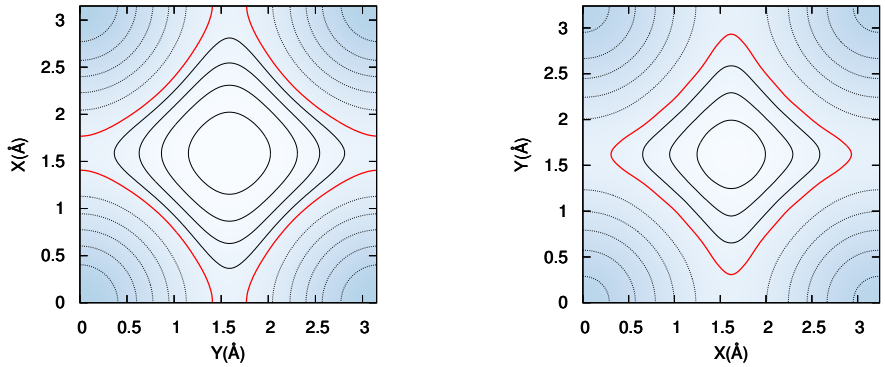

FIGURE 3.6: 2D (X,Y)-cuts of the PW91-PES (left panel) and vdW-DF2-PES (right panel). The molecule is located at a distance of $Z = 3$ Å from the surface with a perpendicular orientation $\theta = 0°$ and r=r_{eq}=1.11 Å. Red thick line corresponds to the zero of the potential energy. Solid (dashed) black lines represent positive (negative) values separated by intervals of 50 (100) meV.

Fig. 3.6 we present a 2D-cut in (X,Y) of the PW91-PES (left panel) and the vdW-DF2-PES (right panel) for a molecule with a perpendicular orientation ($\theta = 0°$) and at a distance of $Z = 3$ Å from the surface. From the figure it becomes clear that the vdW-DF2-PES is more attractive and molecules can adopt a larger number of configurations to approach the surface without facing energy barriers. This observation becomes quite important for the reactive dynamics of the system as it will be discussed in Chapter 4. It is worth noting that while the position of the energy barriers and local minima do not differ too much in terms of the molecular configuration (r and Z), the height and deepness of these features do look affected for the studied different exchange-correlation functionals. The energy barriers in the entrance channel are smaller in the vdW-DF2-PES, and the potential minima are deeper in the case of the PW91-PES.

In a different work, Bocan *et al.* [26] found that in the RPBE functional the top vertical configuration presents a small potential energy barrier in the entrance channel (∼14 meV). This means that for the RPBE functional, none of the configurations allow molecules to approach the surface without facing a potential energy barrier. The potential well over the top site is located around Z∼2.6 Å for the different functionals, however, the depth of the minimum changes with each PES. In table 3.1 we present the energy value at the bottom of the potential energy minimum located on the top site for the different potential energy surfaces. Experimental adsorption energies obtained using thermal desorption spectroscopy

are presented as well [112]. It is worth noting that the adsorption energy values reported in experiments do not correspond necessarily to adsorption over the top site. Keeping in mind that these results are obtained under the frozen surface approximation, comparison with experimental data should be done carefully given that we are not accounting for surface atom movement. One interesting point about these values, is that even though the RPBE-PES shows a more repulsive character in the entrance channel, the potential well is deeper than the one in the vdW-DF2-PES.

TABLE 3.1: Comparison of the potential energy (in eV) at the bottom (PM) of the adsorption well present in the top vertical configuration when using the PW91, RPBE and vdW-DF2 functionals. Experimental adsorption energies are shown as well.

	PW91-PES	RPBE-PES	vdW-DF2-PES	Experiments (eV)
PM (eV)	-1.048	-0.821	-0.746	0.399[a]
				0.455[a]

Following the analysis of the PES, in Fig 3.7 we shows a series of 2D-cuts in (r,Z) for configurations that are relevant to the study of the reaction dynamics. The configurations shown are located in the three high symmetry sites, namely top, bridge, and hollow. After a thorough examination of these kind of 2D-cuts of the PES, we can confirm the above-mentioned observation about the entrance channel. Panels (a) and (b) of Fig. 3.7 show the most favorable configurations for the molecules to approach from the gas-phase without overcoming any energy barrier. In some of the (r,Z)-cuts one can observe local minima (in 2D) that could represent possible molecular adsorption sites in the multi-dimensional space. In order to check whether these minima are actual potential wells in the 6D-space, we make use of a classical trajectories code as proposed in Ref [25]. The idea consists in putting the molecule at the bottom of the observed minimum in the 2D-cut with a random orientation of the velocity (obtained using a Monte-Carlo sampling) associated to the initial kinetic energy E_i. Then, starting with E_i=0 and slowly increasing the energy, we perform classical trajectory calculations (without considering the ZPE of the N_2 molecule) checking how much energy the molecules need to escape the well. The threshold value for E_i corresponds to the diffusion barrier height at the local minima. If no energy is needed (i.e. for E_i=0) for the molecule to leave the well it means that the tested configuration corresponds to a minima in 2D and not in the full dimensional space. Making use of this procedure, we tested the configurations that present a minimum in the 2D-cut and we

[a] *Reference [112]*

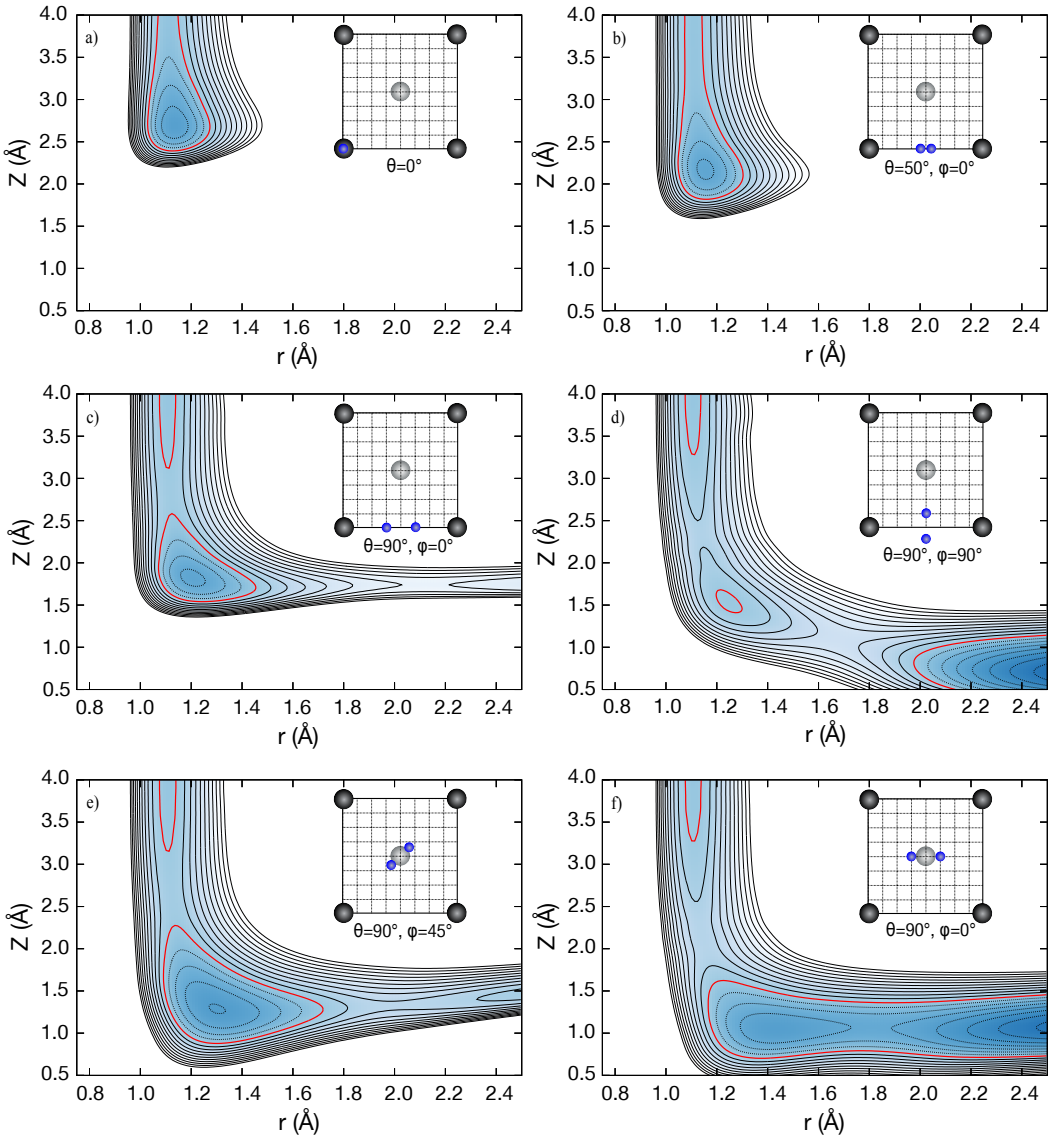

FIGURE 3.7: 2D (r,Z)-cuts of the N_2/W(100) vdW-DF2-PES. The position and orientation of the molecule over the unit cell is schematically shown in each 2D-cut. Red thick line corresponds to the zero of the potential energy. Solid (dashed) black lines represent positive (negative) energy values. All contour lines are separated by intervals of 0.2 eV.

observe the presence of three 6D molecular adsorption sites. They correspond to panels (a), (b) and (e) of Fig. 3.7. The molecular configurations of these minima, along with the value for the potential at the bottom of the well are presented in Table. 3.2.

TABLE 3.2: Properties of molecular adsorption wells present in the vdW-DF2-PES: Adsorption energy (E_{ads}), N-N internuclear distance (r), distance of the N_2 center of mass to the surface (Z), polar (θ) and azimuthal (ϕ) angles.

Site	E_{ads} (eV)	r (Å)	Z (Å)	θ (°)	ϕ (°)
Top	-0.746	1.13	2.68	0	0
Bridge	-0.648	1.16	2.16	50	0
Hollow	-0.809	1.31	1.28	90	45

From the dynamics performed with the molecule starting in the bottom of each potential minimum, we can obtain an accurate picture of the diffusion barriers to leave the minima. In Fig. 3.8 we show a scheme displaying the local minima and the corresponding diffusion barriers. The asymptotic value corresponds to the N_2 binding energy. The exothermicity of the dissociation is calculated as the adsorption energy of the N atoms minus the N_2 binding energy. The value of the adsorption energy for an N atom is obtained from the atomic calculations over the surface (See Appendix B). When a nitrogen atom interacts with the surface, we observe that the deepest potential energy minimum is located with the N atom over the hollow site at a distance of Z=0.7 Å from the surface with a potential energy of -6.77 eV. Desorption experiments reported a value of 4.1 eV per nitrogen molecule for the endothermicity [113]. The latter value is associated with N atoms at the bottom of the adsorption minimum. Adding the corresponding binding energy of the N_2 molecule (9.8 eV) and diving by two, it yields a value of 7 eV for the depth of the adsorption well, not far from the 6.77 eV obtained for our PES. Following the analysis of the potential wells, if the molecule is fixed on the top site minimum, it needs at least 250 meV to be able to move towards the bridge site. Moreover, if less than 400 meV are added, molecules can move back and forth between the minima on top and bridge but none of them can move towards dissociation.

The configuration corresponding to the local minima found in the hollow site is, in fact, the minimum energy configuration for the non-dissociated molecule. From this configuration, dissociation is not possible (See panel (e) of Fig 3.7), it presents a diffusion barrier of $\sim$ 175 meV to stretch the N-N distance and rotate in ϕ to reach the configuration depicted in panel (f) of Fig. 3.7 where dissociation

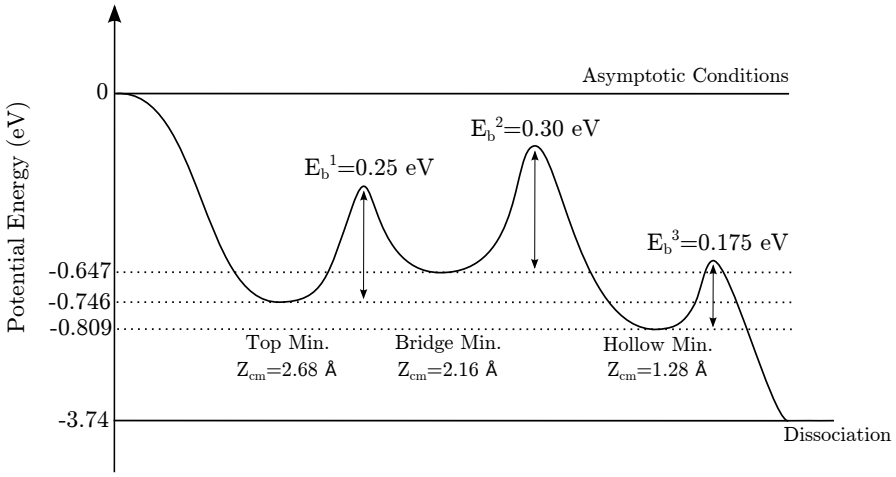

FIGURE 3.8: Scheme of the potential barriers and local minima of the 6D-PES. The asymptotic energy corresponds to the binding energy of the N_2 molecule. The altitude of the center of mass (Z_{cm}) is indicated for each adorption site.

is possible. On the right hand panel of Fig. 3.9 a 2D cut in θ and ϕ for this local minima is presented. In the figure it is clear that the molecules prefer to lie parallel to the surface and with an azimuthal angle of ϕ=45°. The same 2D (θ,ϕ)-cut for the local minima present on the bridge site is shown on the left hand panel of Fig. 3.9. In this configuration, rotation in θ exhibits negative values of the potential with respect to the energy of the molecule in vacuum, except when the molecule is aligned with the N atoms pointing to the hollow site (i.e. with ϕ=90°). Moreover, it can be seen that the energy barrier to rotate in θ starting from the minimum (θ=50°, ϕ=0°) to end up completely parallel to the surface (i.e. with θ=90°) is around 300 meV.

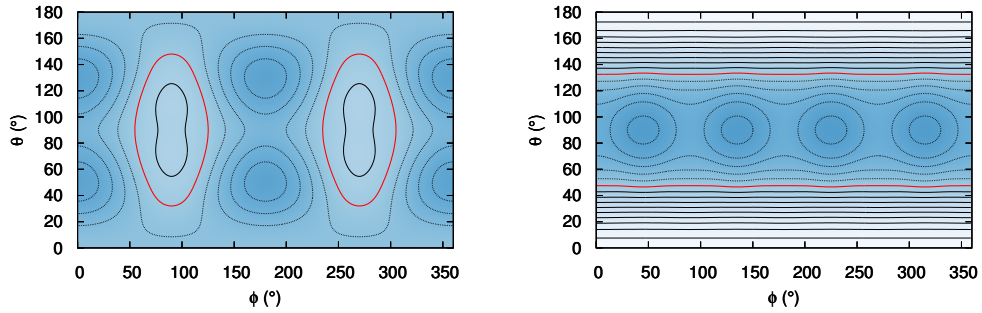

FIGURE 3.9: 2D (θ,ϕ)-cuts of the molecular configurations corresponding to the local minima in the bridge (left hand panel) and the hollow site (right hand panel). Red thick line corresponds to the zero of the potential energy. Solid (dashed) black lines represent positive (negative) values. All contour lines are separated by intervals of 0.15 eV.

This case where the molecule is parallel to the surface and with an azimuthal angle of ϕ=0° is shown in panel (c) of Fig. 3.7. This particular configuration is not accessible from gas-phase without energy barriers, but presents a molecular well in 2D. Rotating the molecule 90° in ϕ we obtain the cut shown in panel (d), notice how this configuration presents an energy barrier towards dissociation of around 650 meV. This fact has attracted our attention given that from this particular configuration dissociation was possible without energy barriers when the PW91-PES was used [25]. In this case a considerable energy barrier appears, indicating that the number of of configurations in which the molecule can dissociate without energy barriers is smaller in the vdW-DF2 PES than in the PW91 PES. One of the configurations where dissociation follows a non-activated path once the molecule is close to the surface corresponds to that of panel (f) discussed above. Naturally, given that a low-energy N_2 molecule is unable to reach this configuration directly from gas-phase, it has to go through some of the others configurations shown.

From this analysis two main observations stand out: first, the vdW-DF2-PES, accounting for long-range interactions exhibits a wider area for the molecule to approach the surface at distances of about 3 Å. Secondly, the usage of this functional causes the appearance of barriers at short distances that were not observed before and that are relevant to the study of the dynamics. Also, molecular adsorption wells are less deep than in the PW91 case. With these changes in the PES, changes in the dynamics are to be expected.

3.3 Summary

In this chapter we have reported the construction of the six-dimensional PES for the N_2/W(100) system based on DFT calculations using the vdW-DF2 functional. Using a well-known interpolation scheme such as the corrugation reducing procedure, more tan 14 000 DFT energy values were used to obtain the continuous 6D PES. The accuracy of the PES was tested using DFT energies of configurations not included in the interpolation procedure. Interpolation error is abut 10 meV in regions important for the dynamics.

After a thorough examination of one and two-dimensional cuts of the PES, it is clear that the description regarding the entrance channel is affected by the choice of the functional. With this new PES, molecules face a wider attractive area in the

region of $Z = 3$ Å along the W-W bond than in the previous PESs. Close to the surface, the PES exhibits new energy barriers to dissociation that were not observed before. One particular configuration over the bridge site ($\theta = 90°$; $\phi = 90°$) that was reported as a non-activated pathways to dissociation in PW91-PES presents now a significant barrier of around 650 meV. This leaves a unique path leading to dissociation without energy barriers (or energy barriers below the zero potential energy). Furthermore, three different molecular adsorption sites were identified along with the corresponding adsorption energies and diffusion barriers. This differences in the topology of the PES were expected given the choice of the XC functional. The next step now is to perform quasi-classical dynamics calculations on the constructed PES.

Chapter 4

Dissociative adsorption dynamics

4.1 N_2 on W(100): A brief background

As discussed in Chapter 1, when it comes to the diatoms-surface interactions, one of the most emblematic examples that comes to mind is the reaction of N_2 with metallic surfaces. In this matter, tungsten surfaces have been widely studied due to the interesting crystallographic anisotropies observed experimentally [17, 18]. The most illustrative example of this anisotropy is the significant difference in the value of the sticking probability of N_2 at room temperature between the W(100) and the W(110) surface, the sticking coefficient being much greater for W(100) than for W(110). To this day, the study of N_2 reactive adsorption dynamics on W surfaces is still undergoing active research. In spite of the great improvements in the dynamics description, agreement between theory and molecular beams measurements is still not achieved. This is predominantly the case for the dissociative and non-dissociative molecular adsorption of N_2 on the W(100) surface.

Aforementioned molecular beam experiments have investigated the effect of many parameters such as the surface temperature (T_s), the initial kinetic energy (E_i) of the N_2 molecules, the angle of incidence (θ_i), the rotational and vibrational states of the colliding molecules on the sticking probability (S_0) [21, 22]. The results of these experiments show a non-monotonous dependence of the initial sticking probability S_0 with translation energy. A significant dependence of S_0 on the surface temperature is observed in the low collision energy regime that corresponds to the decreasing part of S_0. The highest is the surface temperature, the lower is the sticking probability for low collision energies. At higher values of E_i, the dependence of S_0 on the surface temperature vanishes and S_0 converges for all values of T_s. Experimentalists divide the sticking probability into two channels and propose that low-energy N_2 molecules follow a precursor-mediated process

and that high energy molecules follow a more direct mechanism that involve activated reactive pathways. These experiments were also conducted for the reaction with the W(110) surface, where this indirect or precursor-mediated process to dissociation was not observed. Instead, they found that at low values of E_i, the sticking probability at W(110) was extremely low ($\approx 10^{-3}$) [19]. These observations suggest that for the W(100) surface, non activated pathways are present, so that low energy molecules can find a way to dissociate without overcoming any positive potential energy barriers. On the other hand, the W(110) surface presents large energy barriers at low values of E_i, preventing the N_2 molecules to approach the surface and dissociate. One point that it is worth noting, is that in these experiments, the sticking coefficient does not differentiate between non-dissociative and dissociative adsorption. This means that N_2 molecules can end up molecularly adsorbed in the surface without dissociating. This can happen when molecular adsorption wells are present, which is the case for these systems. Studies based on thermal desorption spectroscopy (TDS) measurements, have characterized the adsorption of N_2 on W surfaces [20]. The first of the three adsorption states found corresponds to the so-called α-N_2 state, which desorbs around 300 K, but its formation is not observed on the W(100) surface. A second β-N state that desorbs near 1000 K is observed for both W(100) and W(110) surfaces, with similar adsorption energy. This was found to be counterintuitive given the huge difference in the value of S_0 for both surfaces. Finally, a third γ-N_2 molecular state, that is weakly bounded and desorbs around 150 K, is present for all W surfaces.

All this interesting experimental information motivated different theoretical works dedicated to shed some light on these findings. In 2004, Volphilac et al. [25] built a potential energy surface based on DFT calculations using the PW91 XC functional for N_2 on W(100). Subsequently, they performed classical dynamics calculations using this PES to compute the sticking probability. They carried out and exhaustive characterization of the features of the static PES trying to describe what is observed in the experiments, particularly in the low energy regime. Based on 2D-cuts of the PES, they showed that for the PW91-PES, two different non-activated paths lead to dissociation. The paths were identified based on the configurations that the low-energy N_2 molecules went through during the classical trajectories simulations. Additionally, their results for S_0 exhibited a strange behavior in the low-energy regime. A non-monotonic dependency of S_0 on E_i below 500 meV was obtained, where a steep decrease of S_0 up to $E_i \simeq 40$ meV was observed, followed by an increase in the 40 meV $< E_i <$ 200 meV range with a peak at the latest energy and finally a monotonic decrease for $E_i >$ 200 meV. This

rather strange behavior did not agree with experiments. In addition, no significant dependency of S_0 with the surface temperature was obtained at low values of E_i. Therefore, the explanation was still not complete, and has motivated new studies were the effect of changing the functional was evaluated. Another PES constructed using the RBPE functional (within the GGA approximation, as the PW91) was built in order to see if the description of the reactivity in the low energy regime would improve [26]. These authors reported a qualitative similarity in the topology of the potential energy surfaces. However, comparing 1D and 2D cuts of the PES, the energies obtained with the RPBE functional were larger to those obtained with the PW91 functional. This was expected somehow given the tendency of the RPBE functional to be more repulsive, meaning that the adsorption energies are smaller when RPBE is used. In terms of the sticking coefficient, the repulsive character of the RPBE-PES caused S_0 to be a its minimum at the lowest value of impact energy. Then, S_0 increased up to $E_i = 300$ meV where it started to decrease again to finally stabilize beyond $E_i = 1$ eV. In that work, the striking change in the behavior of S_0 at low values of E_i from one functional to another was attributed to the sensitivity of the dissociation of N_2 to the shape of the PES far from the surface ($Z \geq 3$ Å). Thus, a proper description of the long-range interactions between the molecule and the surface is essential.

At this point, it becomes clear that the choice of the XC functional used to build the PES plays a key role in the problem. More recent studies examined the dynamics of N_2 on the (110) face of tungsten using a functional that accounted for non-local effects like van der Waals interactions in the procedure to build the PES [33, 114]. One of the studies shows that after analyzing the effect of several functionals (PW91, RPBE, optPBE-vdW and vdW-DF), the results were inconclusive. The functionals RPBE and vdW-DF were describing properly the entrance channel but overestimating the energy barriers close to the surface leading to dissociation. On the other hand, the PW91 and the optPBE-vdW functionals exhibited the opposite behavior [114]. However, in posterior studies and making use of a corrected version of the vdW-DF functional (i.e. the vdW-DF2 functional), it was found that by using the vdW-DF2 functional, the molecular depth of adsorption wells and the ratio between the energy barriers for the indirect dissociation and desorption were closer to what experimentally was observed [33].

Assuming the frozen surface approximation, the reaction of the N_2 molecule with the W(100) surface takes place in a 6D-configurational space, hence, the analysis of the static N_2/W(100) PES through the generation of 1 and 2D-cuts can be

useful to have a general picture of the possible reaction paths that the molecule can undergo, but it is still incomplete regarding the high dimensionality of the problem. This chapter is dedicated to study the dissociative adsorption dynamics of N_2 on the W(100) surface performing quasi-classical trajectories (QCT) calculations. The PES has been built assuming that surface atoms are kept fixed in their equilibrium positions. Thus, the forces that derive from the PES are acting only on the N_2 molecular degrees of freedom. In the present chapter, QCT simulations are analyzed within the *Born-Oppenheimer static surface* (BOSS) approximation and no energy exchange is allowed between the molecule and the surface. We will see in next chapters that simple effective models (as GLO and LDFA) are available to go beyond the BOSS approximation using a PES that is not considering explicitly the displacement of surface atoms.

Within this context, the dissociative adsorption probability has been computed for the vdW-DF2-PES and compared to previous results obtained with PESs based on PW91 and/or RPBE functionals as in Refs. [25, 26]. As it will be discussed, the behavior of the sticking probability varies significantly from PES to PES, particularly for low translational energies of the N_2 molecule colliding the surface (i.e. impact energies below 500 meV). These differences are explained regarding the topological changes in the PESs. In addition, the reaction pathways that the molecules undergo at low values of E_i is explored by checking the configurations that the molecules follow throughout the dynamics.

In Sec. 4.2 a description of the most relevant computational details is presented. Next, in Sec. 4.3 the main results of the calculations are discussed, explaining the behavior of the sticking probability in the full range of energies. Finally, a brief summary of the main results is presented in Sec. 4.4.

4.2 Computational details

In order to perform QCT calculations on the multi-dimensional PES we solve the Hamilton equations (2.37) of classical mechanics. Although no significant difference is observed between performing classical or quasi-classical simulations (neglecting or including the ZPE of the N_2 at the beginning of the simulation), all of the calculations were performed accounting for the ZPE. Each trajectory starts with the N_2 molecule at a distance of $Z = 7.5$ Å from the surface. For each value of the impact energy E_i and incidence angle Θ_i a conventional Monte Carlo (MC)

procedure is used to sample all possible initial positions over the unit cell (X,Y), initial molecular orientation (θ,ϕ) and internuclear distance (r) taking into account the initial vibrational energy of the molecule. Associated momenta are also sampled randomly following a MC procedure. The integration time for each trajectory is maximum 50 ps, during which the trajectories are classified in different events:

- Reflection: If the molecular center of mass reaches the starting distance ($Z = 7.5$ Å) with a positive velocity along the surface normal
- Dissociation: If the molecule has a positive radial velocity and its internuclear distance is at least two times the equilibrium distance (i.e. $r \geq 2r_{eq}$)
- Non-dissociative adsorption: If the molecule is neither dissociated nor reflected after the integration time.

4.3 Dissociative adsorption probability

To begin the discussion about the dissociative adsorption probability, it is worth to perform a qualitative comparison of the sticking coefficient S_0 as a function of the impact energy E_i with previous theoretical works. This is precisely what is shown

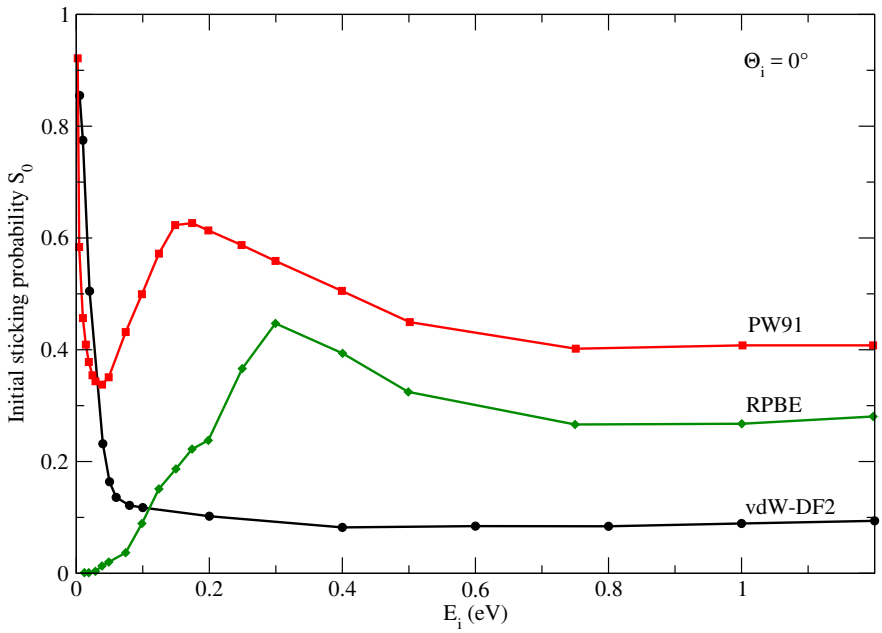

FIGURE 4.1: Initial sticking probability S_0 within the BOSS approximation as a function of the initial kinetic energy E_i under normal incidence for different functionals used to build the PESs. Red line: PW91 results (Ref. [25]); green line: RPBE results (Ref. [26]); black line: vdW-DF2 results.

in Fig. 4.1, where results for classical calculations under normal incidence for the PW91-PES [25], the RPBE-PES [26] and the vdW-DF2-PES are presented. Note that in this comparison, calculations do not include the ZPE of the N_2 molecule to match the conditions used in Refs. [25, 26]. It is quite striking how the shape of the curve changes with the functional chosen to build the PES, particularly for the low impact energies already discussed (i.e. $E_i \leq 500$ meV). The RPBE-PES shows really low values for S_0 in the low energy regime. On the other hand, the PW91-PES results shows the non-monotonic behavior with a minimum at $\sim$40 meV and a peak at $\sim$200 meV. In the case of the vdW-DF2-PES, a steep monotonic decrease of S_0 is observed at low impact energies. At around $\sim$200 meV S_0 it stabilizes with a value close to 0.1. Notice that besides the low-energy regime, the vdW-DF2-PES exhibits a lower value for the sticking coefficient than the PW91 and RPBE-PESs. This could be due to the fact that in the vdW-DF2-PES the number of pathways leading to dissociation is reduced due to the emerging energy barriers close to the surface mentioned in the previous chapter.

As reported in previous works and discussed before, the initial sticking coefficient S_0 is a combination of an indirect mechanism involving many rebounds on the surface prior to dissociation at low values of impact energy E_i (from now on called "indirect" channel) and a direct mechanism at higher values of E_i. To separate both processes we use a concept involving the number of rebounds that the molecule performs before dissociating. In essence, we consider that the molecule performs one rebound every time its velocity changes from pointing away from the surface to pointing towards the surface. Knowing this, we consider a trajectory to contribute to the "indirect" channel if it performs more than 4 rebounds, otherwise it is said to contribute to the "direct" channel. The decomposition of S_0 under normal incidence into these two mechanisms is presented in Fig. 4.2 for the vdW-DF2 PES. In addition, the total initial sticking probability is shown for the classical calculations (i.e. not including the N_2 ZPE at the beginning of the trajectory). The main difference between CT and QCT simulations is observed for very low values of E_i, where CT results exhibit a higher value of S_0. This increase can be due to the fact that the molecules are more easily driven through the "indirect" channel when no initial ZPE is accounted for. Moreover, studies have shown that at low impact energies, S_0 can be reduced artificially in QCT simulations due to energy transfer processes associated to closed channels in a quantum approach [115]. Then, as the energy increases, the results of CT present no significant difference to those obtained performing QCT. Regarding the separations of

the total S_0, it is clear that below 100 meV, the sticking is dominated by the "indirect" process. Then, as the energy increases the "direct" process increases as the molecules perform less rebounds on the surface before dissociating.

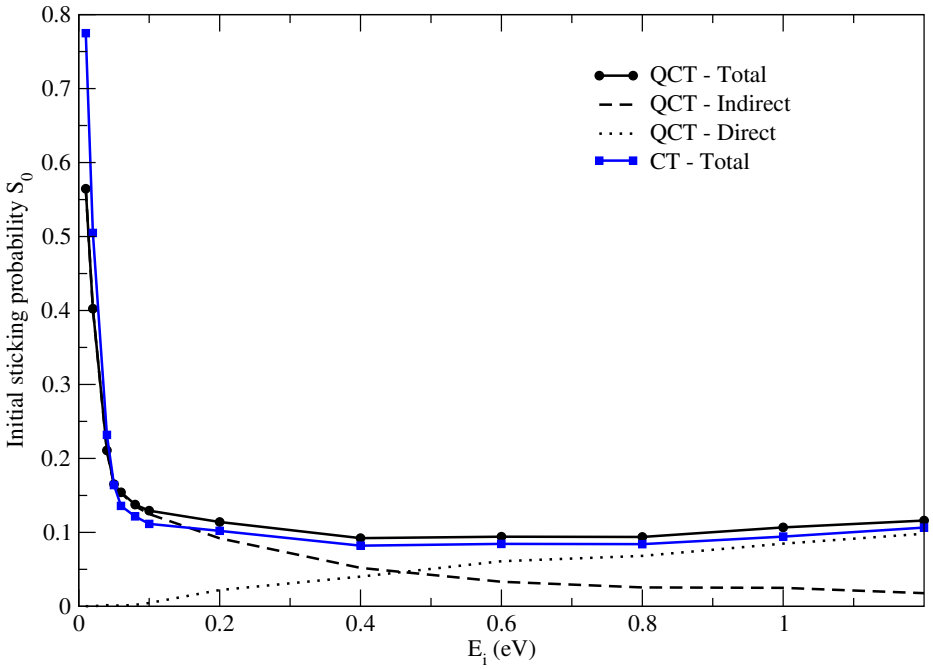

FIGURE 4.2: Total sticking probability S_0 for the classical (CT) and quasi-classical (QCT) trajectories under normal incidence as a function of the initial kinetic energy E_i for the vdW-DF2-DF2. The decomposition of S_0 for the QCT calculations into the so-called indirect and direct contributions is also presented.

A simple way to visualize this is by checking the distribution of the number of rebounds at different values of E_i. This is shown in Fig. 4.3 for four values of the incidence energy (10, 50, 200 and 800 meV) to see the evolution of the distribution of the number of rebounds. In the figure we can see how the molecules perform less rebounds in average (41, 32, 13 and 4 for the respective values of E_i presented) on the surface when E_i is increasing. For the case where E_i=10 meV, we can compare the average number of rebounds obtained (41) to the 17 reported by Volphilac *et al.* [25] using the PW91-PES. This considerable difference can be partially due to the reduced number of paths to dissociation present in the vdW-DF2-PES, causing the molecules to spend more time dynamically "trapped" finding the optimal non-activated path to dissociate. A better understanding of this "indirect" process can be obtained by looking at Fig. 4.4. The figure shows the evolution of the position of the center of mass in X and Y (top panels), the polar angle θ (middel panels) and the azimuthal angle ϕ (bottom panels) of the dissociating molecules

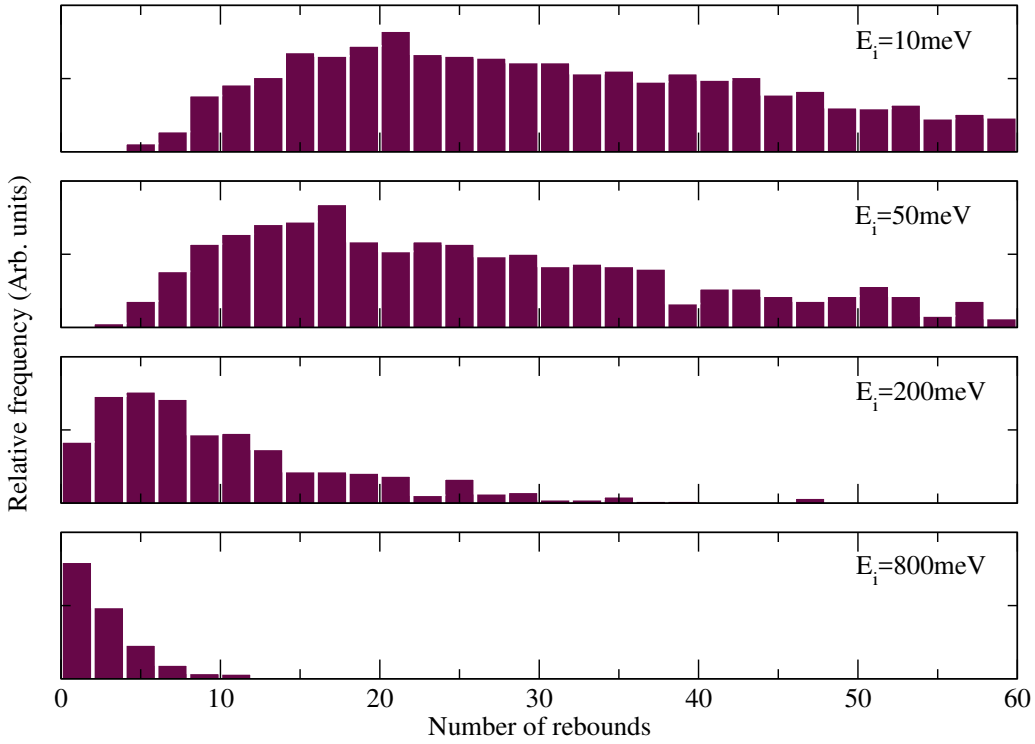

FIGURE 4.3: Distribution of the numbers of rebounds of the N_2 molecule before dissociating for different impact energies E_i. The results are for calculations under normal incidence ($\Theta_i = 0°$).

impinging on the surface with an energy of E_i=10 meV under normal incidence. Each column represents a distance Z from the surface. On top of each column the percentage of dissociating trajectories N_z is written followed by the percentage of the total amount of molecules reaching that value of Z (the latter is written in parenthesis). We can see that at a distance of Z=2.5 Å the molecules have displaced laterally towards the top sites of the unit cell, where the W atoms are located. This observation agrees with the shape of the PES at around Z=3 Å discussed in chapter 3. The attractive area at long distances is focused mainly over the top sites, spreading a bit towards the bridge sites. Looking at the distribution in the polar angle θ it is clear that the molecules tend to be oriented perpendicularly to the surface or a a bit tilted, but no parallel configurations are observed.

To understand better the differences in S_0 between functionals shown in Fig. 4.1, we can compare the approach of the trajectories for low values of E_i for the different PESs. The left panels of Fig. 4.5 show the distribution of the center of mass of the molecules able to reach a distance of Z=2.5 Å from the surface for the vdW-DF2-PES (upper panel) and the PW91-PES (bottom panel) for an impact energy

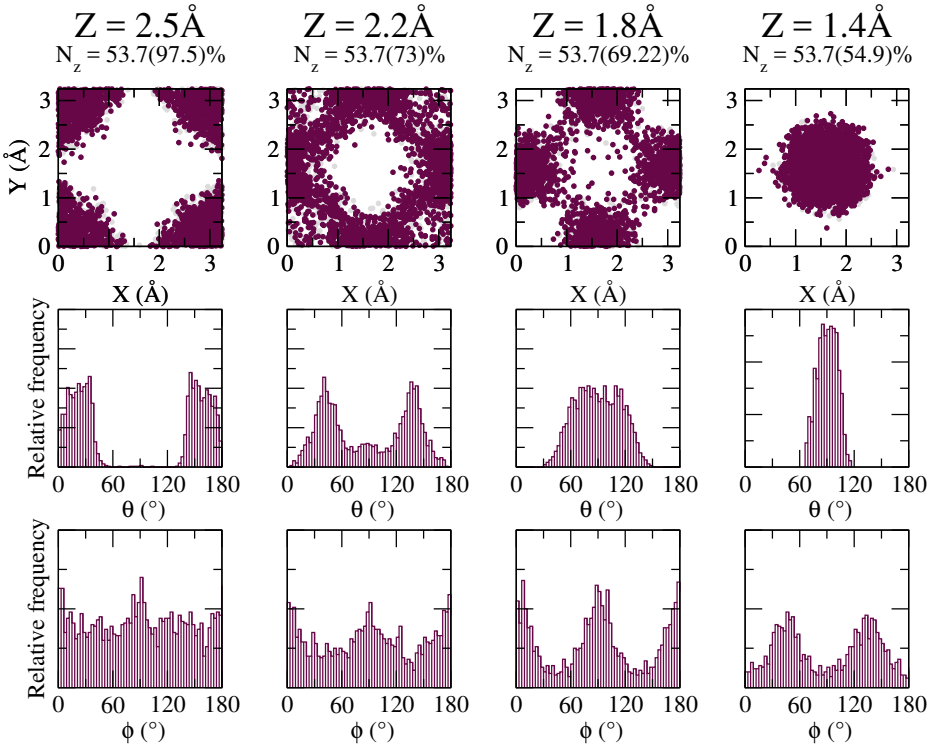

FIGURE 4.4: Evolution of N_2 trajectories on the W(100) surface. They correspond to 10 000 trajectories under normal incidence and impact energy E_i=10 meV. Top panels: position of the center of mass of the molecules at the moment of reaching a distance Z from the surface. The dissociating molecules are plotted in maroon and the total amount of molecules in grey. On top of the panels the percentage of dissociating molecules N_z reaching Z is written and the total percentage of molecules reaching Z is written in parenthesis. Middle panels: Distribution in the polar angle θ of the dissociating molecules. Bottom panels: Distribution in the azimuthal angle ϕ of the dissociating molecules.

of E_i=40 meV. This value of impact energy corresponds to the minimum obtained for S_0 when the PW91-PES is used. The right hand panel of Fig. 4.5 displays the probability for the molecules to reach this distance of 2.5 Å from the surface as a function of the initial kinetic energy. From the figure, we can see that the difference in the sticking probability at low values of E_i is related to the fact that for the PW91-PES, molecules have a wider repulsive area over the unit cell and at the particular energy of 40 meV a significant amount of trajectories are unable to move and orient in a perpendicular way, increasing the scattering probability. At higher energies this is not an issue anymore given that molecules can overcome these entrance barriers. A detailed description of this behavior can be found in Ref. [116].

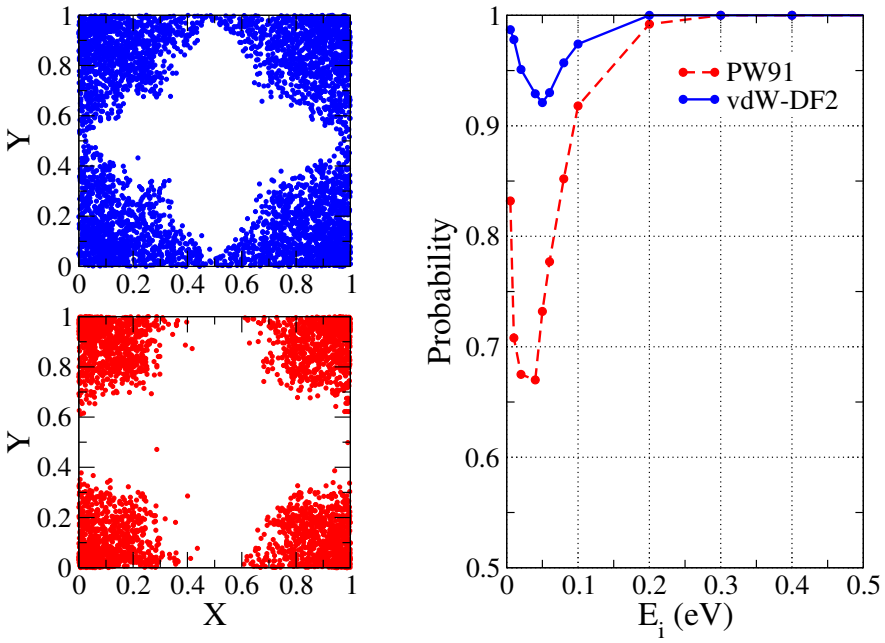

FIGURE 4.5: Left: Location of the molecular center of mass for 10 000 trajectories over the unit cell when the molecule reaches a distance of Z=2.5 Å to the surface with an impact energy of 40 meV. X and Y coordinates are given in units of the lattice constant for the vdW-DF2-PES (upper panel) and PW91-PES (bottom panel). The W atoms are located at the corners of the plots. Right: Probability for the N_2 molecules to reach a distance of Z=2.5 Å from the surface as a function of the initial kinetic energy under normal incidence for both PESs.

After reaching this value of Z=2.5 Å, Fig. 4.4 shows that the dissociating trajectories continue their paths displacing in X and Y towards the bridge site as they start to rotate in θ, having a predominant orientation to the surface of θ=50° (equivalent to θ=130°). Then, as they keep moving towards the surface, at Z=1.8 Å trajectories concentrate almost exclusively on the bridge site with a polar angle equally distributed in the range 50°<θ<130°. At this point, the dissociating molecules align almost entirely along the W-W bond ($\phi = 0°$ for the X axis and $\phi = 0°$ for the Y axis). There are very few molecules parallel to the surface and with the N atoms pointing towards the hollow site ($\phi = 90°$), configuration which was reported by Volpilhac et al. using PW91 to lead to dissociation without barrier. [25] In this case, that configuration presents a large barrier ($\approx$ 650 meV measured from the energy in vacuum) to dissociation and is less favorable energetically (See panels (c) and (d) of Fig. 3.7). Later, the molecules shift laterally in X and Y to reach the hollow site at Z=1.4 Å, where they are parallel to the surface. At this altitude, a great amount of molecules have an azimuthal angles of $\phi = 45°$ (equivalent to $\phi = 135°$). Finally, they can easily leave this molecular well to align

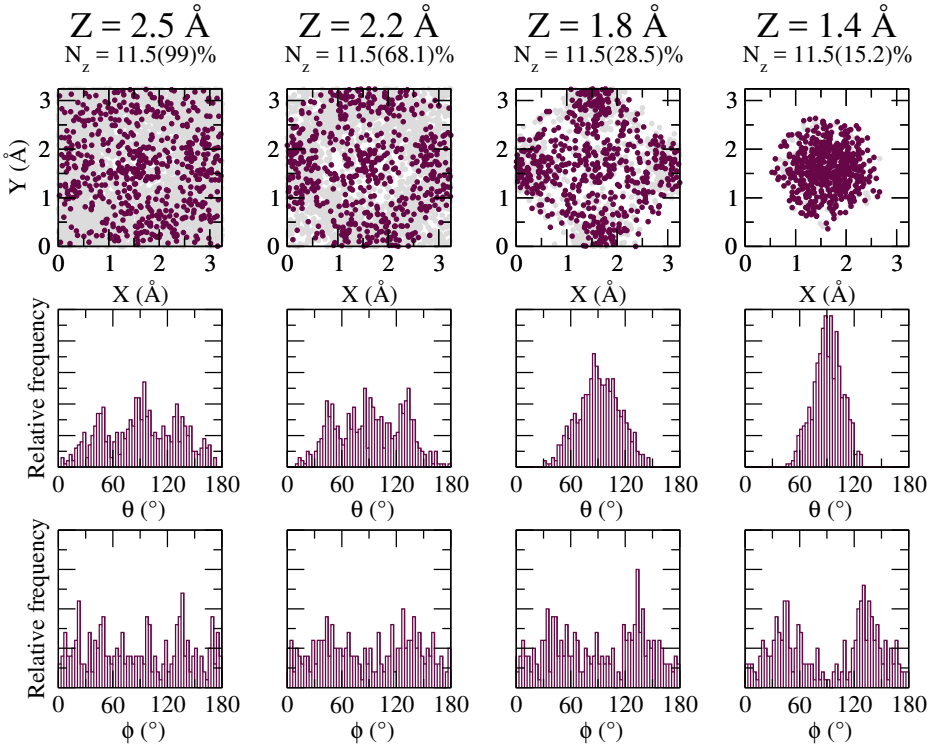

FIGURE 4.6: Same as Fig. 4.4 for E_i=200 meV.

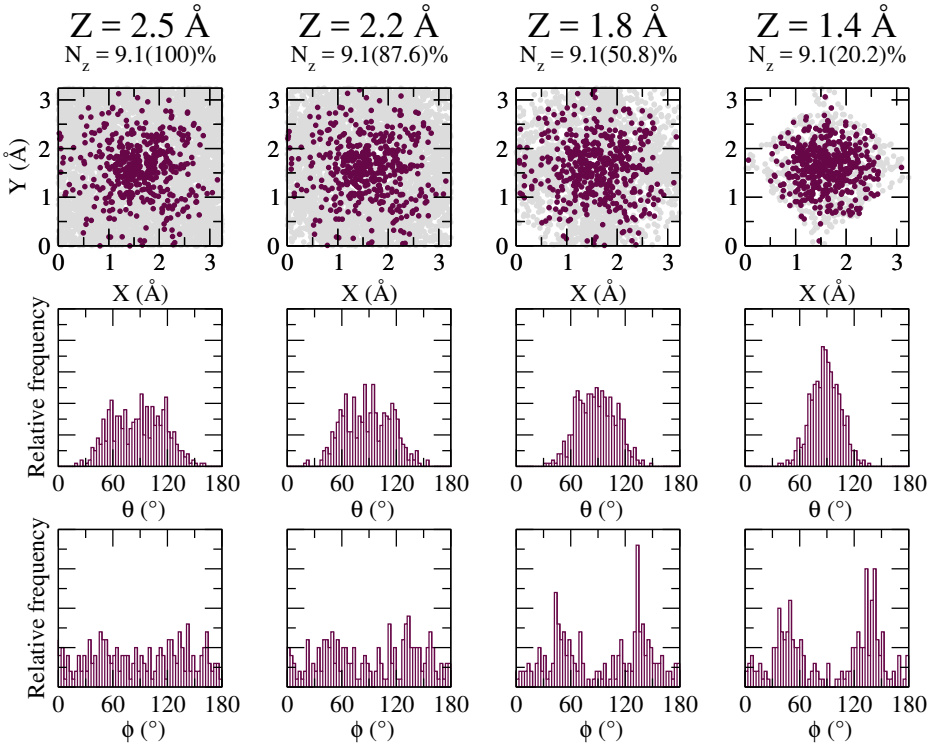

FIGURE 4.7: Same as Fig. 4.4 for E_i=800 meV.

properly to dissociate (see panels (e) and (f) of Fig. 3.7). On average, trajectories following this "indirect" mechanism spend a long time of about 15 picoseconds over the surface before dissociating.

Performing the same analysis for higher impact energies (i.e. 200 and 800 meV) we obtain the results presented in Figs. 4.6 and 4.7, respectively. As the incidence energy increases, the molecules are not restricted to approach the surface through the entrance channel over the top sites. At 200 meV (Fig. 4.6) most of the configurations can overcome the entrance energy barriers and the distribution of the molecules is equally spread over the unit cell. Then, similarly to the case where E_i=10 meV, molecules aggregate parallel to the surface in the hollow site region before dissociating. For E_i=800 meV (Fig. 4.7) the approach of the molecules is done primarily through the hollow site. In addition, practically none of the dissociating molecules have the perpendicular orientation as observed for low values of E_i.

Additonally, we can check the effect of the incidence angle on S_0. For that, we performed QCT calculations varying Θ_i. In Fig. 4.8 the sticking probability as a function of the incidence energy is presented for different values of incidence angle. No significant difference between the normal and off-normal incidences at low impact energies is observed, except for the results when Θ_i=60°. In the latter case, the value of S_0 is much smaller at low E_i. However as the energy increases, the normal incidence calculations exhibit the lower value for S_0, and the larger is the incidence angle the larger is the sticking coefficient. This effect could be due to the fact that at a more grazing incidence, the molecules can reach a configuration where dissociation is more favorable in an easier way than trajectories at normal incidence.

To understand in a better way these results, in Fig. 4.9 we show a comparison of the average number of rebounds that the molecules perform for the different incidence angles studied as a function of the impact energy. From the figure we can see that the number of rebounds decreases significantly as the incidence angle increases for every value of impact energy. These observations suggest that the molecules dissociate through a "direct" mechanism at more grazing incidence. This can also be confirmed by looking at the average time that molecules spend on the surface before dissociating. For E_i=100 meV, the dissociating molecules spend in average 6.4 ps on the surface before dissociating at normal incidence, whereas for an incidence angle of θ=60° the average time until dissociation is reduced to 1.8 ps. The precursor-mediated process or "direct" channel towards dissociation

is favored by molecules impinging at normal incidence.

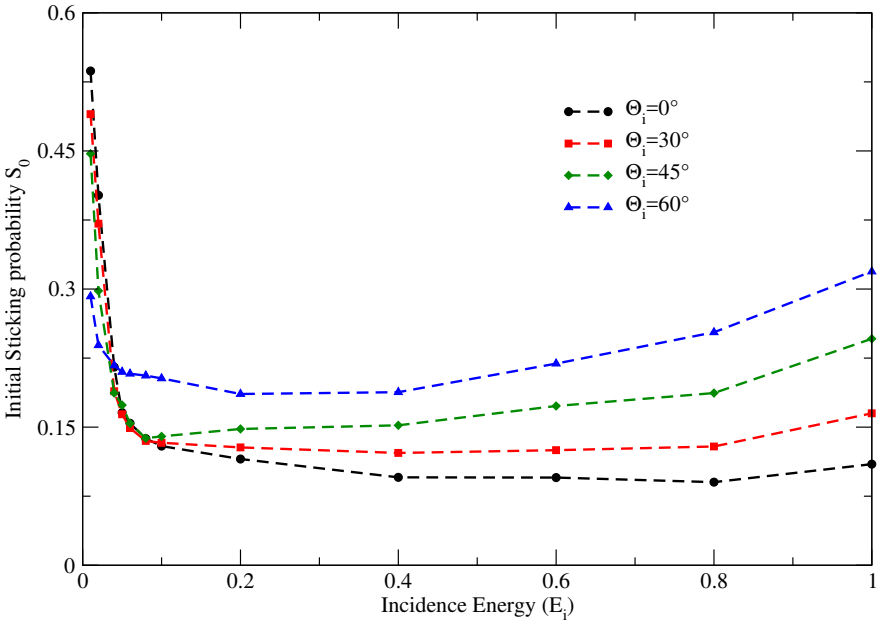

FIGURE 4.8: Initial dissociative adsorption probability S_0 as a function of the initial kinetic energy E_i for different incident angles Θ_i.

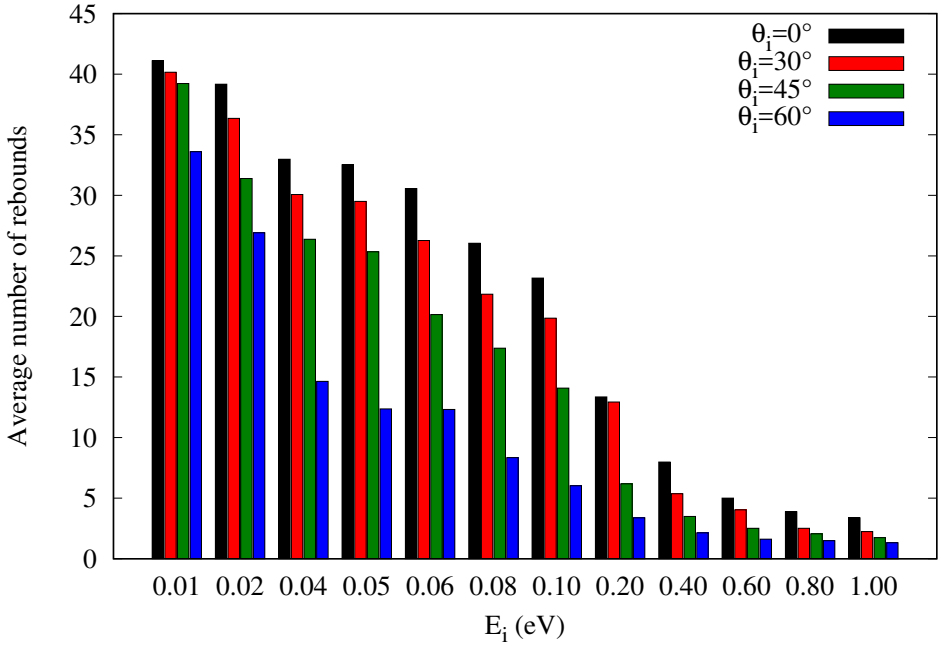

FIGURE 4.9: Average number of rebounds of the N_2 molecules before dissociating as a function of the initial kinetic energy E_i for different incident angles Θ_i.

4.4 Summary

In this chapter we have studied the dynamics of the dissociative adsorption of N_2 on the W(100) surface. We have performed quasi-classical trajectories simulation on the vdW-DF2-PES for different values of impact energy and incidence angle. The resulting sticking probability was compared to that obtained in previous theoretical works using different functionals to build the DFT-PES. In this respect, a strong effect of the choice of the XC functional on the value for the sticking probability is observed. In the low-energy regime, the vdW-DF2-PES exhibits a monotonic decay for S_0, whereas the PW91-PES shows a non-monotonic behavior not observed in experiments, and the RPBE-PES exhibits low values of S_0 due to the large repulsive character of the PES. Moreover, we have compared the probability of the molecules to overcome the barriers at Z=3 Å from the surface for both the PW91-PES and the vdW-DF2-PES. This analysis showed that a large amount of molecules are unable to reach a distance of Z=2.5 Å in the PW91-PES case, resulting in a lower value of S_0 and explains somehow the non-monotonic behavior in the shape of S_0.

Focusing on the large dissociative adsorption probability obtained at low values of E_i, we have analyzed the path that most of the molecules undergo to reach dissociation following this "indirect" channel. A clear approach is done through the top site and along the W-W bond with a molecular orientation close to perpendicular. Approaching the surface, the molecules move towards the bridge site and subsequently to the hollow site where they align in a parallel way to dissociate. This "indirect" process takes place up until $E_i \sim$100 meV. . At higher energies, the molecules dissociate without going through the precursor wells by overcoming the entrance channel barriers.

Quasi-classical simulations performed varying the initial incidence angle Θ_i showed that the greater the incidence angle, S_0 decreases at low impact energies, but increases as the energy increases. It appears that at high impact energies, the molecules can reach more easily a particular configuration that favors dissociation if the incidence angle is higher. This observation has to do with the fact that at more grazing incidence, molecules perform less rebounds (and thus, spend less time) on the surface before dissociating. In this case, the "indirect" channel is favored by molecules impinging at normal incidence.

It is worth noting that up to this point, the results have not been discussed in

relation to experimental data. Under the static surface approximation, the simulation is not taking into account energy dissipation effects, which can result in non-dissociative adsorption, not observed in the calculations of this chapter. The incorporation of the energy exchange effects has to be done in order to perform a more meaningful comparison with what is observed in experiments. This issue will be addressed in the next chapter.

Chapter 5

Energy dissipation effects in reactive scattering of N_2 on W(100)

So far, we have neglected any energy dissipation effects that can occur in the molecule-surface interactions, which are necessary to include in the simulations if we want to make a meaningful comparison with experimental data. Motivated by this and by the presence of N_2 adsorption wells on W(100), in this chapter we study also the dynamics of the non-dissociative adsorption. This process occurs when there exists an energy exchange between the diatomic molecule and the surface, and from this energy exchange the molecule can loose energy and then remain "trapped" in an adsorption well, not having enough energy to escape. To this aim, we performed new QCT calculations accounting for two different energy dissipation channels making use of the six-dimensional N2/W(100) PES that we have obtained. On one hand, we study the role of electron-hole pair excitations through the inclusion of electronic friction by means of the local density friction approximation (LDFA) [96], as described in Chapter 2. On the other hand we include surface motion and surface temperature effects using the generalized Langevin oscillator (GLO) model [85–88]. The combination of both dissipation channels has been tested as well. For simplicity we will refer to the results of this combination as LDFA+GLO.

This chapter is organized as follows: in Sec. 5.1 a description of the computational and theoretical details is given. Next, in Sec. 5.2 the usage of LDFA and GLO is tested in the dynamics and the comparison to experimental data is provided. In this chapter we also include results for *Ab Initio* Molecular Dynamics (AIMD) calculations to account for explicit movement of the surface W atoms. In sec. 5.3 we present the computational details and the main results of the AIMD simulations together with the comparison with the GLO calculations. Finally, the main conclusions of the chapter are presented in sec. 5.4.

5.1 Computational details

To go beyond the Born-Oppenheimer static surface (BOSS) approximation and to compare with experimental data, new sets of quasi-classical trajectories simulations accounting for energy exchange with the lattice and electronic friction effects were performed on the vdW-DF2-PES. Within the GLO model, the values for the frequencies associated with the surface and ghost oscillators are taken as $\omega_x = \omega_y$ =19 meV and ω_z =16 meV [117]. The friction coefficients associated to the ghost oscillators are obtained from the Debye frequencies of tungsten following Ref. [85]. All the observables studied have a low dependency on the value of these parameters, as long as they remain within the same order of magnitude (See Appendix C). In this particular work we examine temperature effects above 200 K, ignoring the c(2×2) atomic rearrangement that the W(100) undergoes below this temperature. [118, 119] On the other hand, electron-hole ($e-h$) pair excitation effects are introduced via the LDFA. For this, the electronic density is obtained from DFT calculations and is taken at each point of the trajectory as that of the surface alone at the position of the atom. The left panel of Fig. 5.1 shows the friction coefficient η for the nitrogen atom in an electron gas as a function of the mean electron radius r_s. On the right panel, the value for r_s is shown in a plane normal to the W(100) surface. The plane cuts the unit cell passing through the bridge sites (i.e.

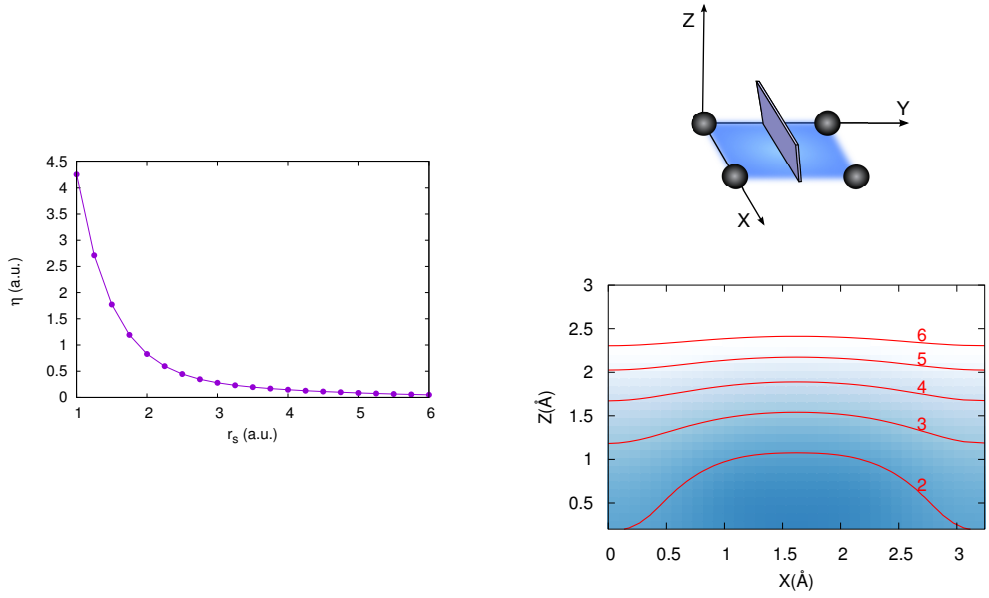

FIGURE 5.1: Left: Friction coefficient η for the nitrogen atom in an electron gas as a function of the mean electron radius r_s. Both η and r_s are given in atomic units. Upper right: Scheme of the plane normal to the W(100) surface for wich the r_s values are shown in the bottom right panel.

parallel to the W-W bond). This orientation is representative for the dissociation of N_2 as shown in previous chapters. Both models have been widely used in the past, and given their simplicity, the coupling between the two can be achieved in a simple manner. [30]

Similar to the BOSS calculations, simulated trajectories start with the center of mass (CM) of the molecule at a distance of Z=7.5 Å from the surface. The positions of the CM over the unit cell and the molecular orientations are sampled using a Monte-Carlo procedure. The initial vibrational energy of the molecules is set equal to the ZPE of N_2, E_0=142.9 meV. For each value of the impact energy E_i, 10 000 trajectories are simulated with a maximum integration time of 50 ps. In addition to the possible exit channels considered in the previous section (i.e. reflection and dissociation), here we consider the non-dissociative adsorption as well. A trajectory is said to contribute the non-dissociative adsorption curve if after the dynamics is over (in this case, after 50 ps) the molecule remains close to the surface without being dissociated.

5.2 Non-dissociative adsorption

5.2.1 Surface motion and surface temperature effects

Firstly, we check how the sticking probability is affected by introducing surface motion and temperature effects in the QCT calculations. In Fig. 5.2 we show results for the sticking probability S_0 at three different surface temperatures T_s (namely 300, 800 and 1000 K) along with the BOSS results. With respect to the static surface results, an increase in S_0 is observed in the whole range of energies shown for the three values of T_s presented. The increase in S_0 is more prominent at low values of the impact energy. When $E_i < 500$ meV a large dependence of S_0 with the surface temperature T_s is obtained. At the lowest impact energy computed (i.e. E_i=10 meV) the sticking coefficient at T_s=1000 K is half of that obtained at T_s=300 K. This is due to the fact that when the surface temperature increases the surface atoms move faster, and this might give low-energy adsorbed molecules enough energy to escape a potential minima in which they are "trapped". This would allow them to go back to the gas-phase and cause a reduction of S_0. As the impact energy increases, molecules may overcome entrance barriers and other energy barriers present close to the surface regardless of the surface temperature, presenting as a consequence a convergence in the sticking coefficients for the different values of T_s.

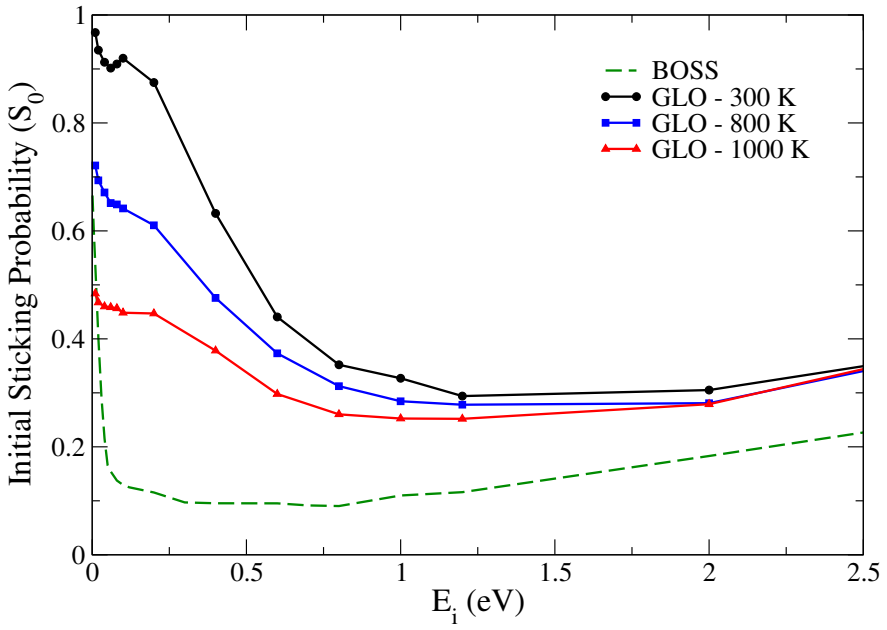

FIGURE 5.2: Total sticking probability S_0 as a function of impact energy for static surface (green dashed) and using GLO for three different surface temperatures T_s. Calculations were performed under normal incidence conditions.

The dependence of S_0 for low-energy molecules with the surface temperature has been observed experimentally in the past. [21, 22] In Fig. 5.3 we present a comparison between the experimental data and the results obtained within the GLO model. The sticking probability includes both dissociative and non-dissociative adsorption. It can be seen that a qualitative agreement in the trend of S_0 between theory and experiments is achieved. In particular, this is the case for the already discussed temperature dependence at low values of E_i, which is a feature that was not obtained with other potential energy surfaces. [116] However, with these results, an overall overestimation of S_0 in the whole range of energies is obtained. To understand better the effect of accounting for energy exchange with the lattice in S_0, we can decompose the sticking probability into dissociative and non-dissociative adsorption. In Fig. 5.4 we present the decomposition for the three values of T_s studied. We observe that for T_s=300 K, at low values of E_i the contribution to S_0 comes almost exclusively from non-dissociative adsorption, then it decreases as the energy increases along with the dissociative adsorption contribution. For higher values of T_s, dissociative adsorption has the largest contribution to S_0 in the whole range of energies.

Further analysis of the case in which non-dissociative adsorption takes its highest values, that is, with T_s=300 K and collision energy of E_i=10 meV, is made

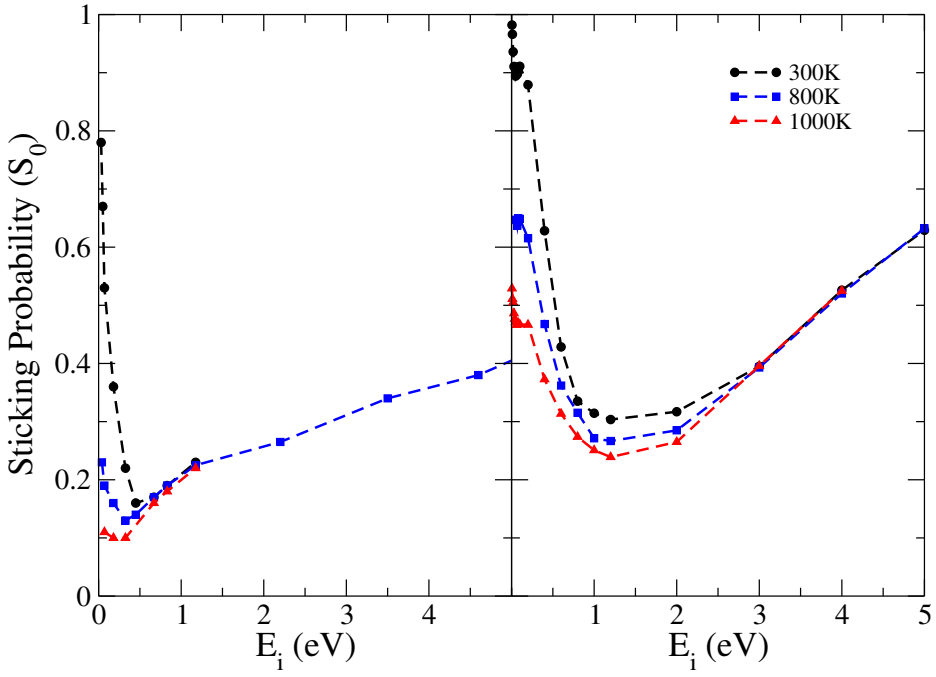

FIGURE 5.3: Left panel: Exprimental sticking probability S_0 as a function of impact energy for T_s=300, 800 and 1000 K. Data extracted from [22]. Right panel: Sticking probabilities obtained obtained within the GLO model for the same values of T_s. Calculations were performed under normal incidence conditions.

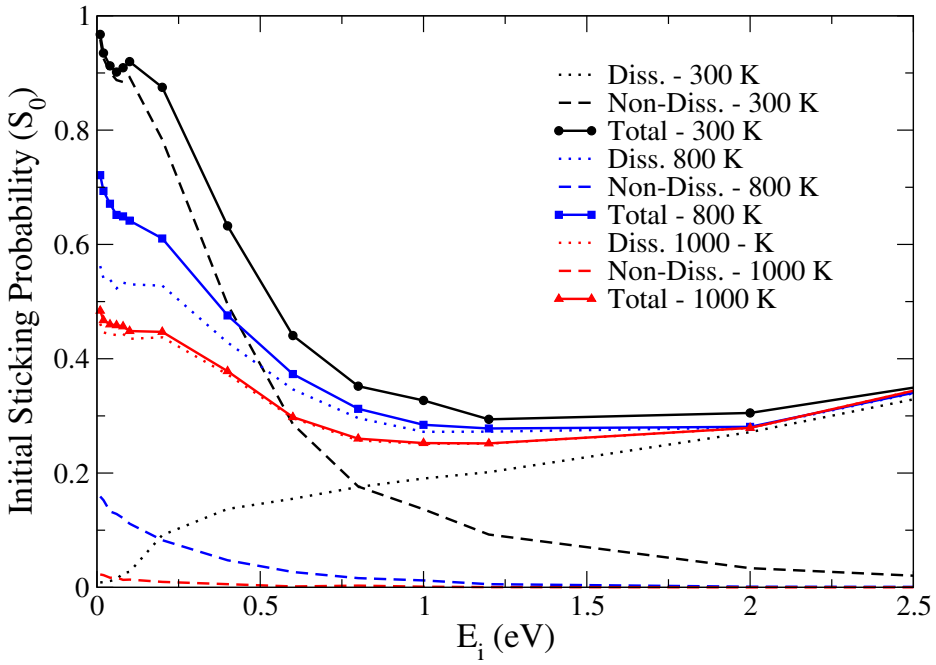

FIGURE 5.4: Decomposition of the sticking probability S_0 (solid lines) into dissociative (dotted lines) and non-dissociative (dashed lines) adsorption for three values of surface temperature T_s as a function of the impact energy E_i.

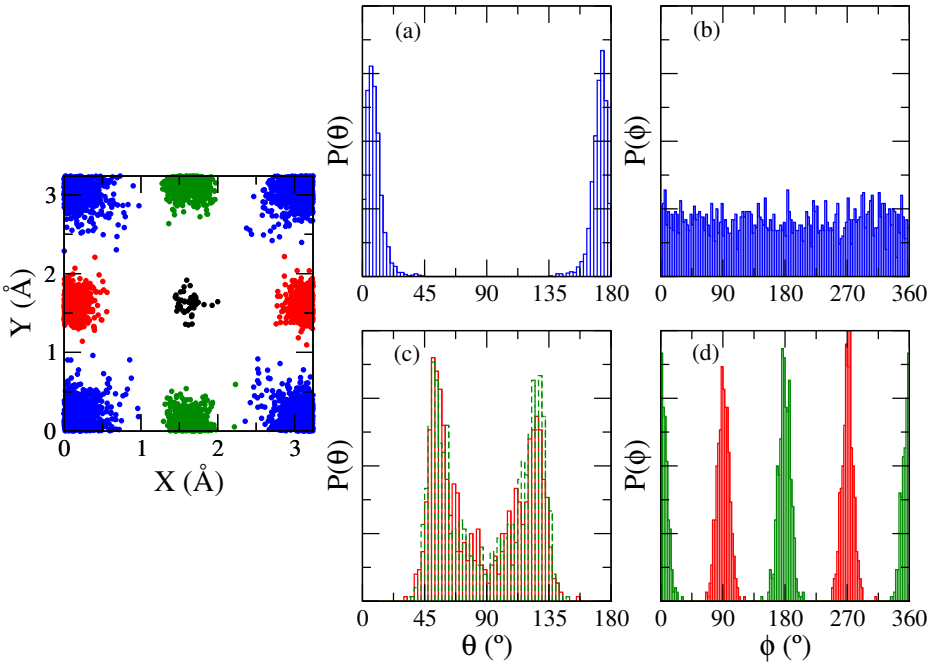

FIGURE 5.5: Left panel: Distribution of the center of mass of the molecules over the unit cell at the end of the dynamics calculations performed with GLO under normal incidence. Initial kinetic energy is E_i=10 meV and surface temperature is T_s=300 K. Blue points represent molecules with its center of mass over the top site, red and green over the bridge site and black over the hollow site. Panels (a) and (b) show the distribution in θ for the molecules over the top and bridges sites, respectively, panel (c) shows the distribution in ϕ for molecules over the bridge site. The color criteria in panels a,b,c and d corresponds to that used in the left panel.

by checking the distribution of the center of mass of the molecularly adsorbed molecules at the end of the dynamics. On the left panel of Fig. 5.5 we present the position of the center of mass over the unit cell for the molecules that remain "trapped" close to the surface at the end of the dynamics (50 ps from an initial set of 10 000 trajectories. Under these conditions, non-dissociative adsorption amounts to almost 96% of the trajectories: 60% correspond to molecules adsorbed over the top site, 35% over the bridge site and less than 1% remain over the hollow site. In panels (a) and (b) of Fig. 5.5 we show the distribution in the polar θ and azimuthal ϕ angles respectively of the molecules adsorbed over the top site. In panels (c) and (d) we show the same distributions for the molecules adsorbed over the bridge site. With this information, it becomes clear that the N_2 molecules stay in the potential minima found and discussed in Chapter 3. Molecules located in the potential minimum over the bridge site are always aligned with the W-W bond. As for the few remaining molecules in the hollow site, they end up adsorbed in the potential minima described in the previous section where they have

a polar angle θ close to 90° and an azimuthal angle ϕ close to 45°.

5.2.2 *e-h* pair excitation effects

The sticking probabilities S_0 of N_2 on the W(100) surface with and without the inclusion of electronic friction are presented in Fig. 5.6. The results are presented as a function of the incidence energy E_i and under normal incidence. Results show an increase of S_0 for E_i<700 meV when we include electronic friction effects, where the most significant changes are observed when E_i<200 meV. This is precisely the regime of energies where the molecules follow the "indirect" channel towards dissociation explained in previous chapters.

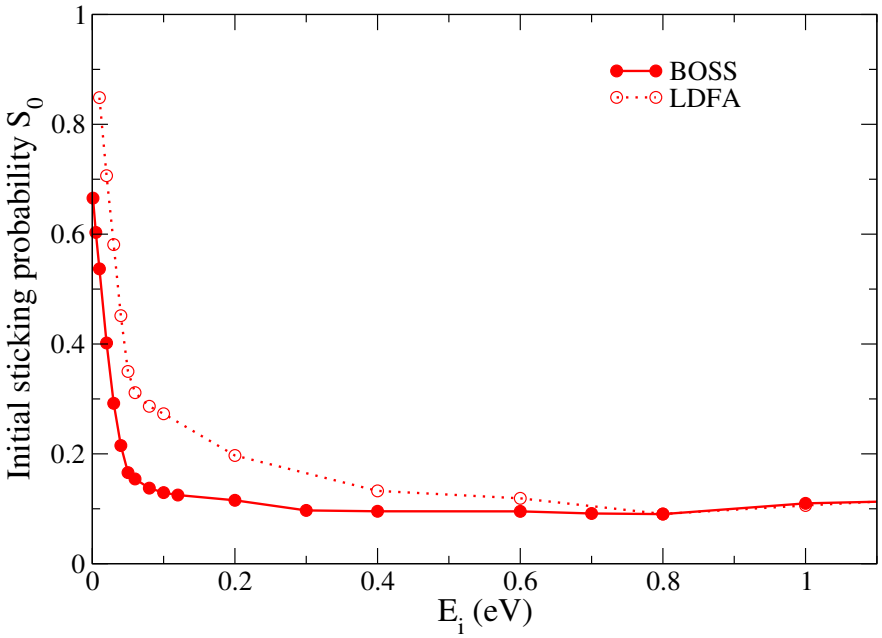

FIGURE 5.6: Initial sticking coefficient S_0 as a function of the impact energy E_i for N_2 over W(100) under normal incidence. Full red circles (red open circles) correspond to results obtained with (without) electronic friction.

t

A more thorough analysis of the LDFA results is presented in Fig. 5.7, where the total sticking probability obtained including friction effects is decomposed into dissociative and non-dissociative adsorption. It can be seen that at low values of impact energy, S_0 is dominated by this non-dissociative adsorption. This observation is consistent with the fact that under these conditions the molecules spend some time in the molecular wells present in the PES, and when the molecule loses enough energy (caused in this case by the introduction of electronic friction), it

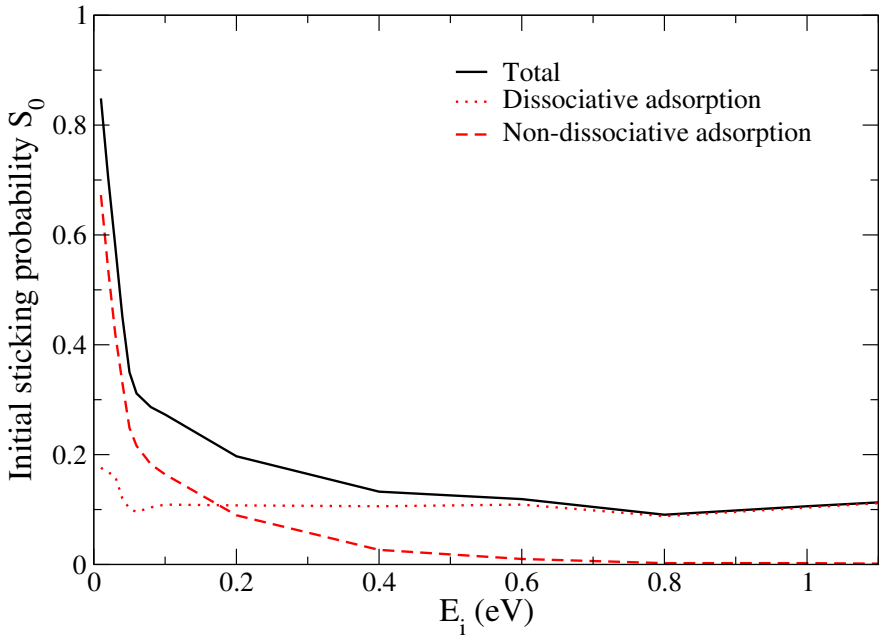

FIGURE 5.7: Decomposition of the initial sticking coefficient S_0 into dissociative and non dissociative adsorption contributions as a function of the impact energy E_i obtained under normal incidence including electronic friction.

remains "trapped" in one of the local minima present. On the other hand, the dissociative adsorption probability is roughly constant in the range of energies shown, and for values of $E_i \geq 600$ meV, it represents the only contribution to S_0.

We can perform the same analysis as with the GLO calculations for the molecularly adsorbed molecules at a low value of impact energy (i.e. E_i=10 meV) regarding its final position. At the end of the dynamics the trajectories are distributed as follows: out of the total amount of adsorbed molecules, 22% are located in the top site (X=0,Y=0) with a polar orientation close to θ=0° at an average distance of Z=2.65Å from the surface, 66% are located in the bridge sites (X=a/2,Y=0) with θ=50°, ϕ=0° (or ϕ=90°, depending on the axis, always being aligned with the W-W bond) and Z=2.0Å. The remaining 12% have their center of mass located over the hollow site (X=a/2,Y=a/2) with θ=90°, ϕ=45° and Z=1.25Å. One notable result is the fact that although the top site is more attractive when the molecule is approaching the surface, it is the bridge site that ends up with the largest percentage of molecules at the end of the dynamics.

5.2.3 GLO+LDFA

Finally, we have also combined both dissipations channels to calculate the sticking probability. In Fig. 5.8 we present the comparison between GLO and GLO+LDFA

results. No significant change is noticed in S_0 when electronic friction is included in the GLO dynamics. From these results we can state that the energy exchange with the lattice phonons appears to play a major role for this particular system in comparison with the energy loss due to $e-h$ pair excitations. The qualitative agreement in the trend of S_0 with experiments is observed in the same way as in Fig. 5.3, where at low values of E_i, a clear dependence of S_0 with T_s is observed in both theory and experiments. As the energy increases, S_0 tends towards the same value regardless of the surface temperature. It is important to note that even though there is still an overestimation of S_0, our results represent an upper bound for S_0. We cannot exclude that a small number of the molecules that remain adsorbed after 50 ps, can not go back to vacuum at longer times.

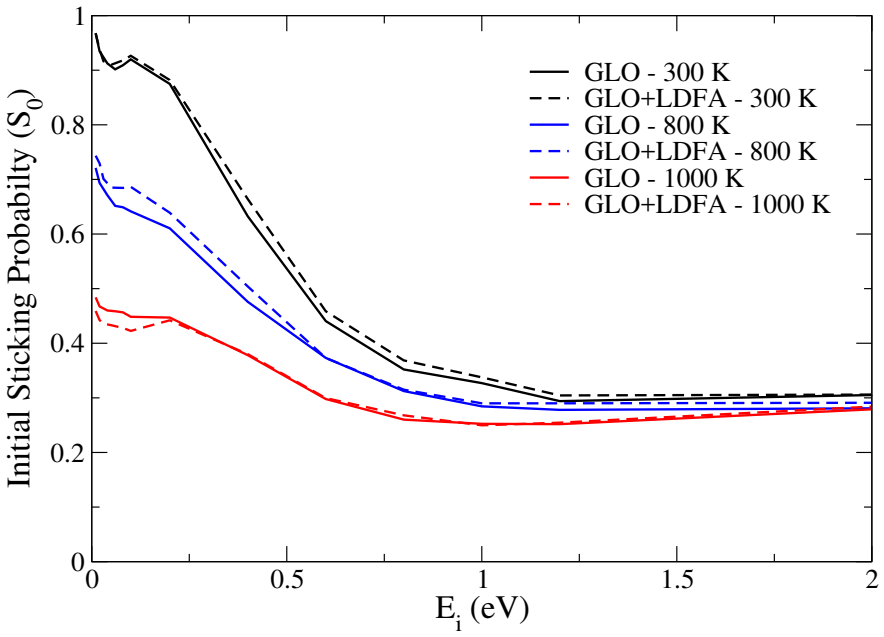

FIGURE 5.8: Initial sticking probabilities as a function of the initial kinetic energy for GLO (solid lines) and GLO+LDFA (dashed lines) calculations under normal incidence.

Even though the effect of electronic friction on S_0 is minimal in comparison with the effect of energy exchange with the lattice, we do observe changes in the ratio between dissociative and non-dissociative adsorption mechanisms when performing GLO+LDFA calculations. In Fig. 5.9 we have decomposed S_0 for both the GLO and GLO+LDFA data obtained under normal incidence into dissociative (left panel) and molecular adsorption (right panel) contributions. In general, what we observe is a reduction in the dissociation probability when including electronic friction and, as a consequence, non-dissociative molecular adsorption probability

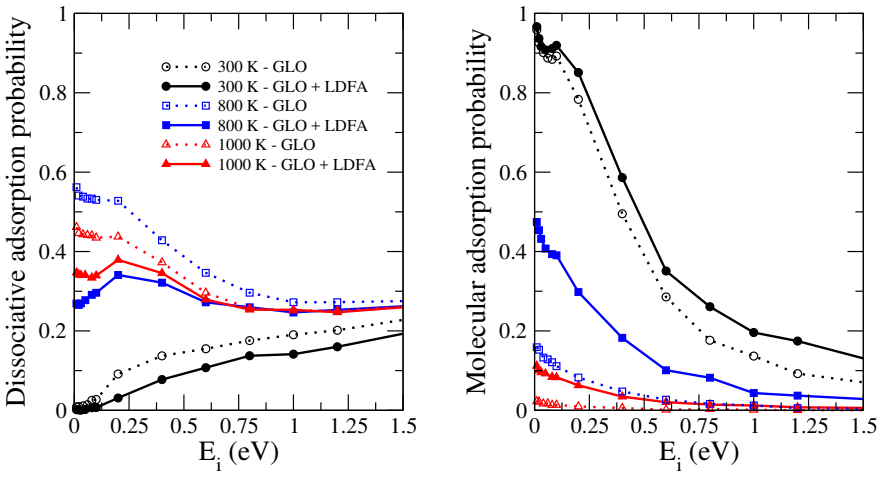

FIGURE 5.9: Left panel: Dissociative adsorption probability as a function of incidence energy for three different surface temperatures T_s under normal incidence conditions using GLO with (filled symbols and solid lines) and without (empty symbols and dotted lines) electronic friction. Right panel: Molecular adsorption probability, same conventions are used.

is enhanced. The most prominent changes appear in the low energy regime for T_s=800 K. In this case, a decrease in the dissociation probability of more than a 30% is observed at almost zero impact energy. This result is a direct consequence of including both energy dissipation effects in the dynamics, since molecules are more likely to remain adsorbed and not go towards dissociation due to energy losses. Regarding the molecular adsorption probability (right panel of Fig. 5.9), the counterbalance of the reduction in the dissociative adsorption is clear. For all values of T_s the molecular adsorption is higher when $e-h$ pair excitations are taken into acount. Again, this effect is more prominent at low values of the impact energy and when T_s=800 K.

5.3 *Ab Initio* Molecular Dynamics

As we have seen, the GLO is a commonly used model to account for surface motion during the dynamics. However, the model is not capable to describe the possible distortions on the lattice that can occur when a molecule spends a large amount of time over the surface, changing the shape of the PES. To tackle this, *Ab Initio* Molecular Dynamics (AIMD) is usually chosen as a methodology to account explicitely for the movement of the surface atoms. [120–123] The AIMD approach is a DFT-based methodology where the forces acting on the atoms are computed

on the fly.

In our calculations, the W(100) surface is modelled by a five-layer (3×3) periodic slab. The use of a bigger cell is necessary to avoid spurious periodic distortions. The initial positions and velocities of the W surface atoms are those of different configurations obtained from a previous thermalization of the surface. The thermalization is done for each value of the surface temperature T_s and run for 5000 steps with a time step of 0.7 fs. An example of this is shown in Fig. 5.10. In order this choice of initial conditions is physically meaningful, we need to make sure that the stantard deviation of the temperature obtained is in the same order of magnitude as that calculated from the equations of a canonical ensemble, where the standard deviation in T can be expressed as:

$$\sqrt{\langle T^2\rangle - \langle T\rangle^2} = \frac{2}{3}\frac{T}{N}\sqrt{\frac{C_v}{N_A k}} \tag{5.1}$$

In Eq. 5.1 N is the number of thermalized atoms in the surface, C_v is the specific heat of the metal, and N_A and k correspond to Avogadro's and Boltzmann constants respectively. For the case in which T=300 K, a theoretical value of $\sqrt{\langle T^2\rangle - \langle T\rangle^2}$=6.35 K is obtained. This value compares well to 6.80 K, which is the value obtained following the thermalization procedure stated above starting from equilibrium (See Fig. 5.10).

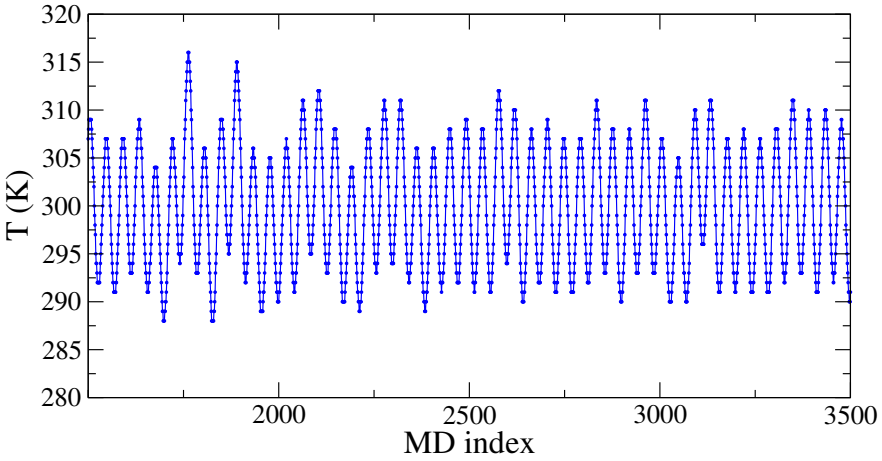

FIGURE 5.10: Surface temperature as a function of time for the thermalization of the bare W(100) surface with an initial temperature of T_s=300 K. The thermalization is performed employing a Nose-Hoover thermostat.

We performed calculations for three values of the initial kinetic energy: E_i=50, 250 and 600 meV for two surface temperatures, T_s=300 and T_s=800 K. For each

value of the impact energy, 100 trajectories were simulated allowing the first three W layers to move. Each N_2 molecule started with the center of mass at a distance of Z_{cm}=7 Å from the surface with the equilibrium internuclear distance. The position in X and Y and the molecular orientation were taken randomly from a Monte Carlo sampling. The time step for solving the classical equations of motion was taken as 0.7 fs to ensure conservation of the energy. The simulations were computed for 3572 steps to end up with an upper time of 2.5 ps per trajectory. The evolution of the altitude of the center of mass and the N-N distance were followed at each time step to check if the molecule was reflected (Z_{cm}>7 Å) or dissociated (r>2.4 Å).

In Fig. 5.11 we show AIMD results for the sticking probability as a function of the impact energy for the three selected values of E_i and a surface temperature of T_s=300 K and T_s=800 K. Results obtained from GLO simulations and experimental data taken from [25] are presented as well. It can be seen that for T_s=300 K, accounting for the individual movement of the surface atoms results in more molecules being reflected than in the GLO approximation and thus, in a decrease of S_0 for the three values of E_i calculated. The values of S_0 are in better agreement with experiments than those obtained within the GLO approximation. In the T_s=800 K case, the same trend is observed when E_i=250 meV and E_i=600 meV, reaching an almost quantitative agreement in the latter case. However, for low-energy N_2 molecules (when E_i=50 meV) we obtain a higher value of S_0.

It is important to remark that due to the computational cost the simulations were limited to 2.5 ps. So in order to understand the reason of this increase in S_0 for low values of E_i at T_s=800 K we first checked the value for S_0 in the GLO calculations at t=2.5 ps, as in our AIMD calculations. From this comparison, we obtained the same value of S_0 for both methodologies. This result agrees with the fact that for this system the low-energy molecules tend to spend a large amount of time over the surface before dissociating or even be reflected back. So 2.5 ps is a too short time to know what will happen with most of the trajectories. Note that this assertion only applies to high values of T_s, since for T_s=300 K the value of S_0 obtained after 2.5 ps is practically the same as that obtained after 50 ps. At high values of T_s, molecules appear to spend more time at the surface before being adsorbed or scattered.

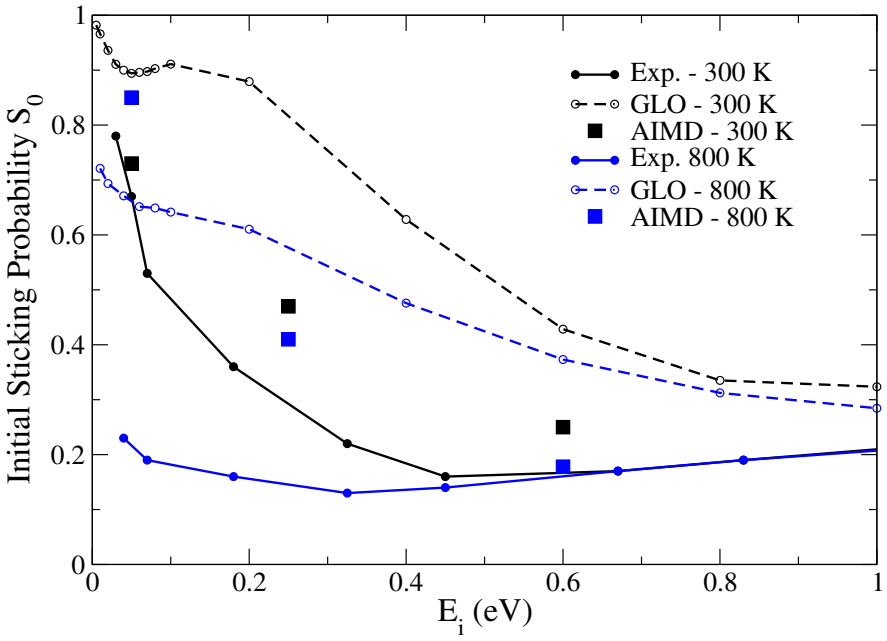

FIGURE 5.11: Initial sticking probability S_0 of N_2 on W(100) as a function of the impact energy E_i for experiments (solid lines), GLO results (dashed lines) and AIMD results (squares). All calculations were done under normal incidence.

With the aim of explaining the overestimation of S_0 at T_s=800 K and low impact energies. We characterized the adsorbed molecules following the kinetic energy of the adsorbed trajectories throughout the dynamics. We observed that the molecules that remain "trapped" at the end of the dynamics can be grouped in four cases. In Fig. 5.12 we present the evolution of the kinetic energy of four trajectories representing these cases with an initial impact energy of E_i=50 meV.

When molecules are approaching the surface they can:

- Be trapped directly over the attractive top site and remain adsorbed there (black line)
- Enter the top site and bounce out of it to diffuse over the surface (blue line)
- Approach through a non-attractive zone and diffuse until reaching a potential well to be adsorbed (red line)
- Diffuse over the surface during the whole time without entering a potential minimum or being reflected back (orange line)

To visualize the final state of the molecules in the dynamics, we show in Fig. 5.13 a distribution of the center of mass of the molecularly adsorbed trajectories for an impact energy of 50 meV and T_s=800 K. The red and green points correspond to

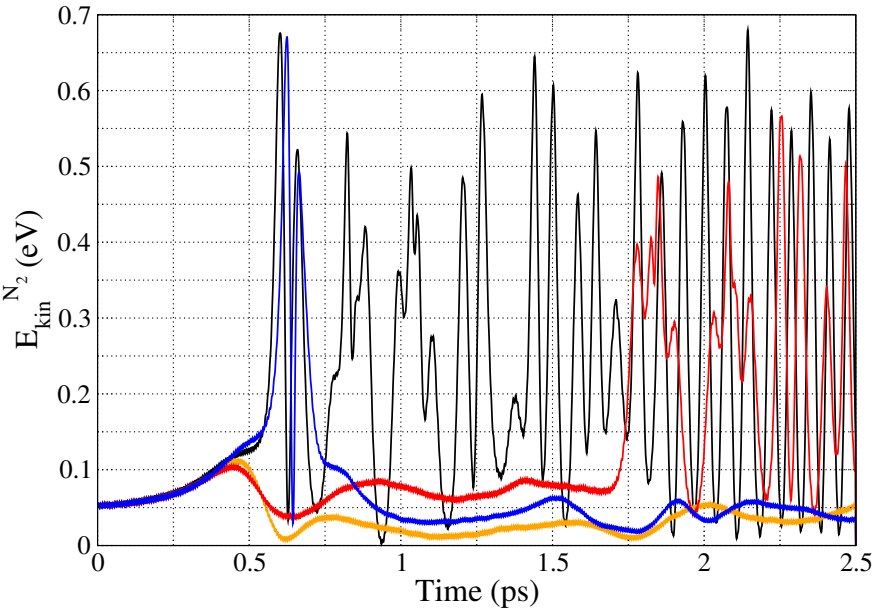

FIGURE 5.12: Evolution of the kinetic energy of N_2 for four trajectories throughout the dynamics. Each color represents a different trajectory. The initial kinetic energy is E_i=50 meV and the surface temperature is T_s=800 K.

molecules adsorbed on the top and bridge sites respectively, and the blue points are the molecules that are diffusing over the surface at the end of the dynamics. As it can be seen, a large amount of molecules that are considered as molecularly adsorbed are actually diffusing on the surface without entering a potential minimum. To see what actually happens with these trajectories, we took 10 out of the molecularly adsorbed trajectories that have not entered a potential minimum after the 2.5 ps and extended the dynamics time up to 10 ps. Interestingly, out of the 10 trajectories, 4 of them were reflected at the end of the simulation, 3 entered the adsorption well in the top site and 3 remained diffusing on the surface. If we extrapolate this result, the sticking probability obtained for E_i=50 meV and T_s=800 K would be reduced in almost in one half, getting closer to what it is observed experimentally. However, to have a meaningful statistical average, more trajectories have to be computed for longer times.

It can also be seen that from the molecules that reach a potential minimum, the majority are located on the top site, and only five trajectories reach the minimum on the bridge site. On top of each point representing a trajectory in Fig. 5.13 the polar angle is indicated. The orientation of the molecules on the top and bridge minima agrees with that observed in the GLO calculations, where an orientation close to vertical is preferred over the top site and molecules on the bridge site are tilted around $\theta = 50^{\circ}$. On the other hand, the blue trajectories are rotating during

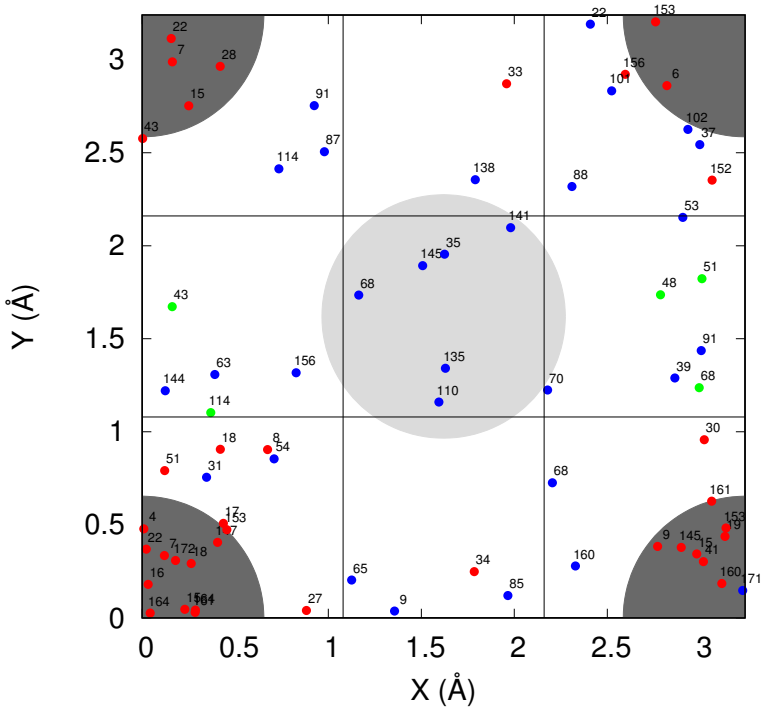

FIGURE 5.13: Position over the unit cell (X,Y) of the center of mass of the N_2 molecules that remain molecularly adsorbed at the end of the dynamics. Molecules adsorbed on the top and bridge sites are in red and green, respectively, blue points represent the trajectories diffusing over the surface without entering a potential minimum. Grey circles represent the W surface atoms. The polar angle of the final state of the N_2 molecules is written on top of each trajectory.

their diffusion over the surface, so the orientation at the end of the dynamics does not appear to be meaningful.

In addition to the final orientation of the molecules, another meaninful information comes from the average kinetic energy of the adsorbed molecules. Fig. 5.14 shows this result for the GLO and AIMD calculations. For both cases, the kinetic energy of the molecules increases when they reach the attractive part of the PES after 0.5 ps, then it tends to decrease more abruptly in the GLO case, where after 2.5 ps the average kinetic energy is almost 0.1 eV lower than that obtained with AIMD. This result could explain why more molecules are able to go towards the minimum on the bridge site in the case of the GLO dynamics and why most of them remain adsorbed on the top site for the AIMD results. From the energy scheme shown in Fig. 3.8, we can see that if a molecule enters the minimum on the bridge site, it needs around 150 meV to overcome the diffussion energy barrier towards the minimum in the top site. From Fig. 5.14 we observe that the

average kinetic energy of the molecules in GLO calculations is under this threshold, whereas in AIMD simulations, molecules have the necessary energy to escape the minimum in the bridge site. The energy barrier in the opposite direction has a height of around 250 meV. Meaning that once a molecule enters the minimum in the top site, it cannot go back to the bridge site if its energy is below this value, which is the case for both GLO and AIMD trajectories as can be observed in Fig. 5.14. It is worth noting that the movement of the surface atoms can change the shape of the PES and make some areas less accesible for the trajectories.

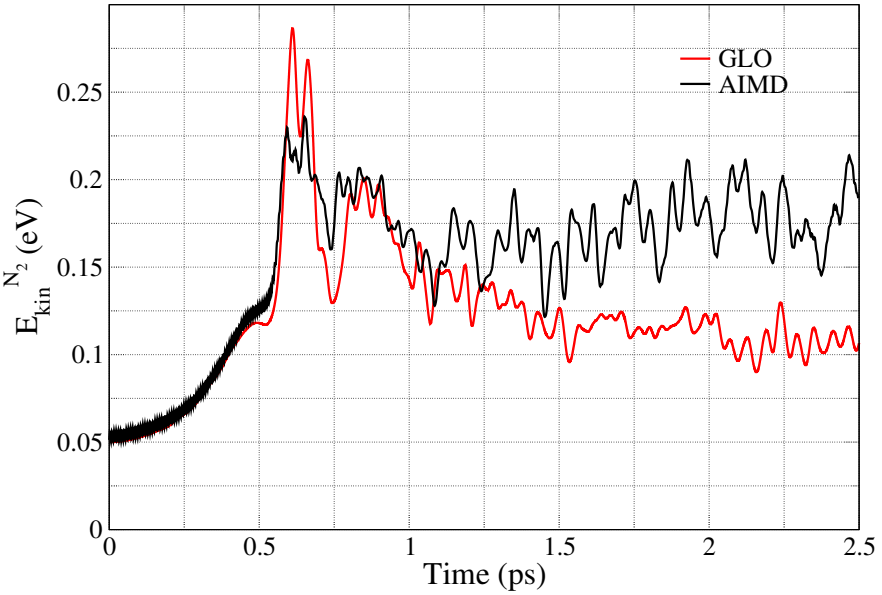

FIGURE 5.14: Average kinetic energy for the molecularly adsorbed trajectories with initial energy of E_i=50 meV as a function of time for GLO and AIMD calculations. The surface temperature is T_s=800 K

5.4 Summary

In summary, we have studied the effect of including energy dissipation channels through energy exchange with the electrons and phonons of the lattice in the dynamics of N_2 on W(100). The usage of both GLO and LDFA in the dynamics preserves the multi-dimensionality of the PES while allowing to introduce the energy dissipation terms. In comparison to the BOSS results, GLO and LDFA data exhibit an overall increase in the sticking probability, being particularly high at low values of the impact energy. This effect is related to the “indirect" dissociation mechanism found in the BOSS calculations. When energy exchange with the lattice is included in the calculations, molecules following the "indirect" path lose

energy and stay adsorbed moelcularly in the minima of the PES present along the path. A characterization of the adsorbed molecules show that they end up located exclusively in the local minima present in the top, bridge and hollow sites. The energy exchange with phonons plays a bigger role, whereas the inclusion of electronic friction does not affect significantly the total sticking probability. However, accounting for $e-h$ pair excitations changes the ratio between dissociative and molecular adsorption, increasing the latter and thus, decreasing the dissociation.

In addition, results obtained from AIMD simulations for selected values of impact energies and two surface temperatures show that accounting for individual explicit movement of the W surface atoms lowers the value for the sticking probability, reaching a better agreement with experimental data. However, the results also show that longer dynamics are needed for a better description, particularly at low values of initial kinetic energy.

Chapter 6

Dynamics of Eley-Rideal recombination and non-reactive Scattering of N_2 on W(100)

In view of the significant improvement in the description of the adsorption of N_2 on W(100) with the vdW-DF2-PES presented in the previous chapters, here we report results of dynamics simulations carried out for two other kind of reactions involving interactions betweens N, N_2 and W(100).

Using QCT method, we explored the Eley-Rideal recombination of N_2 over W(100) making use of the vdW-DF2-PES. In Sec. 6.1 we present a brief overview of the past studies, followed by the computational details to study this molecular recombination mechanism. Then, the main results for the reactive cross sections are shown in in Sec. 6.1.2. In Sec. 6.1.3 we present the results of the simulations including the effect of energy exchange with phonons. We also studied the non-reactive scattering of N_2 on W(100). In Sec. 6.2 we present the main results for this process accouting for energy dissipation with phonons and electrons. Finally, we summarize in Sec. 6.3

6.1 Eley-Rideal recombination dynamics

Besides the extensively studied adsorption of N_2 molecules on surfaces, the recombination of a N atom with a pre-adsorbed N atom has also been subject to many recent studies. The theoretical proposition of Eley-Rideal (ER) processes was made in the late 1940s [124, 125], however, experimental evidence was not observed until 50 years later for H_2 reacting on metals [126–128]. It was shown that these processes exhibited small cross sections and showed that the recombination process is done mainly via a hot atom (HA) mechanism [129–134]. In this

process, an atom is deflected with a motion parallel to the surface upon collision with the surface. Then, before being thermalized on the surface, it may react with another adsorbed atom and go to the gas phase as a molecule. ER process on the other hand, is a more direct mechanism that involves a single collision between the projectile and the adsorbed specie. Both ER and HA mechanisms are characterized by short reaction times (sub-picosecond order), whereas a third recombination mechanism, such as the Langmuir-Hinshelwood (LH) it is said to occur in a larger time scale given that both atoms are thermalized before recombination (i.e. only fast atoms of the Boltzmann distribution are able to react). For the case of H_2 recombinating on metallic surfaces, ER processes have been found to be around one order of magnitude less likely to occur than HA processes [135–138].

In the case of N_2 on the W(100) surface, a value for the adsorption energy of the N atom measured from the bottom of the lowest potential minimum (around 7 eV) has been observed both experimentally and theoretically [139]. Due to this high value of adsorption energy, a recombination of the LH type has a large endothermicity and is it not expected to occur easily. On the other hand, ER and HA processes have been described as exothermic and thus, more likely to occur when a projectile hits a thermalized atom. In view of this, theoretical works have adressed this reaction making use of DFT-based potential energy surfaces and extensions of the London-Eyring-Polanyi-Sato (LEPS) function to describe the six-dimensional PES [102, 138, 140–143]. In these works, the authors found a particular potential energy bump (for the W(100) surface) of about 500 meV located above the adsorbed N atom preventing thus a direct collision between the projectile and the adsorbate with a close to zero impact parameter. This repulsive potential structure plays a major role in the whole recombination process. In addition, they report the HA formation as one order of magnitude more probable than ER recombination.

6.1.1 Computational details

All the simulations are performed within quasi-classical initial conditions in which the zero point energy (ZPE) of the adsorbate atom is included in the initial conditions of the trajectories. Within the molecular dynamics calculation, the adsorbate is placed in the lowest adsorption energy site (X_A=0.5a, Y_A=0.5a, Z_A=0.7 Å) and it is given initial energies and random initial vibrational phases corresponding to the quasi-classical ZPE of each mode within the harmonic approximation. Each

DOF (X, Y and Z) is picked randomly in the interval between the classical turning points. The knowledge of the position determines the momentum absolute value for each coordinate and its direction is then chosen randomly.

All the calculations were performed using the vdW-DF2-PES, restricted to the description of only one adsorbed atom and one projectile (i.e. zero coverage limit). In Fig. 6.1 we show the topology of the vdW-DF2-PES in the ER entrance channel along with data using different functionals. The 2D cuts are shown as a function of the altitude of the projectile (Z_P) and the impact parameter (b) with respect to the adsorbed atom, which is schematically explained in the top panel of Fig. 6.1. The 2D (Z_P-b) cuts are presented for the vdW-DF2-PES and for calculations done using the PW91 functional, the RPBE functional and a flexible periodic LEPS (FPLEPS) as reported in Ref. [138]. Looking at the ER entrance channel for the different functionals, a clear difference in the potential energy topology in a region of Z_P located above the already adsorbed atom can be noticed. For all cases (except for the vdW-DF2-PES) the potential energy bump is above the zero of the potential energy. The RPBE exhibits a greater repulsive energy barrier, while the PW91 is slightly less repulsive. The results obtained with the FPLEPS show a repulsive barrier of around 500 meV, being somewhere in between the PW91 and the RPBE. For the vdW-DF2-PES, the interaction between the projectile and the adsorbate is purely attractive and no energy bumps is present. This vanishing of the repulsive area when the projectile approaches the surface on top of the adsorbate agrees with our observations of the vdW-DF2-PES, shown to be more attractive than the previous PESs at large distances. Once more, we can attribute this feature to the inclusion of non-local interactions in the functional used to build the PES. The disappearance of the potential energy bump could imply a significant change in the reactivity since impinging atoms have a broader barrierless area to approach the target. Due to the high symmetry of the surface, the initial coordinates of the projectile (X_P, Y_P) were chosen within in an octant of the unit cell, as shown in the highlighted area in the bottom panel of Fig. 6.1. Since the topology of the PES does not show any potential energy barriers, several non-activated reaction pathways for ER can be found. To illustrate, in Fig. 6.2 we present a 2D cut of the PES a a function of the altitude for the projectile (Z_P) and the adsorbate (Z_A) keeping fixed the impact paramenter at b=0.7 Å in the diagonal direction. In the figure, it can be seen that the ER abstraction can take place keeping the potential energy lower than the reactant asymptote all along the path. This is only one of many possible configurations where the ER recombination process does not present energy barriers above the asymptote.

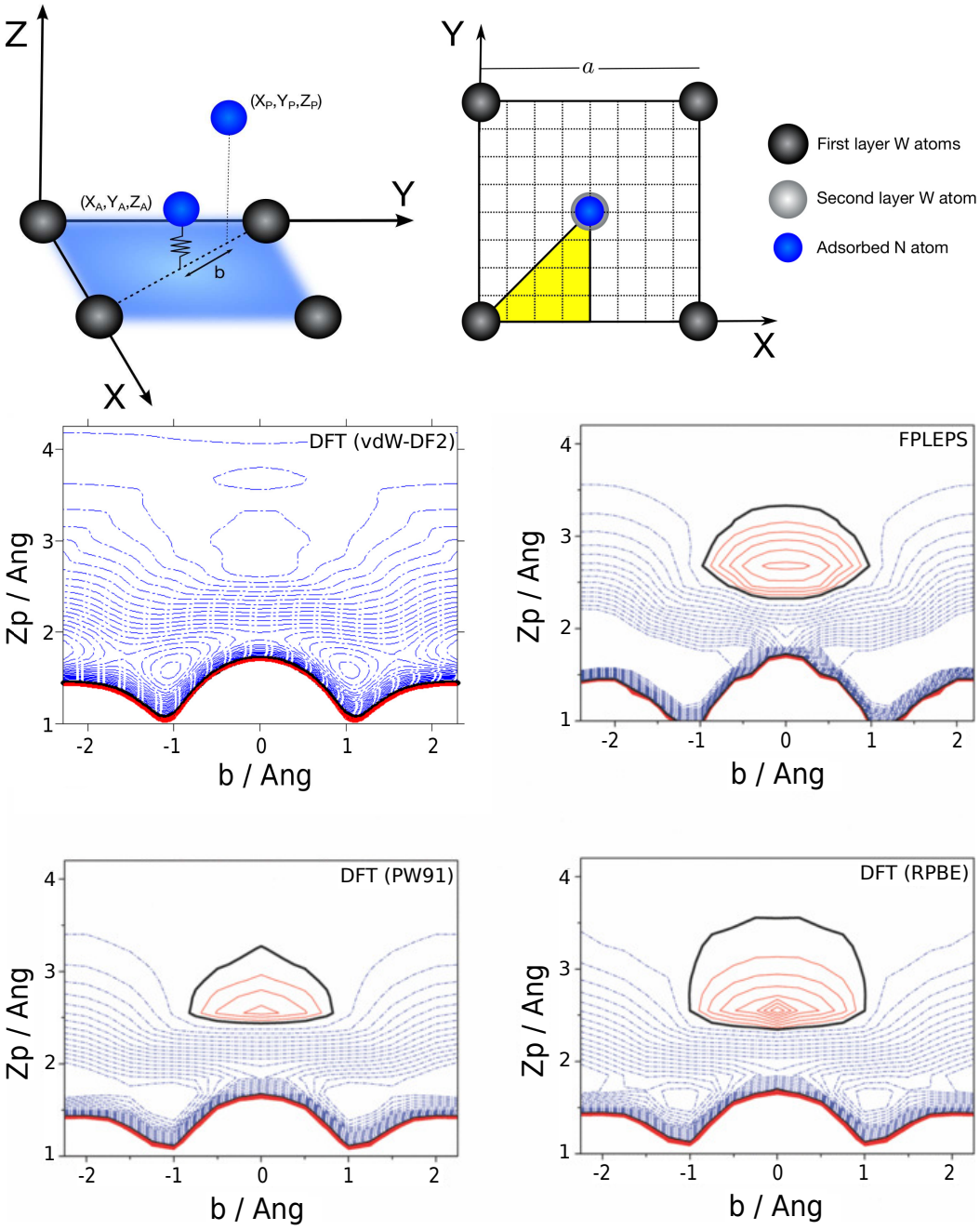

FIGURE 6.1: Upper Left: Coordinates system and the W(100) unit cell. Surface atoms are shown in grey and nitrogen atoms in blue. The origin of the coordinate system is placed on top of a surface atom. Upper Right :Sampling of initial conditions. The target atom is in blue and the yellow area represents the sampling area of the initial position of the projectile (X_P, Y_P). Middle and bottom panels: 2D cuts of the potential energy surface as a function of the projectile altitude Z_p and the impact paramenter b in the diagonal plane. The method used for each 2D-cut is shown in the upper right side of each panel. The thick black lines indicates the zero energy level, taken as the N atom adsorption energy. Full lines (dashed lines) are positive (negative) isovalues, separated by 0.1 eV (0.2 eV)

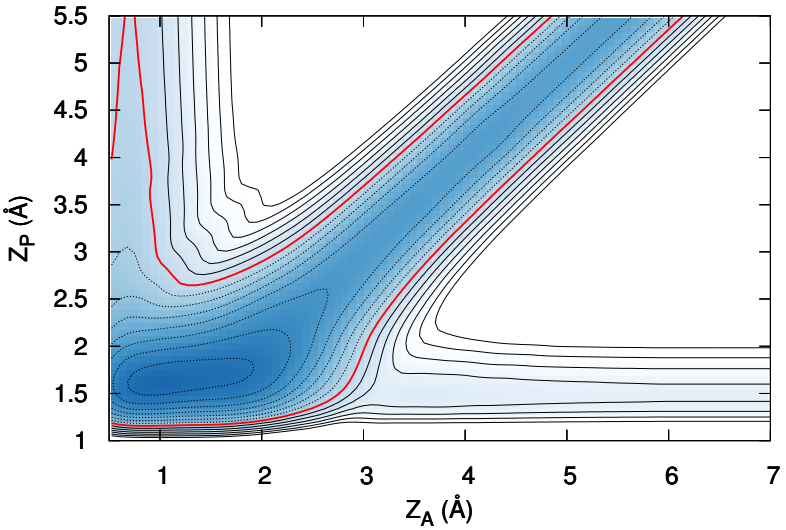

FIGURE 6.2: 2D cut of the PES as a function of the altitude of both the projectile (Z_P) and the adsorbate Z_A for b = 0.7 Å impact parameter in the diago nal direction. The thick red line indicates the zero energy level, taken as the N atomic adsorption energy. Full lines (dashed lines) are positive (negative) energies and separated by 0.5 eV.

To define the exit channels of the simulations, we have to take into account the many possible processes that can occur when an atom collides a surface in which atoms are already adsorbed. In this work, we limit the study to the zero coverage limit (only one adsorbate). This simplifies the possible processes while providing significant information of the reaction. In this case, following Ref. [137], the dynamics is divided in two steps:

1. $t \leq t_0$: Trajectories are integrated up to the first collision of the projectile with the surface ($t = t_0$), this is defined as a sign change in the Z linear momentum. At this moment, two different situations are considered depending on the interatomic distance r between the two atoms:

   - If the interatomic distance $r > r_{max}$, we consider that the projectile has become a hot atom. By evaluating the energy of this hot atom, the trajectory is identified as metastable hot atom (MHA) formation if the energetics allows it to leave the surface, i.e., its has a positive energy (E_p>0). Otherwise the hot atom will not be able to escape the surface as long as it does not react with an adsorbate, this is referred to as a bound hot atom (BHA). In practice, we set a value of r_{max}=4Å for N_2.

- If r$\leq$r$_{max}$ the integration of the trajectory continues.

2. t>t$_0$: After the first rebound, in each integrating step the conditions described below are checked. If fulfilled, the corresponding exit channel is identified and the integration of the equations of motion finishes.

   - Absorption: the Z coordinate of any N atom gets lower than 0.5 Å.
   - Reflection: any of the atoms reaches the initial altitude of the projectile within one rebound.
   - Hot atom: the interatomic distance is larger than r$_{max}$. As well as in the first step, the energy of the projectile is checked in order to decide wether is a BHA or a MHA trajectory.
   - Abstraction: both atoms reach the initial altitude of the projectile with a positive momentum of the diatom center of mass along the surface normal (Z-axis) and an interatomic distance r < 2.3 Å. The ER process occurs when the formed molecule moves definitively toward the vacuum before the second rebound of the projectile.

6.1.2 Eley-Rideal reactivity

We start with results obtained within the BOSS approximation. In Fig. 6.3 we show a representation of the initial coordinates of the projectile (X_P, Y_P) over the surface unit cell for 0.3, 1.0 and 2.6 eV impact energies. The colors of the trajectories depict the different exit channels. At 0.3 eV, most of the trajectories lead to bound HA formation (cyan dots), which are formed by transferring all of the impact energy to the target nitrogen atom since we are not accounting for energy exchange with the lattice so far. ER reactions (red dots) occur in the area around the target atom, opposite to what is reported in Ref. [138], where at such low collision energies, no ER product were found due to the energy barrier on top of the adsorbed atom. At 1.0 eV the reflection (violet dots) and metastable HA (blue dots) channels increase, particularly close to the surface W atoms. Then, for an impact energy of 2.6 eV, absorption (black dots) starts to be more prominent and the area for ER trajectories spreads towards the top sites.

The cross sections for the possible exit channels upon collision is presented in Fig. 6.4 together with the results obtained using the FPLEPS in Ref. [138]. We have separated the exit channels in two plots due to the large diference in the value of the cross sections. On the left hand panel of Fig. 6.4 we present the competition between bound (cyan lines) and metastable (blue lines) hot atom mechanisms as

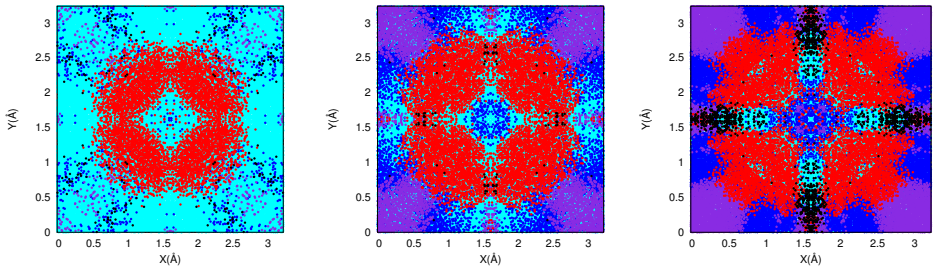

FIGURE 6.3: Opacity maps of initial coordinates (X,Y) of the projectile N atom for 0.3 eV (left), 1.0 eV (center) and 2.6 eV (right) impact energy. The exit channels depicted correspond to: ER (red dots), BHA (cyan dots), MHA (blue dots), reflection (violet dots) and absorption (black dots).

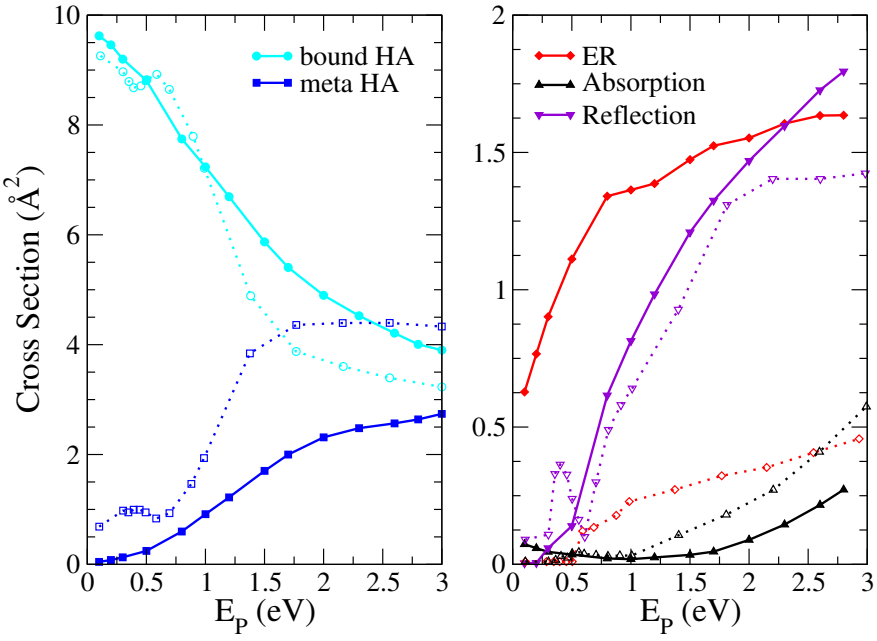

FIGURE 6.4: Left: Cross sections for bound (cyan circles) and metastable (blue squares) HA formation as a function of the projectile impact energy E_P. Right: Cross sections for absorption (black up triangles), ER reaction (red diamonds) and reflection (violet down triangles). The full lines correspond to calculations using the vdW-DF2-PES and the dotted lines to those using the FPLEPS reported in Ref. [138].

a function of the impact energy for both the vdW-DF2-PES and the FPLEPS. The FPLEPS shows a non-monotonic behavior between 0 eV<E_P<1 eV for both channels, whereas the vdW-DF2-PES does not present this feature. Moreover, it shows a greater amount of metastable HA (and consequently a decrease in the bound HA) formation as the energy increases compared to the vdW-DF2-PES results. The increase in metastable HA formation as a function of E_P is due to the fact

that at higher values of E_P, the energy transferred to the adsorbed atom is not enough to avoid the projectile going back to the gas-phase, hence the increase in the reflection process.

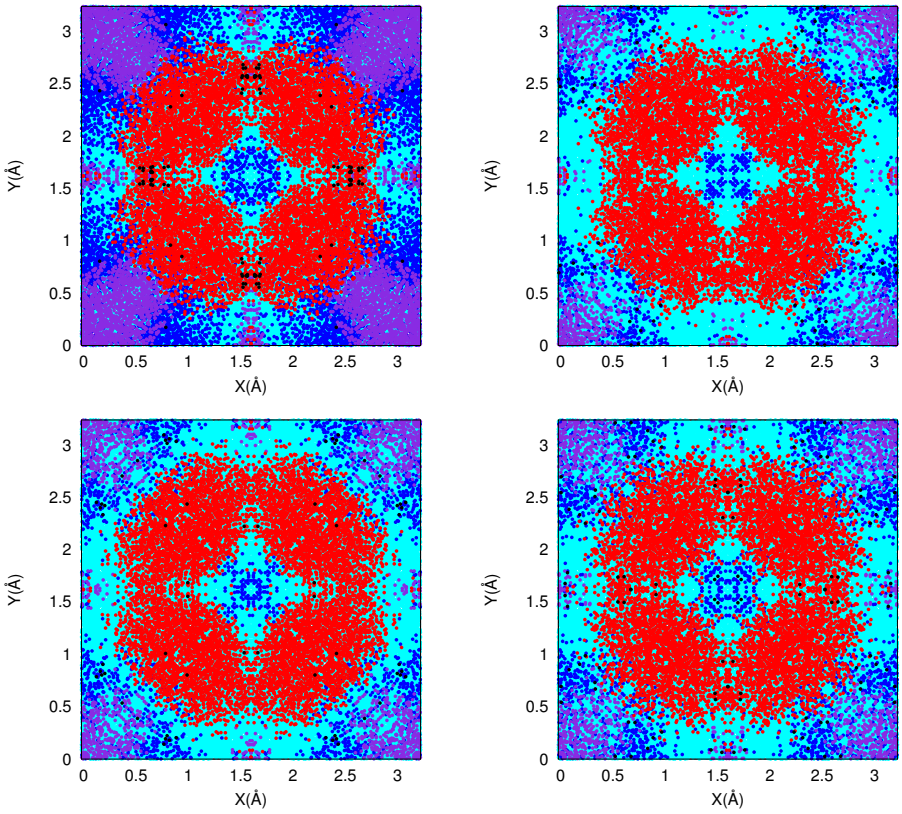

FIGURE 6.5: Opacity maps of initial coordinates (X,Y) of the projectile N atom for 1.0 eV impact energy and different temperatures. Upper left: BOSS model; Upper right: 300 K; Bottom left: 800 K; Bottom right: 1500 K. The exit channels depicted correspond to: ER (red dots), BHA (cyan dots), MHA (blue dots), reflection (violet dots) and absorption (black dots).

On the right panel we show the cross section for the reflection, absorption and ER recombination channels. The main and most striking result is the significant difference in the ER reactivity comparing both PESs. For the vdW-DF2-PES, ER reaction is non-zero in the whole range of energies shown. It appears that the main effect of the vanishing of the potential bump is to decrease the number of MHA at the benefits of ER molecular recombination. The FPLEPS on the other hand, presents ER reactivity from E_P>500 meV, value that corresponds to the energy bump observed in the 2D-cut of the PES. The reflection channel shows a non-monotonic behavior in the low energy regime for the FPLEPS, but then increases rather rapidly for both PESs. Finally, the vdW-DF2-PES exhibits a non-zero value

for the absorption at low values of the impact energy, feature that is not observed for the FPLEPS. Then, as the energy increases, the absorption decreases and then increases again.

6.1.3 Energy Dissipation effects on ER mechanisms

The GLO model has been used to account for possible energy transfers to the lattice. In Fig. 6.5 we present the opacity maps for an impact collision energy of 1.0 eV and three surface temperatures (300, 800 and 1500 K), as well as the results for the BOSS simulations. Including surface temperature in the calculations causes an increase in the bound HA formation and the area for reflection to occur is smaller. This is consistent with the fact that allowing energy exchange with the lattice, projectile atoms that had enough energy to eventually go back to the gas-phase, now can lose enough energy to remain over the surface as bound HA. Regarding the ER recombination, no significant changes are obtained within the GLO model.

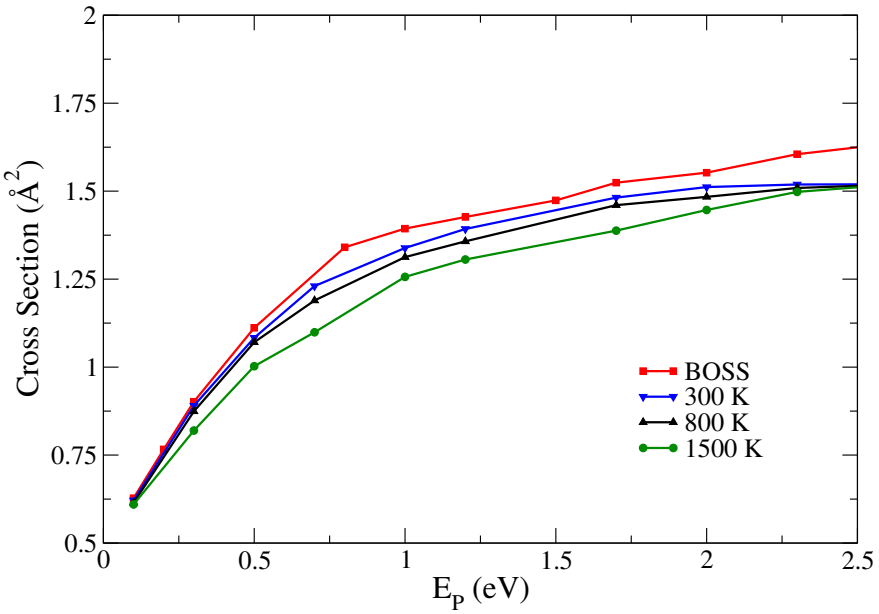

FIGURE 6.6: Cross sections for ER formation for the BOSS simulations (black circles) and the GLO for three different surface temperatures, 300 (red squares), 800 (green diamonds) and 1500 K (blue triangles) as a function of the collision energy.

In Fig. 6.6 we present the ER recombination cross section for the BOSS and the GLO results. In the figure it can be seen that accounting for energy exchange with phonons reduces the ER cross section as compared to the rigid surface data. This

result was not obvious in the opacity maps of Fig. 6.5 given that the difference is small. Increasing the temperature yields lower values for the ER cross section up to an impact energy of E_P=2.5 eV. For high energy values, the ER process seems to be insensitive to the surface temperature. Finally, it is worth to mention that regarding the HA formation cross sections we do not observe a significant dependence on the temperature.

6.2 Scattering dynamics

In addition to the ER recombination dynamics, nonreactive scattering of diatomic molecules on metal surfaces has also been studied with the vdW-DF2-PES. In this respect, the distributions of scattering polar angles (with respect to the surface normal) have been of great interest since they are extremely sensitive to the normal vs parallel differential momentum transfer which originates from the motion of surface atoms and the corrugation of the potential energy surface. These distributions, associated with the angle-resolved velocities, have long been used to characterize scattering regimes for molecules. Given the importance of the description of the PES, and the good results obtained for the reactive sticking of N_2 on the W(100) surface, we have studied the scattering using the vdw-DF2-PES and including the already mentioned energy dissipation effects. To this aim, we characterized the molecules scattered back to the gas phase in the dynamics. To simulate experimental conditions, we use an angle collection of $\pm$ 1° about the scattering plane, defined by the direction vector of the incoming beam and that of the surface normal.

One of the observables commonly reported by experiments corresponds to the full-width at half maximum (FWHM) of the in-plane scattering angle distribution. In Fig. 6.7 we show the evolution of the experimental and theoretical FWHM (with and without including energy dissipation effects) as a function of the normal energy for two values of incidence angle. In simulations, the FWHMs were extracted from the in-plane angular distributions with an estimated error of $\pm$2°. The results obtained exhibit a reasonable agreement with experimental data. Previous works were unable to reproduce the behavior at low values of collision energy, in the same way they failed to describe the reactive sticking dynamics. With this PES this problem is partially solved, most likely due to the vanishing of the barriers in the entrance channel as a consequence of the non-local forces accounted for in the vdW-DF2 functional. This can be investigated further by checking the altitude at which the molecules bounce over the surface. For the vdW DF2-PES, an important

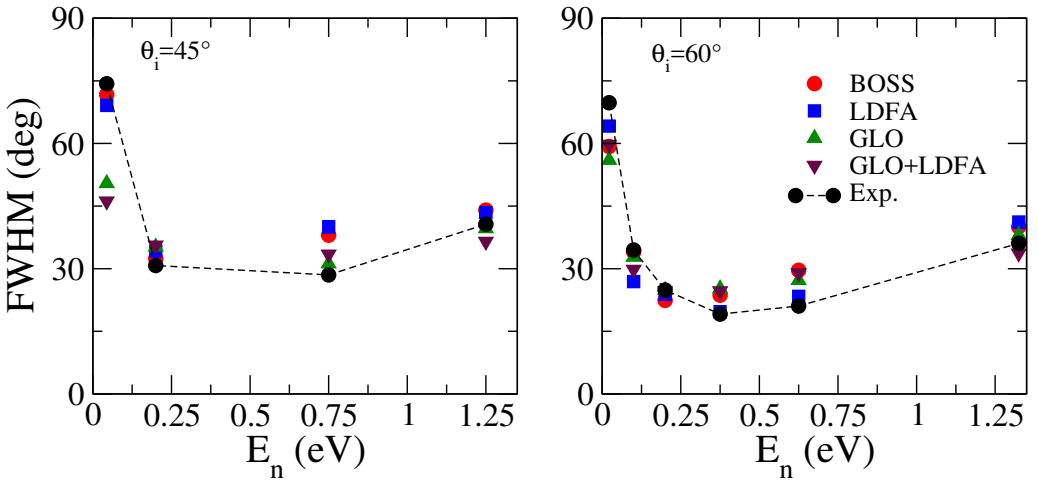

FIGURE 6.7: Results for the full width at half maximum (FWHM) of the in-plane scattering angle distributions as a function of the normal energy E_n for θ=45° (left panel) and θ=60° (right panel).

fraction of N_2 molecules sample regions of the PES where the corrugation is high (close to the surface). This results in the molecule performing multiple rebounds, which causes a broadening of the angular distribution, agreeing with what it is observed experimentally. Previous works performed using the PW91-PES, show that molecules mostly bounce far from the surface, where the corrugation is minimal, thus leading to a narrow distributions around the specular angle [144] at variance with the experimental measurements.

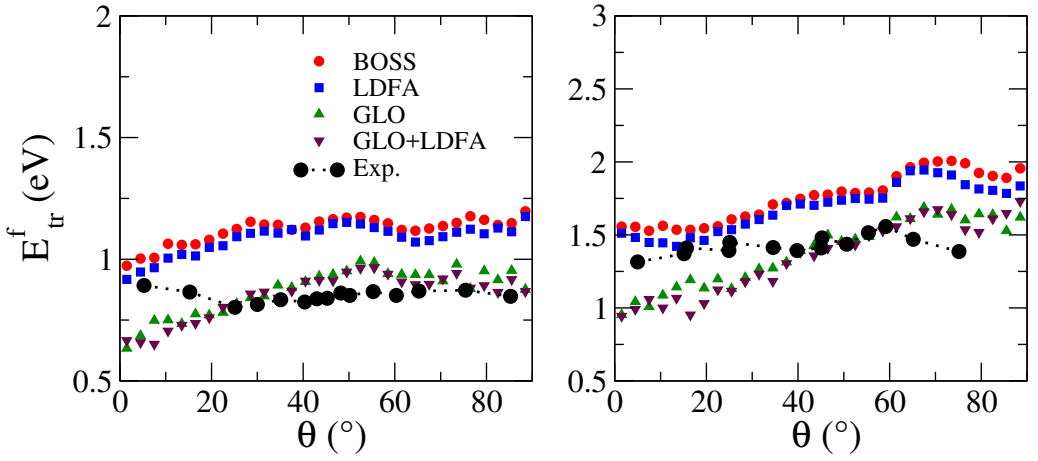

FIGURE 6.8: Angle-resolved average translation energies a function of the scattering angle. Simulated trajectories and experimental data are shown for a surface temperature of T_s=800 K and impact energy of 1.5 eV (left) and 2.5 eV (right).

In order to evaluate the energy dissipation to the W(100) surface upon N_2 scattering, we take a look at the final average translation energies of the scattered molecules as a function of the scattering angles. In Fig. 6.8 we show experimental and theoretical results for two values of the impact energy. It can be seen that the best agreement with experiments is obtained when accounting for dissipation to phonons and electrons. Electronic friction by itself does not have a large influence with respect to the BOSS results. These results are quite satisfactory given that we are able to obtain a qualitative agreement in the full range of scattering angles, as compared to the results reportes in Ref. [144] where at scattering angles $\geq 60^{\circ}$ the average translation energy decreased drastically.

6.3 Summary

In summary, we have studied the Eley-Rideal recombination process making use of the vdW-DF2-PES. Our PES exhibits no potential energy barriers as it was observed in previous works preventing the projectile to approach freely towards the adsorbate and the surface even at low impact energies. This difference as compared to other works leads to higher values for the ER cross sections, which are non-zero in the whole range of energies studied. At zero coverage limit, the reaction process shows that the HA formation is around one order of magnitude higher than ER at low impact energies, however, the ratio between this process reduces as the collision energy increases.

In addition, the effect of the surface temperature was also studied, and it appears to be minor regarding the ER process. Accounting for energy exchange with the lattice causes an increase in the HA formation, particularly the bound HA. This increase is counterbalanced by the decrease in metastable HA and reflection processes.

We have also analyzed the non reactive scattering of molecules off W(100), taking a look at the in-plane scattering angle distributions and the angle-resolved average translation energies of the molecules. For the former, a satisfactory agreement is obtained for the first time in the low-energy regime, where previous works failed to describe properly this observable. This is due to the vanishing energy barriers present in the entrance channel, allowing for the molecules to get closer to the surface where corrugation is high. The consequence of which being the broadening of the angular distribution of reflected back molecules that leads to an almost quantitative agreement with experiments. For the case of the final average translation energies, the energy dissipation channels have to be included to reach

an agreement with the energy loss observed experimentally.

Chapter 7

Conclusions and outlook

The aim of the present work was to contribute to a better understanding of several processes occurring when N_2 molecule is interacting with W(100) surface. For that purpose, we first constructed a six-dimensional potential energy surface (PES) making use of a set of first principles electronic structure calculations data grid obtained using a functional that accounts for non-local interactions, such as van der Waals (vdW) forces. The data grid was subsequentially interpolated via tha corrugation reducing procedure (CRP). The accuracy of the interpolation procedure was tested and it showed errors below 10 meV in the regions of the interest for the dynamics.

Analyzing the static surface through 1D and 2D cuts of the PES we identified three adsorption wells located over the three high symmetry sites of the W(100) surface. Two of those potential wells were identified as accessible to low energy molecules without overcoming energy barriers. When compares to previous built PESs the so called vdW-DF2-PES was shown to be more attractive when molecules are located at about 3 Å from the surface. At the opposite, the appearance of energy barriers close to the surface with respect to previous works led to a decrease in the number of configurations that the molecules can adopt to dissociate. The exothermicity of the dissociation was -3.74 eV, close to the -4.1 eV obtained with TDS measurements.

Afterwards, quasi-classical trajectories (QCT) simulations using the constructed PES were performed within the Born-Oppenheimer Static Surface (BOSS) approximation to study the dissociative adsorption of N_2. The results showed a high value for the sticking coefficient (S_0) at low values of the impact energy (E_i), followed by a steep monotonic decrease. Comparing the results to data obtained using different functionals (i.e. PW91 and RPBE), we observed that the main difference in S_0 was seen in the low energy regime. The shape of the PES in the

entrance channel plays a key role in the value of S_0 at low energies. In the case of the vdW-DF2-PES, more molecules can orient in a way that they can approach the surface without being reflected back to the gas-phase. Focusing on the low-energy N_2 molecules, we studied the path they follow to dissociation. A non-activated pathway was identified in which the molecules spend a long time bouncing over the surface.

Next, we performed dynamics including energy dissipation effects to the surface phonons and electrons using the generalized Langevin oscillator (GLO) model and the local density friction approximation (LDFA) respectively. The results from these calculations showed that accounting for energy exchange with phonons has a greater impact on S_0 than accounting for $e-h$ pair excitations. For both cases, the initial sticking coefficient is greater than that obtained from BOSS calculations. This increase is due to the non-dissociated molecules that remain trapped in the previouly identified adsorption wells. The most important results from these simulations is the temperature dependence of S_0 at low impact energies obtained within the GLO model. This dependence is observed in experiments and was not reproduced theoretically until now. In spite of the qualitative agreement with experiments, an overestimation of S_0 was observed in the whole range of energies studied. Trying to tackle this, we performed *Ab Initio* Molecular Dynamics (AIMD) to allow the explicit movement of the surface atoms. Due to the computational cost, we performed 100 trajectories for three values of the impact energy and two surface temperatures. The results showed a decrease in S_0 for most of the energies studied, obtaining a value closer to the experimental one. However, at low values of impact energy and high surface temperature, we obtained a higher value for S_0. A deeper analysis showed that this can be due to the short time of the dynamics, since most of the "trapped" molecules at the end of the dynamics are not adsorbed in the potential minima of the PES, but stay diffusing over the surface. So, longer times for the dynamics are needed to evaluate the final state of these molecules. Nevertheless, the AIMD results proved that accounting for the individual movement of the atoms during the reaction is important to properly describe the adsorption.

Finally, we tested two more mechanisms such as the Eley-Rideal (ER) recombination and the non-reactive scattering. For the ER reaction we observed that the topology of the vdW-DF2-PES when a single N atom is previously adsorbed on the surface (i.e. zero coverage limit) does not display any potential energy bumps,

as compared to what was previously reported for this system. Due to this, we obtained a cross section for the ER recombination significantly higher than previous works. Additionally, energy exchange with phonons does not have a significant effect on the recombination process. The only noticeable effect is a slight decrease of the ER recombination as the surface temperature increases. On the other hand, the study of the non-reactive scattering yielded a qualitative agreement in the low energy regime with experimental data regarding the in-plane scattering angle distributions for the first time. Moreover, a qualitative agreement of the angle-resolved average translation energies a function of the scattering angle with experiments was achieved as well.

All in all, the work in this thesis serves as a contribution in the study of the gas-surface dynamics by solving some long-lasting disagreements between theory and experiments. However, it also leaves many open questions that have to be addressed in future works.

Appendix A

Convergence study for the N_2/W(100) system

The parameters used in the DFT calculations must be chosen carefully since they can have a significant effect on the properties that we want to study. To that aim, we perform a convergence analysis of several properties. First, we must ensure that the vacuum between the slabs is enough for the molecule to not interact with the surface or its periodic image. In Fig. A.1 we show results for DFT calculations of the N_2 molecule in vacuum and halfway between slabs (i.e. at Z=7.5 Å from the surface) as a function of the internuclear distance. From the results it is clear that the choice of the size of the vacuum is good enough to guarantee that the N_2 molecule does not interacts with the surface at this distance. Moreover, DFT non-spin polarized (NSP) calculations of the potential energy of N_2 are shown in Fig. A.1 as well. From the results of spin polarized (SP) and NSP calculations we determine the value of the N-N distance from which we must perform SP calculations to ensure proper convergence.

All the DFT calculations presented in this thesis were carried out usign the VASP code [106–109]. The code contains a set of projector augmented wave (PAW) pseuopotentials (PP) to choose from. For the nitrogen, we used a hard PAW-PP with a suggested value for the E_{cutoff} of 420 EV in the construction of the potential energy surface. However, to perform AIMD calculations we noticed that the computational time was considerably reduced if we used a soft PAW-PP with a suggested energy cutoff of 400 eV. To check if the change in the PP used could affect the results, we performed a set of calculations for different configurations of the molecule on the surface using both PPs. In Fig. A.2 we present results for a molecule approaching the surface in a perpendicular way towards the top site and in a parallel way towards the hollow site using both PPs. We notice that the hard PP is more repulsive, particularly close to the surface, however, the values for the

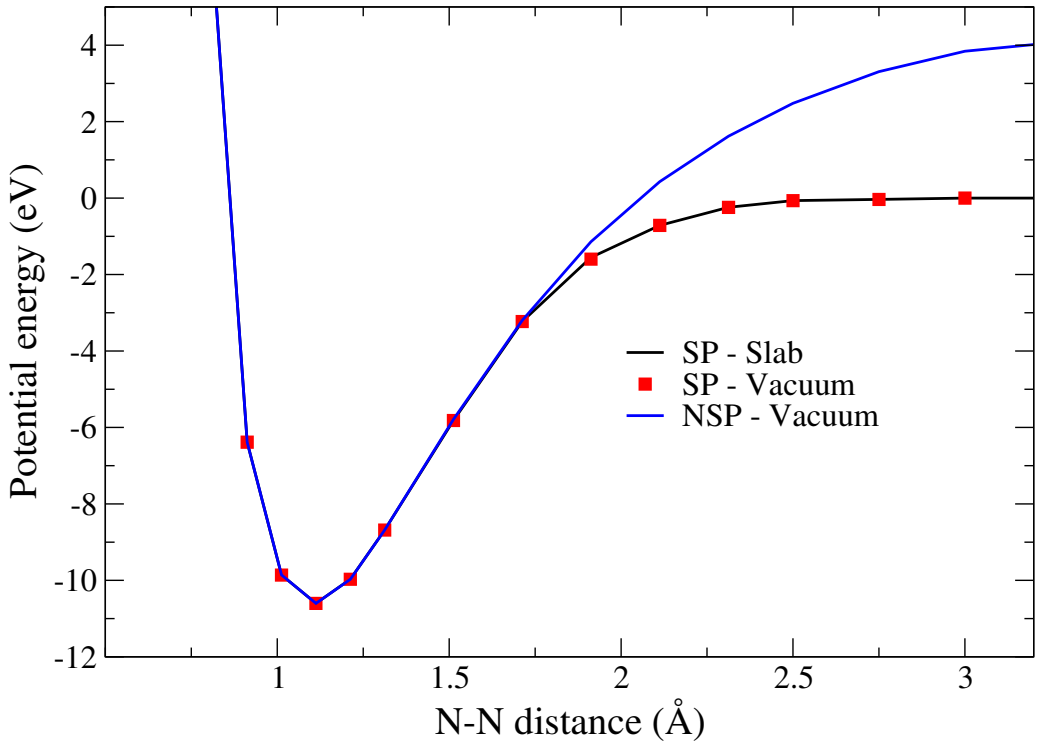

FIGURE A.1: Potential energy of the N_2 molecule as a function of the N-N interatomic distance in vacuum for DFT spin polarized (red squares) and non-spin polarized calculations (blue line). DFT spin polarized calculations with the molecule half way between two slabs of W are also presented (black line).

adsorption minimum in the top site with respect to the asymptotic value for each PP differ in less than 10 meV. From these results we consider that the change in the PP to perform AIMD is adequate and does not represent significant changes in the final results.

Regarding the **k**-point mesh and the value for E_{cutoff}, we noticed that a 8×8×1 mesh is enough to obtain converged values for the properties studied. In Fig. A.3 we present the values of the potential energy as a function of the cut-off energy (upper panel) and the **k**-point mesh (bottom panel) for a N_2 molecule located on the top site of the W(100) surface. In general, for values of **k** ≥8 and E_{cutoff} ≥500, no significant differences are obtained regarding the adsorption energies, internuclear distances and unit cell parameters. Hence our choice of these values.

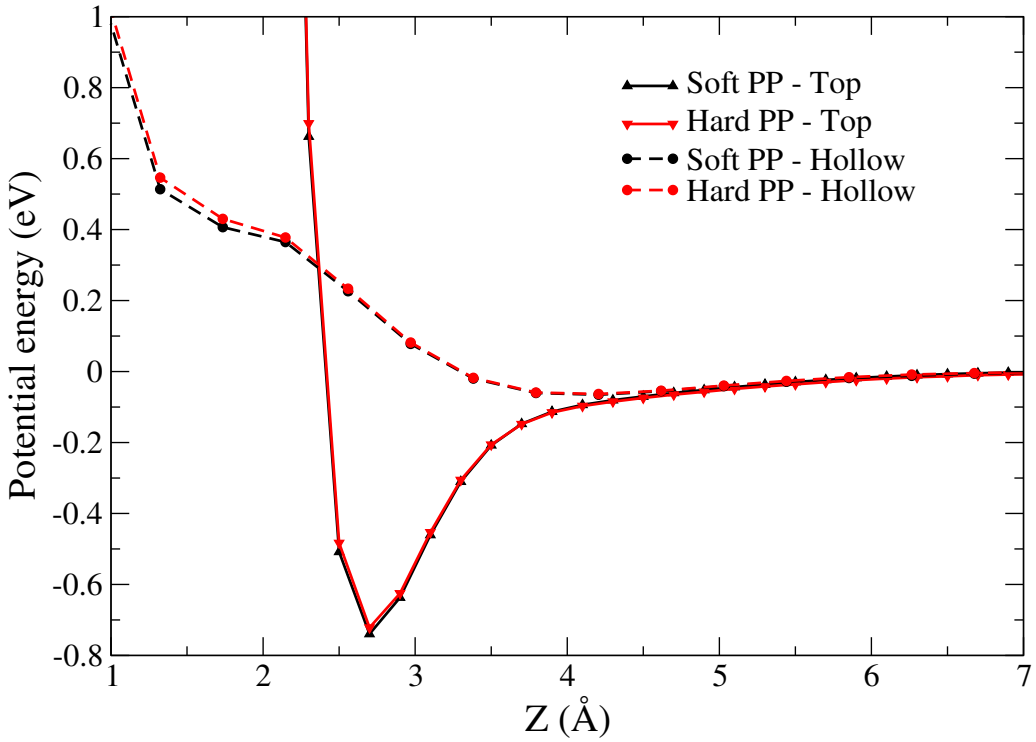

FIGURE A.2: Potential energy of the N_2 molecule from DFT calculations as a function of distance to the surface for two configurations (top vertical and hollow parallel) and two different pseudopotentials.

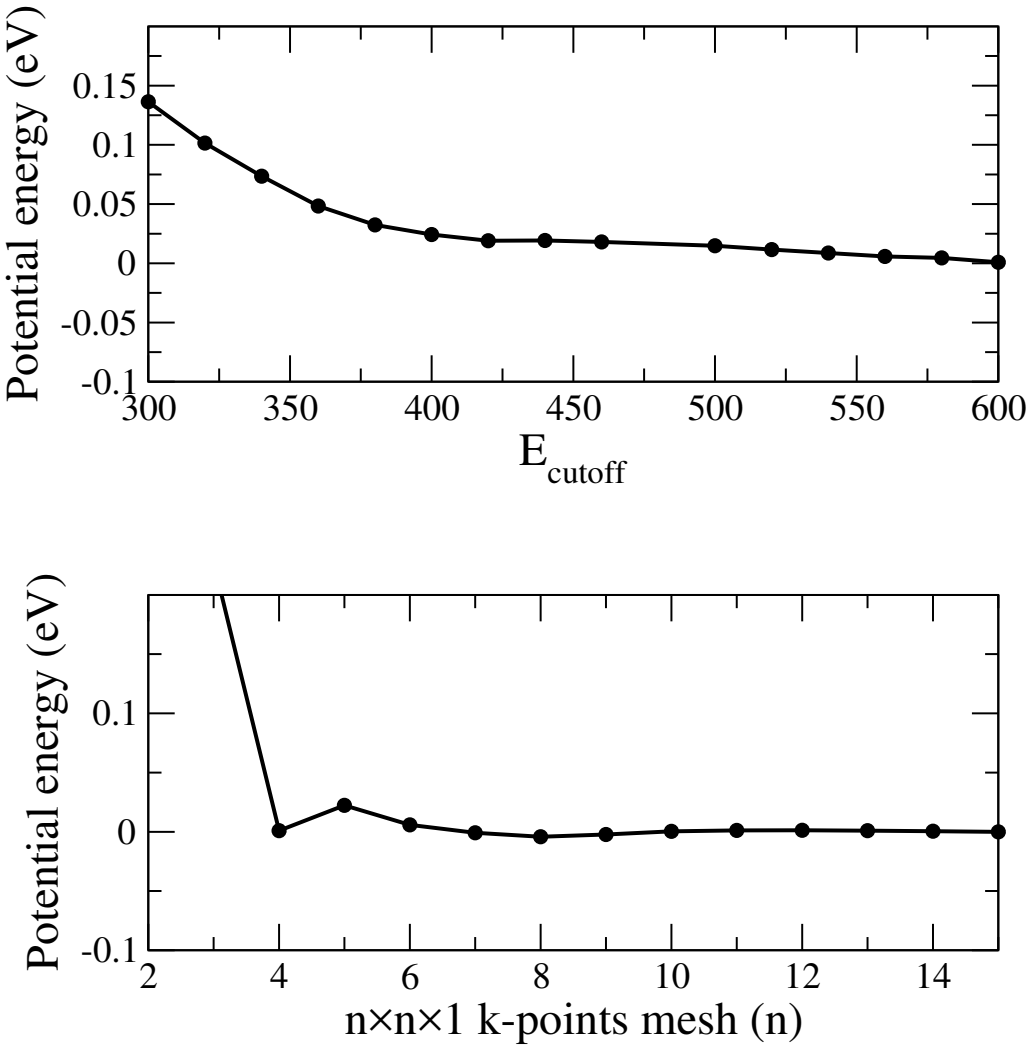

FIGURE A.3: Convergence of potential energy as a function of the E_{cutoff} (upper panel) and the **k**-point mesh (bottom panel) for a molecular configuration of the N_2 molecule over the top site of the W(100) surface.

Appendix B

Details for the Corrugation Reducing Procedure Interpolation

Here we present the interpolation functions used in the Corrugation Reducing Procedure (CRP) to build the N_2/W(100) 6D-PES. As explained in Chapter 2, the first step is to compute a grid of DFT data points for the N atom (V^{3D}) and the N_2 molecule (V^{6D}) over the W(100) surface unit cell.

B.1 3D atomic PES: N/W(100)

The interaction of the N atom with the frozen W(100) surface is described with a 3D PES that depends on the position $\mathbf{R}$ of the N atom over the surface. The spin-polarized DFT calculations are used to obtain the interpolation function I^{3D},

$$I^{3D}(\mathbf{R}) = V^{3D}(\mathbf{R}) - \sum_{i=1}^{n} V^{1D}(|\mathbf{R} - \mathbf{R_i}|), \tag{B.1}$$

where V^{1D} is a potential energy in one dimension that describes the interaction between the N atom and the *ith*-W atom positioned at $\mathbf{R_i}$. The surface atoms of the first and second layers are considered in the summation of Eq. B.1. The obtained interpolation function I^{3D} presents less corrugation that the initial atomic potential V^{3D} and is interpolated using cubic splines in X,Y and Z.

The dependence of the potential energy on the distance of the N atom with the W(100) surface is shown in Fig. B.1 for different positions in X and Y. For every configuration, the approach of the N atom towards the surface is characterized by an adsorption minimum followed by a repulsive barrier. From the analysis of the 1D (Z)-cuts we see that the most attractive position is the one over the hollow site (X=1.612 Å, Y1.612 Å, Z=0.7 Å), with an adsorption energy of 6.77 eV.

Furthermore, a complete inspection of 2D (X,Y)-cuts of the 3D PES at fixed distances from the surface allows us to determine the sites that actually correspond

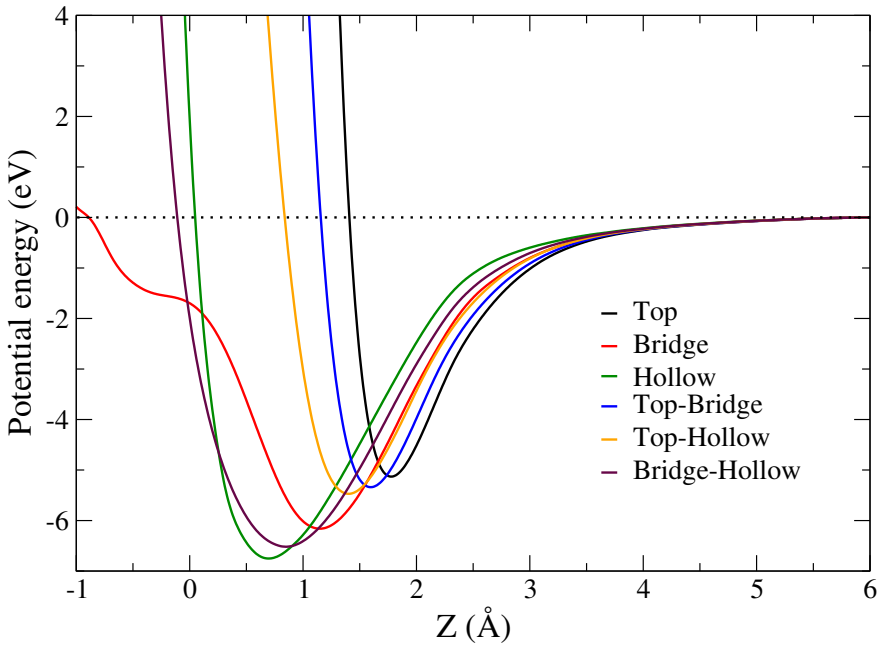

FIGURE B.1: Potential energy as a function of the altitude of the N atom from the W(100) surface for the high-symmetry sites.

to true minima in 3D. On the left panel of Fig. B.2 we show a 2D cut for a distance of Z=0.7 Å, where the lowest adsorption minimum is present. As it can be seen, the attractive region is rather large around the middle of the unit cell. However, a closer look to the minimum shows a rather interesting feature. On the right panel of Fig. B.2 we show the same 2D cut, but closer to the minimum of the potential energy. It appears that the global minimum of the 3D PES is not located directly over the hollow site, as it has been reported before, but slightly displaced (around 0.3 Å) towards the bridge sites. The difference in energy between the lowest energy configurations and the hollow site if of 19 meV. Given that the energy difference is low, an adsorbed atom with an initial ZPE will be moving inside the whole area and would not be restricted to the small potential minima around the hollow site. This feature where the potential over the hollow is slightly higher than the sites around it was not reported in previous works with GGA-type functionals. We attribute this effect to the non-local interactions introduced by the vdW-DF2 functional with the W atom on the second layer, which is located just below the hollow site.

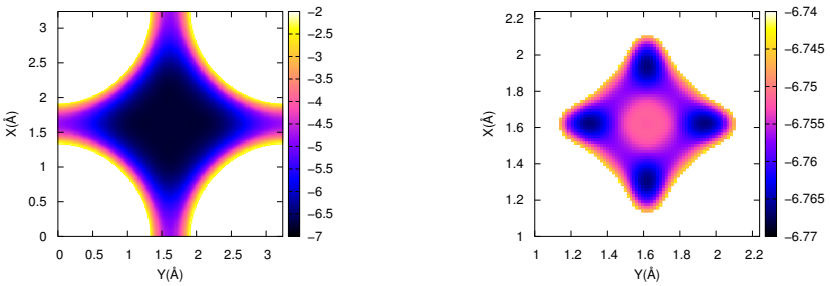

FIGURE B.2: 2D (X,Y)-cuts of the 3D PES for a distance of Z=0.7 Å from the surface. The right panel shows the same cut closer to the minimum of the potential.

B.2 6D molecular PES: N_2/W(100)

Here we will describe in detail the interpolation procedure to obtain the molecular 6D continuous PES in all degrees of freedom $V^{6D}(X, Y, r, \theta, \phi)$. In Chapter 3 we described the 35 configurations (X,Y,θ,ϕ) used to build the DFT data grid from 2D (r,Z)-cuts. For each configuration, we substract the atomic potential from the 6D potential, obtaining what we refer to as the interpolation frunction (I^{6D}). This function is subsequentally interpolated in three steps:

- Interpolation over (r,Z) using cubic splines
- Interpolation over (θ,ϕ) using trigonometric functions
- Interpolation over (X,Y) using periodic cubic splines

Here we will focus on the interpolation over θ and ϕ, site per site. In the notation to be used, I^{6D}(x) represents the value of the interpolation function where (x) denotes the corresponding configuration (X,Y,θ,ϕ) for which the potential energy is available. Then, the I^{6D} terms with the same value of θ are gathered in the interpolation functions I^{6D}_{θ}, which can be interpolated in ϕ, $I^{6D}_{\theta}(\phi)$. Lastly, the interpolation functions over θ and ϕ are detailed.

a) The configurations calculated for the top (X=0, Y=0) and hollow (X=$a/2$, Y=$a/2$) sites are: (1) θ=0°; (2) θ=45° and ϕ=0°; (3) θ=45° and ϕ=45°; (4) θ=90° and ϕ=0°; (5) θ=90° and ϕ=45°. The interpolation functions over ϕ for these configurations are:

$$I^{6D}_{0}(\phi) = I^{6D}(1) \tag{B.2}$$

$$I_{45}^{6D}(\phi) = \frac{1}{2}(I^{6D}(2) + I^{6D}(3)) + \frac{1}{2}(I^{6D}(2) - I^{6D}(3))cos(4\phi) \tag{B.3}$$

$$I_{90}^{6D}(\phi) = \frac{1}{2}(I^{6D}(4) + I^{6D}(5)) + \frac{1}{2}(I^{6D}(4) - I^{6D}(5))cos(4\phi) \tag{B.4}$$

The interpolation function over (θ,ϕ) can be thus expressed as:

$$\begin{aligned} I^{6D}(\theta,\phi) =& \frac{1}{4}[(I_0^{6D} + 2I_{45}^{6D} + I_{90}^{6D} + 2(I_0^{6D} - I_{90}^{6D}))cos(2\theta) \\ &+ (I_0^{6D} - 2I_{45}^{6D} + I_{90}^{6D})cos(4\theta)] \end{aligned} \tag{B.5}$$

b) The configurations calculated for the bridge site (X=$a/2$, Y=0) are: (1) θ=0°; (2) θ=45° and ϕ=0°; (3) θ=45° and ϕ=90°; (4) θ=90° and ϕ=0°; (5) θ=90° and ϕ=90°. The interpolation functions over ϕ for these configurations are:

$$I_0^{6D}(\phi) = I^{6D}(1) \tag{B.6}$$

$$I_{45}^{6D}(\phi) = \frac{1}{2}(I^{6D}(2) + I^{6D}(3)) + \frac{1}{2}(I^{6D}(2) - I^{6D}(3))cos(2\phi) \tag{B.7}$$

$$I_{90}^{6D}(\phi) = \frac{1}{2}(I^{6D}(4) + I^{6D}(5)) + \frac{1}{2}(I^{6D}(4) - I^{6D}(5))cos(2\phi) \tag{B.8}$$

And the interpolation function over (θ,ϕ) is:

$$\begin{aligned} I^{6D}(\theta,\phi) =& \frac{1}{4}[(I_0^{6D} + 2I_{45}^{6D} + I_{90}^{6D} + 2(I_0^{6D} - I_{90}^{6D}))cos(2\theta) \\ &+ (I_0^{6D} - 2I_{45}^{6D} + I_{90}^{6D})cos(4\theta)] \end{aligned} \tag{B.9}$$

c) The configurations calculated for the top-to-hollow (T2H) site (X=$a/4$, Y=$a/4$) are: (1) θ=0°; (2) θ=90° and ϕ=45°; (3) θ=90° and ϕ=135°; (4) θ=45° and ϕ=45°; (5) θ=45° and ϕ=90°; (6) θ=45° and ϕ=135°; (7) θ=45° and ϕ=225°. The interpolation functions over ϕ for these configurations are:

$$I_0^{6D}(\phi) = I^{6D}(1) \tag{B.10}$$

$$I_{90}^{6D}(\phi) = \frac{1}{2}(I^{6D}(2) + I^{6D}(3)) + \frac{1}{2}(I^{6D}(2) - I^{6D}(3))cos(2\phi) \tag{B.11}$$

$$I_{45}^{6D}(\phi) = a_0 + a_1 cos(\phi) + a_2 cos(2\phi) + a_3 cos(3\phi) \tag{B.12}$$

$$I_{135}^{6D}(\phi) = a_0 + a_1 cos(\phi + \pi) + a_2 cos(2(\phi + \pi)) + a_3 cos(3(\phi + \pi)) \tag{B.13}$$

with

$$\begin{aligned} a_3 = &- \frac{1}{4\sqrt{2}}((-\sqrt{2}-1)I^{6D}(4) + 4I^{6D}(5) \\ &- 2I^{6D}(6) + (\sqrt{2}-1)I^{6D}(7)) \end{aligned} \tag{B.14}$$

$$a_2 = a_0 - I^{6D}(6) \tag{B.15}$$

$$a_1 = \frac{1}{\sqrt{2}-1}(-I^{6D}(4) + 2I^{6D}(5) - I^{6D}(6) + (\sqrt{2}+1)a_3) \tag{B.16}$$

$$a_0 = (I^{6D}(4) + I^{6D}(6) - a_1 - a_3)/2 \tag{B.17}$$

and the interpolation function over (θ,ϕ) is:

$$\begin{aligned} I^{6D}(\theta,\phi) = &\frac{1}{4}[I_0^{6D} + I_{45}^{6D} + I_{90}^{6D} + I_{135}^{6D} \\ &+ (I_0^{6D} + I_{90}^{6D} - I_{45}^{6D} - I_{135}^{6D})cos(4\theta)] \\ &+ \frac{1}{2}[(I_0^{6D} - I_{90}^{6D})cos(2\theta) + (I_{45}^{6D} - I_{135}^{6D})sin(2\theta)] \end{aligned} \tag{B.18}$$

d) The configurations calculated for the top-to-bridge (T2B) site (X=$a/4$, Y=0) are: (1) θ=0°; (2) θ=90° and ϕ=0°; (3) θ=90° and ϕ=90°; (4) θ=45° and ϕ=0°; (5) θ=45° and ϕ=180°; (6) θ=45° and ϕ=90°. The interpolation functions over ϕ for these configurations are:

$$I_0^{6D}(\phi) = I^{6D}(1) \tag{B.19}$$

$$I_{90}^{6D}(\phi) = \frac{1}{2}(I^{6D}(2) + I^{6D}(3)) + \frac{1}{2}(I^{6D}(2) - I^{6D}(3))cos(2\phi) \tag{B.20}$$

$$I_{45}^{6D}(\phi) = a_0 + a_1 cos(\phi) + a_2 cos(2\phi) \tag{B.21}$$

$$I_{135}^{6D}(\phi) = a_0 - a_1 cos(\phi) + a_2 cos(2\phi) \tag{B.22}$$

with

$$a_0 = \frac{1}{4}(I^{6D}(4) + I^{6D}(5) + 2I^{6D}(6)) \tag{B.23}$$

$$a_1 = \frac{1}{2}(I^{6D}(4) - I^{6D}(5)) \tag{B.24}$$

$$a_2 = \frac{1}{4}(I^{6D}(4) + I^{6D}(5) - 2I^{6D}(6)) \tag{B.25}$$

and the interpolation function over (θ,ϕ) is:

$$\begin{aligned} I^{6D}(\theta,\phi) =& \frac{1}{4}[I_0^{6D} + I_{45}^{6D} + I_{90}^{6D} + I_{135}^{6D} \\ &+ (I_0^{6D} + I_{90}^{6D} - I_{45}^{6D} - I_{135}^{6D}) cos(4\theta)] \\ &+ \frac{1}{2}[(I_0^{6D} - I_{90}^{6D}) cos(2\theta) + (I_{45}^{6D} - I_{135}^{6D}) sin(2\theta)] \end{aligned} \tag{B.26}$$

e) The configurations calculated for the bridge-to-hollow (B2H) site (X=$a/2$, Y=$a/4$) are: (1) θ=0°; (2) θ=90° and ϕ=0°; (3) θ=90° and ϕ=90°; (4) θ=45° and ϕ=0°; (5) θ=45° and ϕ=90°; (6) θ=45° and ϕ=270°; (7) θ=90° and ϕ=45°. The interpolation functions over ϕ for these configurations are:

$$I_0^{6D}(\phi) = I^{6D}(1) \tag{B.27}$$

$$I_{90}^{6D}(\phi) = a_0 + a_1 cos(2\phi) + a_2 cos(4\phi) \tag{B.28}$$

$$I_{45}^{6D}(\phi) = a_3 + a_4 cos(\phi) + a_5 cos(2\phi) \tag{B.29}$$

$$I_{135}^{6D}(\phi) = a_3 + a_4 cos(\phi + \pi) + a_5 cos(2(\phi + \pi)) \tag{B.30}$$

where

$$a_0 = \frac{1}{4}(I^{6D}(2) + 2I^{6D}(7) + I^{6D}(3)) \tag{B.31}$$

$$a_1 = \frac{1}{2}(-I^{6D}(2) + I^{6D}(3)) \tag{B.32}$$

$$a_2 = \frac{1}{4}(I^{6D}(2) - 2I^{6D}(7) + I^{6D}(3)) \tag{B.33}$$

$$a_3 = \frac{1}{4}(2I^{6D}(4) + I^{6D}(5) + I^{6D}(6)) \tag{B.34}$$

$$a_4 = \frac{1}{2}(I^{6D}(5) - I^{6D}(6)) \tag{B.35}$$

$$a_5 = \frac{1}{4}(-2I^{6D}(4) + I^{6D}(5) + I^{6D}(6)) \tag{B.36}$$

and the interpolation function over (θ,ϕ) is:

$$\begin{aligned} I^{6D}(\theta,\phi) =& \frac{1}{4}[I_0^{6D} + I_{45}^{6D} + I_{90}^{6D} + I_{135}^{6D} \\ &+ (I_0^{6D} + I_{90}^{6D} - I_{45}^{6D} - I_{135}^{6D})cos(4\theta)] \\ &+ \frac{1}{2}[(I_0^{6D} - I_{90}^{6D})cos(2\theta) + (I_{45}^{6D} - I_{135}^{6D})sin(2\theta)] \end{aligned} \tag{B.37}$$

After the interpolation over (r,z,θ,ϕ) is done, we use 2D periodic cubic splines to obtain the full value of the interpolation function I^{6D}(X,Y,Z,r,θ,ϕ). Adding the corresponding atomic potentials V^{3D} to the interpolation function we obtain the value for the molecular potential energy at that particular configuration:

$$\begin{aligned} V^{6D}(X,Y,Z,r,\theta,\phi) =& I^{6D}(X,Y,Z,r,\theta,\phi) + \\ & V^{3D}(X_A,Y_A,Z_A) + V^{3D}(X_B,Y_B,Z_B). \end{aligned} \tag{B.38}$$

Appendix C

Parameters for the GLO calculations

The sensitivity of the sticking probability to the values used for the parameters describing the oscillators within the GLO model is tested by varying them in a systematic way. The parameters correspond to: the friction coefficient associated to the ghost oscillator (γ), and the frequencies for the parallel ($\omega_{x,y}$) and perpendicular (ω_z) motion. The reference values as explained in Chapter 5 are taken as $\omega_x = \omega_y$ =19 meV (7 10^{-4} a.u.), ω_z =16 meV (6 10^{-4} a.u.) and γ=6.6x10^{-4} a.u. For the test, the value of one of these parameters was changed while keeping the rest fixed. The results presented in Fig. C.1 shows the sticking probabilities S_0 obtained after varying each one of the parameteres by a factor of 10 for γ and by a factor of 2 for the frequencies $\omega_{x,y,z}$. The results obtained show that the sticking probabilites are not sensitive to the choice of these parameters, as long as they are kept within the same order of magnitude.

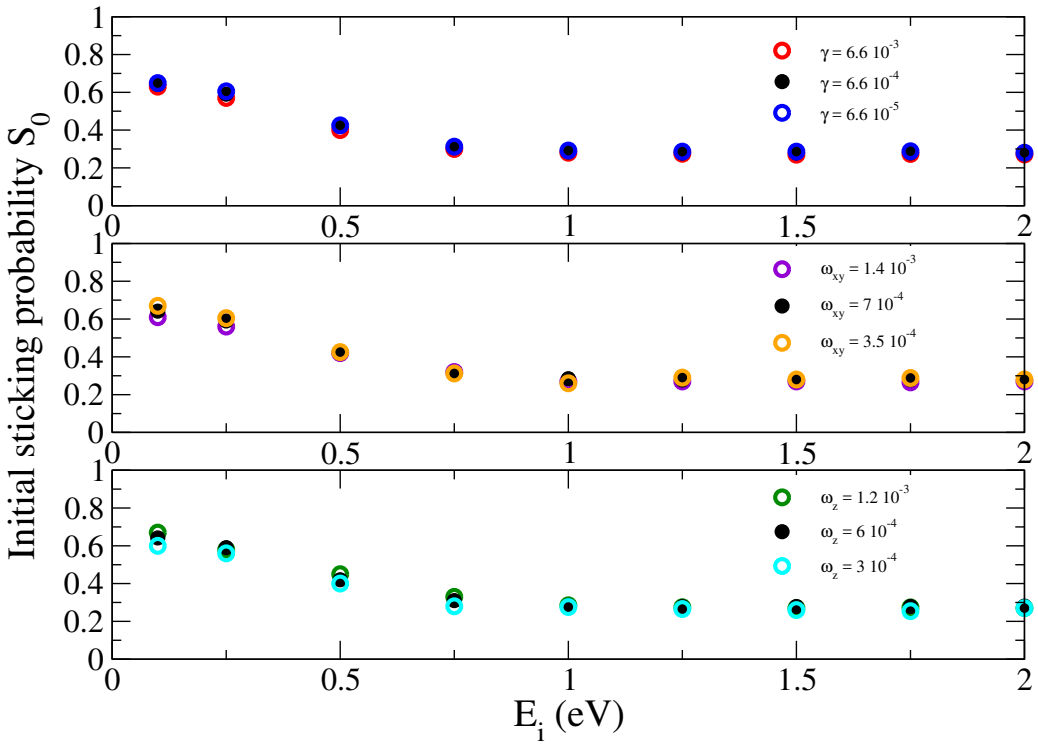

FIGURE C.1: Sticking probabilities as a function of the impact energy for calculations within the GLO model varying the different values for the oscillator parameters. Results are for calculations at normal incidence and surface temperature T_s=800 K. Variation of γ, $\omega_{x,y}$ and ω_z correspond to the top, middel and bottom panels, respectively. The reference values are displayed in black circles.

Bibliography

[1] Uwe Dingerdissen, Andreas Martin, Daniel Herein, and Hans Jürgen Wernicke. In: "The Development of Industrial Heterogeneous Catalysis". Chap. 1.3, pp. 37–56. American Cancer Society, 2008. (Cited on p. 1).

[2] Kathleen C. Taylor. "Nitric Oxide Catalysis in Automotive Exhaust Systems". *Catalysis Reviews* 35, pp. 457–481, 1993. (Cited on p. 1).

[3] Martyn V. Twigg. "Progress and future challenges in controlling automotive exhaust gas emissions". *Applied Catalysis B: Environmental* 70, pp. 2–15, 2007. (Cited on p. 1).

[4] G Ertl. "Surface science and catalysis—studies on the mechanism of ammonia synthesis: the PH Emmett award address". *Catal. Rev.* 21, pp. 201–223, 1980. (Cited on p. 1).

[5] David C. Knauth, B Andersson, S R Mccandliss, and H. Warren Moos. "The interstellar N2 abundance towards HD 124314 from far-ultraviolet observations". *Nature* 429, pp. 636–638, 2004. (Cited on p. 1).

[6] Julien J. Daranlot, U. Hincelin, Astrid Bergeat, Michel Costes, Jean-Christophe Loison, Valentine Wakelam, and Kevin M. Hickson. "Elemental nitrogen partitioning in dense interstellar clouds". *Proceedings of the National Academy of Sciences of the United States of America* 109, pp. 10233–10238, 2012. (Cited on p. 1).

[7] Bret Halpern and Daniel E. Rosner. "Chemical energy accommodation at catalyst surfaces. Flow reactor studies of the association of nitrogen atoms on metals at high temperatures". *J. Chem. Soc., Faraday Trans. 1* 74, pp. 1883–1912, 1978. (Cited on p. 1).

[8] *ITER*. URL: https://www.iter.org/mach/divertor (visited on 05/30/2018) (Cited on p. 1).

[9] J. Libuda and H.-J. Freund. "Molecular beam experiments on model catalysts". *Surface Science Reports* 57, pp. 157–298, 2005. (Cited on p. 3).

[10] Sebastiaan Y. T. van de Meerakker, Hendrick L. Bethlem, Nicolas Vanhaecke, and Gerard Meijer. "Manipulation and Control of Molecular Beams". *Chemical Reviews* 112 PMID: 22449067, pp. 4828–4878, 2012. (Cited on p. 3).

[11] F. Pirani, D. Cappelletti, F. Vecchiocattivi, L. Vattuone, A. Gerbi, M. Rocca, and U. Valbusa. "A simple and compact mechanical velocity selector of use to analyze/select molecular alignment in supersonic seeded beams". *Review of Scientific Instruments* 75, pp. 349–354, 2004. (Cited on p. 3).

[12] M. N. R. Ashfold and J. D. Howe. "Multiphoton Spectroscopy of Molecular Species". *Annual Review of Physical Chemistry* 45, pp. 57–82, 1994. (Cited on p. 4).

[13] Marcos Dantus, Mark J. Rosker, and Ahmed H. Zewail. "Real-time femtosecond probing of "transition states" in chemical reactions". *The Journal of Chemical Physics* 87, pp. 2395–2397, 1987. (Cited on p. 4).

[14] J. L. Kinsey. "Laser-Induced Fluorescence". *Annual Review of Physical Chemistry* 28, pp. 349–372, 1977. (Cited on p. 4).

[15] A. Groß. *Theoretical Surface Science: A Microscopic Perspective*. Springer Berlin Heidelberg, 2009. (Cited on pp. 4, 24).

[16] R. D. Muino and H. F. Busnengo, eds. *Dynamics of Gas-surface Interactions*. Springer, Heidelberg, 2013. (Cited on p. 4).

[17] P.W. Tamm and L.D. Schmidt. "Crystallographic anisotropies in condensation: N2 on (110) W". *Surface Science* 26, pp. 286–296, 1971. (Cited on pp. 5, 45).

[18] S.P. Singh-Boparai, Michael Bowker, and David A. King. "Crystallographic anisotropy in chemisorption: Nitrogen on tungsten single crystal planes". *Surface Science* 53, pp. 55–73, 1975. (Cited on pp. 5, 45).

[19] H. E. Pfnür, C. T. Rettner, J. Lee, R. J. Madix, and D. J. Auerbach. "Dynamics of the activated dissociative chemisorption of N2 on W(110): A molecular beam study". *The Journal of Chemical Physics* 85, pp. 7452–7466, 1986. (Cited on pp. 5, 46).

[20] J. Lee, R.J. Madix, J.E. Schlaegel, and D.J. Auerbach. "Molecular beam studies of the dynamics of activated adsorption of N2 on W(110): Dissociation threshold and new binding states". *Surface Science* 143, pp. 626–638, 1984. (Cited on pp. 5, 46).

[21] C. T. Rettner, H. Stein, and E. K. Schweizer. "Effect of collision energy and incidence angle on the precursor-mediated dissociative chemisorption of *N*_2 on W(100)". *J. Chem. Phys* 89, pp. 3337–3341, 1988. (Cited on pp. 5, 45, 64).

[22] C. T. Rettner, E. K. Schweizer, and H. Stein. "Dynamics of the chemisorption of N2 on W(100): Precursor-mediated and activated dissociation". *J. Chem. Phys.* 93, pp. 1442–1454, 1990. (Cited on pp. 5, 6, 45, 64, 65).

[23] M. Alducin, R. Díez-Muiño, H. F. Busnengo, and A. Salin. "Why N_2 Molecules with Thermal Energy Abundantly Dissociate on W(100) and Not on W(110)". *Phys. Rev. Lett.* 97, p. 056102, 2006. (Cited on pp. 5, 22).

[24] M. Alducin, R. Díez, H. F. Busnengo, and A. Salin. "Dissociative adsorption of *N*_2 on W(110): Theoretical study of the dependence on the incidence angle". *Surf. Sci.* 601, pp. 3726–3730, 2007. (Cited on pp. 5, 22).

[25] G. Volpilhac and A. Salin. "Dissociative adsorption of *N*_2 on the W(100) surface". *Surf. Sci.* 556, pp. 129–144, 2004. (Cited on pp. 5, 6, 36, 38, 42, 46, 48–51, 54, 72).

[26] G.A. Bocan, R. Díez, M. Alducin, and H. F. Busnengo. "The role of exchange-correlation functionals in the potential energy surface and dynamics of *N*_2 dissociation on W surfaces". *J. Chem. Phys.* 128, p. 154704, 2008. (Cited on pp. 5, 37, 47–50).

[27] Francesco Nattino, Francesca Costanzo, and Geert-Jan Kroes. "N2 dissociation on W(110): An ab initio molecular dynamics study on the effect of phonons". *The Journal of Chemical Physics* 142, p. 104702, 2015. (Cited on p. 5).

[28] C. Díaz, J. K. Vincent, G. P. Krishnamohan, R. A. Olsen, G. J. Kroes, K. Honkala, and J. K. Nørskov. "Reactive and nonreactive scattering of N2 from Ru(0001): A six-dimensional adiabatic study". *J. Chem. Phys.* 125, p. 114706, 2006. (Cited on p. 5).

[29] I. Goikoetxea, J. Meyer, J. I. Juaristi, M. Alducin, and K. Reuter. "Role of Physisorption States in Molecular Scattering: A Semilocal Density-Functional Theory Study on O2/Ag(111)". *Phys. Rev. Lett.* 112, p. 156101, 2014. (Cited on p. 5).

[30] L. Martin-Gondre, M. Alducin, G. A. Bocan, R. Díez Muiño, and J. I. Juaristi. "Competition between Electron and Phonon Excitations in the Scattering of Nitrogen Atoms and Molecules off Tungsten and Silver Metal Surfaces". *Phys. Rev. Lett.* 108, p. 096101, 2012. (Cited on pp. 5, 28, 63).

[31] Pablo Nieto, Ernst Pijper, Daniel Barredo, Guillaume Laurent, Roar A. Olsen, Evert-Jan Baerends, Geert-Jan Kroes, and Daniel Farías. "Reactive and Non-reactive Scattering of H2 from a Metal Surface Is Electronically Adiabatic". *Science* 312, pp. 86–89, 2006. (Cited on p. 5).

[32] D. Farías, C. Díaz, P. Rivière, H. F. Busnengo, P. Nieto, M. F. Somers, G. J. Kroes, A. Salin, and F. Martín. "In-Plane and Out-of-Plane Diffraction of H2 from Metal Surfaces". *Phys. Rev. Lett.* 93, p. 246104, 2004. (Cited on p. 5).

[33] Davide Migliorini, Francesco Nattino, and Geert-Jan Kroes. "Application of van der Waals functionals to the calculation of dissociative adsorption of N2 on W(110) for static and dynamic systems". *J. Chem. Phys.* 144, p. 084702, 2016. (Cited on pp. 6, 16, 47).

[34] Ivor Lon čari ć, Gernot Füchsel, J. I. Juaristi, and Peter Saalfrank. "Strong Anisotropic Interaction Controls Unusual Sticking and Scattering of CO at Ru(0001)". *Phys. Rev. Lett.* 119, p. 146101, 2017. (Cited on pp. 6, 16).

[35] H. F. Busnengo, A. Salin, and W. Dong. "Representation of the 6D potential energy surface for a diatomic molecule near a solid surface". *J. Chem. Phys.* 112, pp. 7641–7651, 2000. (Cited on pp. 6, 19, 22, 31).

[36] M. Born and R. Oppenheimer. "Zur Quantentheorie der Molekeln". *Annalen der Physik* 389, pp. 457–484, 1927. (Cited on p. 10).

[37] P. Hohenberg and W. Kohn. "Inhomogeneous Electron Gas". *Phys. Rev.* 136, B864–B871, 1964. (Cited on p. 12).

[38] W. Kohn and L. J. Sham. "Self-Consistent Equations Including Exchange and Correlation Effects". *Phys. Rev.* 140, A1133–A1138, 1965. (Cited on pp. 13, 14).

[39] D. M. Ceperley and B. J. Alder. "Ground State of the Electron Gas by a Stochastic Method". *Phys. Rev. Lett.* 45, pp. 566–569, 1980. (Cited on p. 15).

[40] S. H. Vosko, L. Wilk, and M. Nusair. "Accurate spin-dependent electron liquid correlation energies for local spin density calculations: a critical analysis". *Canadian Journal of Physics* 58, pp. 1200–1211, 1980. (Cited on p. 15).

[41] John P. Perdew and Yue Wang. "Accurate and simple analytic representation of the electron-gas correlation energy". *Phys. Rev. B* 45, pp. 13244–13249, 1992. (Cited on p. 15).

[42] R. O. Jones and O. Gunnarsson. "The density functional formalism, its applications and prospects". *Rev. Mod. Phys.* 61, pp. 689–746, 1989. (Cited on p. 15).

[43] J. P. Perdew, K. Burke, and M. Ernzerhof. "Generalized Gradient Approximation Made Simple". *Phys. Rev. Lett.* 77, pp. 3865–3868, 1996. (Cited on p. 15).

[44] A. D. Becke. "Density-functional exchange-energy approximation with correct asymptotic behavior". *Phys. Rev. A* 38, pp. 3098–3100, 1988. (Cited on p. 15).

[45] Chengteh Lee, Weitao Yang, and Robert G. Parr. "Development of the Colle-Salvetti correlation-energy formula into a functional of the electron density". *Phys. Rev. B* 37, pp. 785–789, 1988. (Cited on p. 15).

[46] B. Hammer, L. B. Hansen, and J. K. Nørskov. "Improved adsorption energetics within density-functional theory using revised Perdew-Burke-Ernzerhof functionals". *Phys. Rev. B* 59, pp. 7413–7421, 1999. (Cited on p. 15).

[47] John P. Perdew, J. A. Chevary, S. H. Vosko, Koblar A. Jackson, Mark R. Pederson, D. J. Singh, and Carlos Fiolhais. "Atoms, molecules, solids, and surfaces: Applications of the generalized gradient approximation for exchange and correlation". *Phys. Rev. B* 46, pp. 6671–6687, 1992. (Cited on p. 15).

[48] Henrik Rydberg, Bengt I. Lundqvist, David C. Langreth, and Maxime Dion. "Tractable nonlocal correlation density functionals for flat surfaces and slabs". *Phys. Rev. B* 62, pp. 6997–7006, 2000. (Cited on p. 16).

[49] H. Rydberg, M. Dion, N. Jacobson, E. Schröder, P. Hyldgaard, S. I. Simak, D. C. Langreth, and B. I. Lundqvist. "Van der Waals Density Functional for Layered Structures". *Phys. Rev. Lett.* 91, p. 126402, 2003. (Cited on p. 16).

[50] M. Dion, H. Rydberg, E. Schröder, D. C. Langreth, and B. I. Lundqvist. "Van der Waals Density Functional for General Geometries". *Phys. Rev. Lett.* 92, p. 246401, 2004. (Cited on p. 16).

[51] André K. Kelkkanen, Bengt I. Lundqvist, and Jens K. Nørskov. "Density functional for van der Waals forces accounts for hydrogen bond in benchmark set of water hexamers". *The Journal of Chemical Physics* 131, p. 046102, 2009. (Cited on p. 16).

[52] Andris Gulans, Martti J. Puska, and Risto M. Nieminen. "Linear-scaling self-consistent implementation of the van der Waals density functional". *Phys. Rev. B* 79, p. 201105, 2009. (Cited on p. 16).

[53] Svetla D. Chakarova-Käck, Elsebeth Schröder, Bengt I. Lundqvist, and David C. Langreth. "Application of van der Waals Density Functional to an Extended System: Adsorption of Benzene and Naphthalene on Graphite". *Phys. Rev. Lett.* 96, p. 146107, 2006. (Cited on p. 16).

[54] Aaron Puzder, Maxime Dion, and David C. Langreth. "Binding energies in benzene dimers: Nonlocal density functional calculations". *The Journal of Chemical Physics* 124, p. 164105, 2006. (Cited on p. 16).

[55] D C Langreth, B I Lundqvist, S D Chakarova-Käck, V R Cooper, M Dion, P Hyldgaard, A Kelkkanen, J Kleis, Lingzhu Kong, Shen Li, P G Moses, E Murray, A Puzder, H Rydberg, E Schröder, and T Thonhauser. "A density functional for sparse matter". *Journal of Physics: Condensed Matter* 21, p. 084203, 2009. (Cited on p. 16).

[56] Lingzhu Kong, Guillermo Román-Pérez, José M. Soler, and David C. Langreth. "Energetics and Dynamics of $\mathbf{H}_2$ Adsorbed in a Nanoporous Material at Low Temperature". *Phys. Rev. Lett.* 103, p. 096103, 2009. (Cited on p. 16).

[57] T. Thonhauser, Valentino R. Cooper, Shen Li, Aaron Puzder, Per Hyldgaard, and David C. Langreth. "Van der Waals density functional: Self-consistent potential and the nature of the van der Waals bond". *Phys. Rev. B* 76, p. 125112, 2007. (Cited on p. 16).

[58] Kyuho Lee, Éamonn D. Murray, Lingzhu Kong, Bengt I. Lundqvist, and David C. Langreth. "Higher-accuracy van der Waals density functional". *Phys. Rev. B* 82, p. 081101, 2010. (Cited on pp. 16, 31).

[59] Per Hyldgaard, Kristian Berland, and Elsebeth Schröder. "Interpretation of van der Waals density functionals". *Phys. Rev. B* 90, p. 075148, 2014. (Cited on p. 16).

[60] Kristian Berland, Valentino R Cooper, Kyuho Lee, Elsebeth Schröder, T Thonhauser, Per Hyldgaard, and Bengt I Lundqvist. "van der Waals forces in density functional theory: a review of the vdW-DF method". *Reports on Progress in Physics* 78, p. 066501, 2015. (Cited on p. 16).

[61] Richard M. Martin. *Electronic Structure: Basic Theory and Practical Methods*. Cambridge University Press, 2004. (Cited on p. 17).

[62] Felix Bloch. "Über die Quantenmechanik der Elektronen in Kristallgittern". *Zeitschrift für Physik* 52, pp. 555–600, 1929. (Cited on p. 17).

[63] D. R. Hamann, M. Schlüter, and C. Chiang. "Norm-Conserving Pseudopotentials". *Phys. Rev. Lett.* 43, pp. 1494–1497, 1979. (Cited on p. 18).

[64] David Vanderbilt. "Soft self-consistent pseudopotentials in a generalized eigenvalue formalism". *Phys. Rev. B* 41, pp. 7892–7895, 1990. (Cited on p. 18).

[65] Kari Laasonen, Roberto Car, Changyol Lee, and David Vanderbilt. "Implementation of ultrasoft pseudopotentials in ab initio molecular dynamics". *Phys. Rev. B* 43, pp. 6796–6799, 1991. (Cited on p. 18).

[66] P. E. Blöchl. "Projector augmented-wave method". *Phys. Rev. B* 50, pp. 17953–17979, 1994. (Cited on p. 18).

[67] G. Kresse and D. Joubert. "From ultrasoft pseudopotentials to the projector augmented-wave method". *Phys. Rev. B* 59, pp. 1758–1775, 1999. (Cited on pp. 18, 31).

[68] Hendrik J. Monkhorst and James D. Pack. "Special points for Brillouin-zone integrations". *Phys. Rev. B* 13, pp. 5188–5192, 1976. (Cited on p. 19).

[69] Murray S. Daw, Stephen M. Foiles, and Michael I. Baskes. "The embedded-atom method: a review of theory and applications". *Materials Science Reports* 9, pp. 251–310, 1993. (Cited on p. 19).

[70] Shin Sato. "On a New Method of Drawing the Potential Energy Surface". *The Journal of Chemical Physics* 23, pp. 592–593, 1955. (Cited on p. 19).

[71] L. Martin-Gondre, C. Crespos, P. Larregaray, J.C. Rayez, B. van Ootegem, and D. Conte. "Is the LEPS potential accurate enough to investigate the dissociation of diatomic molecules on surfaces?" *Chemical Physics Letters* 471, pp. 136–142, 2009. (Cited on p. 19).

[72] Ludovic Martin-Gondre, C Crespos, Pascal Larregaray, J C. Rayez, D Conte, and B van Ootegem. "Detailed description of the flexible periodic London-Eyring-Polanyi-Sato potential energy function". 367, pp. 136–147, 2010. (Cited on p. 19).

[73] Jörg Behler. "Neural network potential-energy surfaces in chemistry: a tool for large-scale simulations". *Phys. Chem. Chem. Phys.* 13, pp. 17930–17955, 2011. (Cited on p. 19).

[74] C. Crespos, M.A. Collins, E. Pijper, and G.J. Kroes. "Multi-dimensional potential energy surface determination by modified Shepard interpolation for a molecule–surface reaction: H2+Pt(111)". *Chemical Physics Letters* 376, pp. 566–575, 2003. (Cited on p. 19).

[75] E Pijper, M.F Somers, G.J Kroes, R.A Olsen, E.J Baerends, H.F Busnengo, A Salin, and D Lemoine. "Six-dimensional quantum dynamics of scattering of (v=0, j=0) H2 from Pt(111): comparison to experiment and to classical dynamics results". *Chemical Physics Letters* 347, pp. 277–284, 2001. (Cited on p. 22).

[76] R. A. Olsen, H. F. Busnengo, A. Salin, M. F. Somers, G. J. Kroes, and E. J. Baerends. "Constructing accurate potential energy surfaces for a diatomic molecule interacting with a solid surface: H2+Pt(111) and H2+Cu(100)". *The Journal of Chemical Physics* 116, pp. 3841–3855, 2002. (Cited on p. 22).

[77] M. Alducin, H. F. Busnengo, and R. Díez-Muiño. "Dissociative adsorption of spin-triplet and spin-singlet O2 on Ag(100)". *J. Chem. Phys.* 129, p. 224702, 2008. (Cited on p. 22).

[78] K. R. Geethalakshmi, J. I. Juaristi, R. Díez Muiño, and M. Alducin. "Non-reactive scattering of N2 from the W(110) surface studied with different exchange-correlation functionals". *Phys. Chem. Chem. Phys.* 13, pp. 4357–4364, 2011. (Cited on p. 22).

[79] C. Diaz, E. Pijper, R. A. Olsen, H. F. Busnengo, D. J. Auerbach, and G. J. Kroes. "Chemically Accurate Simulation of a Prototypical Surface Reaction: H2 Dissociation on Cu(111)". *Science* 326, pp. 832–834, 2009. (Cited on p. 22).

[80] I. Goikoetxea, M. Alducin, R. Díez Muiño, and J. I. Juaristi. "The dynamics of adsorption and dissociation of N2 in a monolayer of iron on W(110)". *Phys. Chem. Chem. Phys.* 17, pp. 19432–19445, 2015. (Cited on p. 22).

[81] Axel Groß. "Reactions at surfaces studied by ab initio dynamics calculations". *Surface Science Reports* 32, pp. 291–340, 1998. (Cited on p. 24).

[82] A. Lozano, A. Gross, and H. F. Busnengo. "Adsorption dynamics of H2 on Pd(100) from first principles". *Phys. Chem. Chem. Phys.* 11, pp. 5814–5822, 2009. (Cited on p. 24).

[83] P. Ehrenfest. "Bemerkung über die angenäherte Gültigkeit der klassischen Mechanik innerhalb der Quantenmechanik". *Zeitschrift für Physik* 45, pp. 455–457, 1927. (Cited on p. 24).

[84] J. Stoer and R Bulirsch. *Introduction to numerical analysis*. Texts in applied mathematics. Springer, 2002. (Cited on p. 25).

[85] J. C. Tully. "Dynamics of gas-surface interactions: 3D generalized Langevin model applied to fcc and bcc surfaces". *J. Chem. Phys.* 73, pp. 1975–1985, 1980. (Cited on pp. 26, 61, 62).

[86] J. C. Polanyi and R. J. Wolf. "Dynamics of simple gas-surface interaction. II. Rotationally inelastic collisions at rigid and moving surfaces". *J. Chem. Phys.* 82, pp. 1555–1566, 1985. (Cited on pp. 26, 61).

[87] H. F. Busnengo, W. Dong, and A. Salin. "Trapping, Molecular Adsorption, and Precursors for Nonactivated Chemisorption". *Phys. Rev. Lett.* 93, p. 236103, 2004. (Cited on pp. 26, 61).

[88] H. F. Busnengo, M. A. Di Césare, W. Dong, and A. Salin. "Surface temperature effects in dynamic trapping mediated adsorption of light molecules on metal surfaces: H_2 on Pd(111) and Pd(110)". *Phys. Rev. B* 72, p. 125411, 2005. (Cited on pp. 26, 61).

[89] S. A. Adelman and J. D. Doll. "Generalized Langevin equation approach for atom/solid-surface scattering: General formulation for classical scattering off harmonic solids". *The Journal of Chemical Physics* 64, pp. 2375–2388, 1976. (Cited on p. 26).

[90] Brian Gergen, Hermann Nienhaus, W. Henry Weinberg, and Eric W. McFarland. "Chemically Induced Electronic Excitations at Metal Surfaces". *Science* 294, pp. 2521–2523, 2001. (Cited on p. 27).

[91] D. Krix, R. Nünthel, and H. Nienhaus. "Generation of hot charge carriers by adsorption of hydrogen and deuterium atoms on a silver surface". *Phys. Rev. B* 75, p. 073410, 2007. (Cited on p. 27).

[92] M Lindenblatt, J van Heys, and E Pehlke. "Molecular dynamics of nonadiabatic processes at surfaces: Chemisorption of H/Al(111)". 600, pp. 3624–3628, 2006. (Cited on p. 27).

[93] M. Lindenblatt, E. Pehlke, A. Duvenbeck, B. Rethfeld, and A. Wucher. "Kinetic excitation of solids: The concept of electronic friction". *Nuclear Instruments and Methods in Physics Research B* 246, pp. 333–339, 2006. (Cited on p. 27).

[94] Neil Shenvi, Sharani Roy, and John C. Tully. "Dynamical Steering and Electronic Excitation in NO Scattering from a Gold Surface". *Science* 326, pp. 829–832, 2009. (Cited on p. 27).

[95] A. C. Luntz and M. Persson. "How adiabatic is activated adsorption/associative desorption?" *The Journal of Chemical Physics* 123, p. 074704, 2005. (Cited on p. 27).

[96] J. I. Juaristi, M. Alducin, R. Diez, H. F. Busnengo, and A. Salin. "Role of Electron-Hole Pair Excitations in the Dissociative Adsorption of Diatomic Molecules on Metal Surfaces". *Phys. Rev. Lett.* 100, p. 116102, 2008. (Cited on pp. 27, 28, 61).

[97] P.M. Echenique, R.M. Nieminen, and R.H. Ritchie. "Density functional calculation of stopping power of an electron gas for slow ions". *Solid State Communications* 37, pp. 779–781, 1981. (Cited on p. 28).

[98] P. M. Echenique, R. M. Nieminen, J. C. Ashley, and R. H. Ritchie. "Nonlinear stopping power of an electron gas for slow ions". *Phys. Rev. A* 33, pp. 897–904, 1986. (Cited on p. 28).

[99] H. Winter, J. I. Juaristi, I. Nagy, A. Arnau, and P. M. Echenique. "Energy loss of slow ions in a nonuniform electron gas". *Phys. Rev. B* 67, p. 245401, 2003. (Cited on p. 28).

[100] J. I. Juaristi, A. Arnau, P. M. Echenique, C. Auth, and H. Winter. "Charge State Dependence of the Energy Loss of Slow Ions in Metals". *Phys. Rev. Lett.* 82, pp. 1048–1051, 1999. (Cited on p. 28).

[101] M. Blanco-Rey, J. I. Juaristi, R. Díez Muiño, H. F. Busnengo, G. J. Kroes, and M. Alducin. "Electronic Friction Dominates Hydrogen Hot-Atom Relaxation on Pd(100)". *Phys. Rev. Lett.* 112, p. 103203, 2014. (Cited on p. 28).

[102] O. Galparsoro, R. Pétuya, J. I. Juaristi, C. Crespos, M. Alducin, and P. Larregaray. "Energy Dissipation to Tungsten Surfaces upon Eley–Rideal Recombination of N2 and H2". *The Journal of Physical Chemistry C* 119, pp. 15434–15442, 2015. (Cited on pp. 28, 80).

[103] I Goikoetxea, J I Juaristi, M Alducin, and R Díez Muiño. "Dissipative effects in the dynamics of N2on tungsten surfaces". *Journal of Physics: Condensed Matter* 21, p. 264007, 2009. (Cited on p. 28).

[104] Loup Verlet. "Computer "Experiments" on Classical Fluids. I. Thermodynamical Properties of Lennard-Jones Molecules". *Phys. Rev.* 159, pp. 98–103, 1967. (Cited on p. 28).

[105] D. Beeman. "Some multistep methods for use in molecular dynamics calculations". *Journal of Computational Physics* 20, pp. 130–139, 1976. (Cited on p. 28).

[106] G. Kresse and J. Hafner. "Ab initio molecular dynamics for liquid metals". *Phys. Rev. B* 47, pp. 558–561, 1993. (Cited on pp. 31, 97).

[107] G. Kresse and J. Furthmüller. "Efficiency of ab-initio total energy calculations for metals and semiconductors using a plane-wave basis set". *Computational Materials Science* 6, pp. 15–50, 1996. (Cited on pp. 31, 97).

[108] G. Kresse and J. Furthmüller. "Efficient iterative schemes for ab initio total-energy calculations using a plane-wave basis set". *Phys. Rev. B* 54, pp. 11169–11186, 1996. (Cited on pp. 31, 97).

[109] J. Hafner and G. Kresse. In: "The Vienna AB-Initio Simulation Program VASP: An Efficient and Versatile Tool for Studying the Structural, Dynamic, and Electronic Properties of Materials". Antonios Gonis, Annemarie Meike, and Patrice E. A. Turchi, eds. Pp. 69–82. Boston, MA: Springer US, 1997. (Cited on pp. 31, 97).

[110] Jayant S. Shah and M. E. Straumanis. "Thermal Expansion of Tungsten at Low Temperatures". *Journal of Applied Physics* 42, pp. 3288–3289, 1971. (Cited on p. 32).

[111] K Griffiths, D A King, G C Aers, and J B Pendry. "LEED structural analysis of N2 and CO (2 x 2)R45 structures on W(100)". *Journal of Physics C: Solid State Physics* 15, p. 4921, 1982. (Cited on p. 32).

[112] L.R. Clavenna and L.D. Schmidt. "Interaction of N2 with (100) W". *Surface Science* 22, pp. 365–391, 1970. (Cited on p. 38).

[113] D.O. HAYWARD. "Chapter 4 - Gas Adsorption". In: *Chemisorption and Reactions on Metallic Films*. Ed. by J.R. Anderson. Vol. 1. Physical Chemistry: A Series of Monographs. Academic Press, 1971. Pp. 225–326. (Cited on p. 40).

[114] L. Martin-Gondre, J. I. Juaristi, M. Blanco-Rey, R. Díez Muiño, and M. Alducin. "Influence of the van der Waals interaction in the dissociation dynamics of N2 on W(110) from first principles". *J. Chem. Phys.* 142, p. 074704, 2015. (Cited on p. 47).

[115] H. F. Busnengo, C. Crespos, W. Dong, J. C. Rayez, and A. Salin. "Classical dynamics of dissociative adsorption for a nonactivated system: The role of zero point energy". *The Journal of Chemical Physics* 116, pp. 9005–9013, 2002. (Cited on p. 50).

[116] Alejandro Peña-Torres, H. Fabio Busnengo, J. Iñaki Juaristi, Pascal Larregaray, and Cedric Crespos. "Dynamics of N2 sticking on W(100): the decisive role of van der Waals interactions". *Phys. Chem. Chem. Phys.* 20, pp. 19326–19331, 2018. (Cited on pp. 53, 64).

[117] M. Balden, S. Lehwald, and H. Ibach. "Substrate and hydrogen phonons of the ordered p(2x1) and (2x2) phase and of the anomalous (1x1) phase of hydrogen on W(110)". *Phys. Rev. B* 53, pp. 7479–7491, 1996. (Cited on p. 62).

[118] H.-J. Ernst, E. Hulpke, and J. P. Toennies. "Helium-atom-scattering study of the structure and phonon dynamics of the W(001) surface between 200 and 1900 K". *Phys. Rev. B* 46, pp. 16081–16105, 1992. (Cited on p. 62).

[119] S. Titmuss, A. Wander, and D. A. King. "Reconstruction of Clean and Adsorbate-Covered Metal Surfaces". *Chemical Reviews* 96 PMID: 11848790, pp. 1291–1306, 1996. (Cited on p. 62).

[120] Axel Gross, Michel Bockstedte, and Matthias Scheffler. "Ab Initio Molecular Dynamics Study of the Desorption of D_2 from Si(100)". *Phys. Rev. Lett.* 79, pp. 701–704, 1997. (Cited on p. 70).

[121] Axel Groß and Arezoo Dianat. "Hydrogen Dissociation Dynamics on Precovered Pd Surfaces: Langmuir is Still Right". *Phys. Rev. Lett.* 98, p. 206107, 2007. (Cited on p. 70).

[122] A. Lozano, A. Groß, and H. F. Busnengo. "Molecular dynamics study of H_2 dissociation on H-covered Pd(100)". *Phys. Rev. B* 81, p. 121402, 2010. (Cited on p. 70).

[123] Francesco Nattino, Hirokazu Ueta, Helen Chadwick, Maarten E. van Reijzen, Rainer D. Beck, Bret Jackson, Marc C. van Hemert, and Geert-Jan Kroes. "Ab Initio Molecular Dynamics Calculations versus Quantum-State-Resolved Experiments on CHD3 + Pt(111): New Insights into a Prototypical Gas–Surface Reaction". *The Journal of Physical Chemistry Letters* 5 PMID: 26269970, pp. 1294–1299, 2014. (Cited on p. 70).

[124] D. D. Eley and E. K. Rideal. "The catalysis of the parahydrogen conversion by tungsten". *Proceedings of the Royal Society of London A: Mathematical, Physical and Engineering Sciences* 178, pp. 429–451, 1941. (Cited on p. 79).

[125] D. D. Eley. "The interchange of hydrogen in the adsorbed film on tungsten". *Proceedings of the Royal Society of London A: Mathematical, Physical and Engineering Sciences* 178, pp. 452–464, 1941. (Cited on p. 79).

[126] C. T. Rettner. "Dynamics of the direct reaction of hydrogen atoms adsorbed on Cu(111) with hydrogen atoms incident from the gas phase". *Phys. Rev. Lett.* 69, pp. 383–386, 1992. (Cited on p. 79).

[127] Charles T. Rettner. "Reaction of an H-atom beam with Cl/Au(111): Dynamics of concurrent Eley–Rideal and Langmuir–Hinshelwood mechanisms". *The Journal of Chemical Physics* 101, pp. 1529–1546, 1994. (Cited on p. 79).

[128] C. T. Rettner, H. A. Michelsen, and D. J. Auerbach. "Quantum-state-specific dynamics of the dissociative adsorption and associative desorption of H2 at a Cu(111) surface". *The Journal of Chemical Physics* 102, pp. 4625–4641, 1995. (Cited on p. 79).

[129] Bret Jackson and Mats Persson. "A quantum mechanical study of recombinative desorption of atomic hydrogen on a metal surface". *The Journal of Chemical Physics* 96, pp. 2378–2386, 1992. (Cited on p. 79).

[130] Bret Jackson and Mats Persson. "Effects of isotopic substitution on Eley–Rideal reactions and adsorbate-mediated trapping". *The Journal of Chemical Physics* 103, pp. 6257–6269, 1995. (Cited on p. 79).

[131] Mats Persson and Bret Jackson. "Flat surface study of the Eley–Rideal dynamics of recombinative desorption of hydrogen on a metal surface". *The Journal of Chemical Physics* 102, pp. 1078–1093, 1995. (Cited on p. 79).

[132] Stavros Caratzoulas, Bret Jackson, and Mats Persson. "Eley–Rideal and hot-atom reaction dynamics of H(g) with H adsorbed on Cu(111)". *The Journal of Chemical Physics* 107, pp. 6420–6431, 1997. (Cited on p. 79).

[133] Chakrapani Kalyanaraman, Didier Lemoine, and Bret Jackson. "Eley–Rideal and hot-atom reactions between hydrogen atoms on metals: quantum mechanical studies". *Phys. Chem. Chem. Phys.* 1, pp. 1351–1358, 1999. (Cited on p. 79).

[134] Bret Jackson and Didier Lemoine. "Eley–Rideal reactions between H atoms on metal and graphite surfaces: The variation of reactivity with substrate". *The Journal of Chemical Physics* 114, pp. 474–482, 2001. (Cited on p. 79).

[135] Bret Jackson, Xianwei Sha, and Ziya B. Guvenc. "Kinetic model for Eley–Rideal and hot atom reactions between H atoms on metal surfaces". *The Journal of Chemical Physics* 116, pp. 2599–2608, 2002. (Cited on p. 80).

[136] Ziya B. Guvenc, Xianwei Sha, and Bret Jackson. "Eley–Rideal and hot atom reactions between hydrogen atoms on Ni(100): Electronic structure and quasiclassical studies". *The Journal of Chemical Physics* 115, pp. 9018–9027, 2001. (Cited on p. 80).

[137] R. Martinazzo, S. Assoni, G. Marinoni, and G. F. Tantardini. "Hot-atom versus Eley–Rideal dynamics in hydrogen recombination on Ni(100). I. The single-adsorbate case". *The Journal of Chemical Physics* 120, pp. 8761–8771, 2004. (Cited on pp. 80, 83).

[138] E. Quintas-Sánchez, P. Larrégaray, C. Crespos, L. Martin-Gondre, J. Rubayo-Soneira, and J.-C. Rayez. "Dynamical reaction pathways in Eley-Rideal recombination of nitrogen from W(100)". *The Journal of Chemical Physics* 137, p. 064709, 2012. (Cited on pp. 80, 81, 84, 85).

[139] G Volpilhac, H.F Busnengo, W Dong, and A Salin. "Scattering of atomic nitrogen on W(100)". *Surface Science* 544, pp. 329–338, 2003. (Cited on p. 80).

[140] L. Martin-Gondre, C. Crespos, P. Larregaray, J.C. Rayez, B. van Ootegem, and D. Conte. "Is the LEPS potential accurate enough to investigate the dissociation of diatomic molecules on surfaces?" *Chemical Physics Letters* 471, pp. 136–142, 2009. (Cited on p. 80).

[141] L. Martin-Gondre, C. Crespos, P. Larrégaray, J.C. Rayez, D. Conte, and B. van Ootegem. "Detailed description of the flexible periodic London–Eyring–Polanyi–Sato potential energy function". *Chemical Physics* 367, pp. 136–147, 2010. (Cited on p. 80).

[142] L. Martin-Gondre, C. Crespos, P. Larregaray, J. C. Rayez, B. van Ootegem, and D. Conte. "Dynamics simulation of N2 scattering onto W(100,110) surfaces: A stringent test for the recently developed flexible periodic London–Eyring–Polanyi–Sato potential energy surface". *The Journal of Chemical Physics* 132, p. 204501, 2010. (Cited on p. 80).

[143] E. Quintas-Sánchez, C. Crespos, P. Larrégaray, J-C. Rayez, L. Martin-Gondre, and J. Rubayo-Soneira. "Surface temperature effects on the dynamics of N2 Eley-Rideal recombination on W(100)". *The Journal of Chemical Physics* 138, p. 024706, 2013. (Cited on p. 80).

[144] R. Pétuya, P.-A. Plötz, C. Crespos, and P. Larregaray. "Revisiting the Non-reactive Scattering of N2 off W(100): On the Influence of the Scattering Azimuth on In-Plane Angular Distributions". *The Journal of Physical Chemistry C* 118, pp. 21904–21910, 2014. (Cited on pp. 89, 90).